Immunotoxin Monotherapy and Combinatorial Therapy With Immune Checkpoint Inhibitors for Malignant Brain Tumors

by

Xuhui Bao

Department of Pathology
Duke University

Date:_____

Approved:

_____
Darell Bigner, Supervisor

_____
Yiping He

_____
Edward Levin

_____
Qi-Jing Li

_____
Hai Yan

Dissertation submitted in partial fulfillment of
the requirements for the degree of Doctor
of Philosophy in the Department of
Pathology in the Graduate School
of Duke University

2016

ABSTRACT

Immunotoxin Monotherapy and Combinatorial Therapy With Immune Checkpoint Inhibitors for Malignant Brain Tumors

by

Xuhui Bao

Department of Pathology
Duke University

Date:_____

Approved:

_____
Darell Bigner, Supervisor

_____
Yiping He

_____
Edward Levin

_____
Qi-Jing Li

_____
Hai Yan

An abstract of a dissertation submitted in partial fulfillment of the requirements for the degree of Doctor of Philosophy in the Department of Pathology in the Graduate School of Duke University

2016

Abstract

Glioblastoma is the most common and aggressive malignant brain tumor among all primary brain and central nervous system (CNS) tumors. The median survival time for glioblastoma patients given the current standard of care treatment (surgery, radiation, and chemotherapy) is less than 15 months. Medulloblastoma is another major malignant brain tumor that most frequently occurs in children. Although recent advances in surgery, radiotherapy, and chemotherapy have led to an increase in 5-year survival rates of medulloblastoma patients, treatment-related toxicity often has a major impact on long-term quality of survival.

As a result, there is an urgent need to develop more efficient and novel therapeutic approaches that specifically target tumor cells while preserving the surrounding normal CNS to improve the poor survival and quality of life of patients with malignant brain tumors. To address this need, we have developed two novel targeted immunotoxins (ITs), D2C7-(scdsFv)-PE38KDEL (D2C7-IT) and NZ-1-(scdsFv)-PE38KDEL (NZ-1-IT). D2C7-IT was developed by fusing the single-chain variable fragment (scFv) of the D2C7 monoclonal antibody (mAb) with domains II and III of *Pseudomonas* exotoxin A (PE38KDEL), and NZ-1-IT was developed by fusing the scFv of the NZ-1 mAb with PE38KDEL. D2C7-IT reacts with both the wild-type epidermal growth factor receptor (EGFRwt) and the EGFR variant III (EGFRvIII), two

overexpressed proteins in glioblastomas. NZ-1-IT reacts with podoplanin (PDPN), a protein that has a high expression in glioblastomas and medulloblastomas.

In vitro cytotoxicity data shows that both ITs effectively inhibited protein synthesis in a variety of epitope-expressing glioblastoma and medulloblastoma xenograft cells and human tumor cell lines. Furthermore, the direct anti-tumor efficacy of D2C7-IT was examined in orthotopic glioma models in immunocompromised mice, while the direct anti-tumor efficacy of NZ-1-IT was observed in medulloblastoma xenograft-bearing immunocompromised mice. Both immunotoxins showed a robust anti-tumor efficacy in the preclinical brain tumor models. D2C7-IT was first investigated in the subsequent studies to accelerate its translation to the clinic. The preclinical toxicity of intracerebral D2C7-IT infusion was subsequently determined in normal Sprague-Dawley (SD) rats. The maximum tolerated dose (MTD) of D2C7-IT was determined to be between a total dose of 0.10 and 0.35 μg, and the no-observed-adverse-effect level (NOAEL) of D2C7-IT was a total dose of 0.05 μg in SD rats. Both the MTD and NOAEL were utilized as references for the D2C7-IT clinical trial design.

In addition to direct tumor cell killing, immunotoxin monotherapy has been shown to induce a secondary anti-tumor immune response through the engagement of T cells. Therefore, the D2C7-IT-induced secondary anti-tumor immune response was investigated using syngeneic mouse glioma models in immunocompetent mice. Moreover, previous studies have demonstrated that immune checkpoint inhibitors have

a robust anti-tumor efficacy by augmenting the T cell response to the tumor cells. Thus, immune checkpoint inhibitors were combined with D2C7-IT in order to enhance the immunotoxin-induced anti-tumor immune response to eliminate residual tumor cells and prevent tumor recurrence in the long term. Meanwhile, studies with NZ-1-IT remain preliminary; thus, this IT will not be as robustly discussed as D2C7-IT throughout this text.

Dedication

To my whole family,

for their endless encouragement, generous support, and great patience.

Contents

List of Tables

List of Figures

Acknowledgements

This thesis work would not have been accomplished without such a collaborative and supportive community where I have grown up not only as a graduate student but also as a scientist. I would like to specifically express my sincerest gratitude to:

My advisor Dr. Darell Bigner: for his leadership, guidance, patience, support, encouragement, immense knowledge, and for entrusting me with many exciting projects. I could not imagine a better advisor.

My committee: Drs. Yiping He, Edward Levin, Qi-Jing Li, John Sampson (preliminary exam committee faculty), and Hai Yan for their guidance, support, and encouragement throughout my PhD training.

Drs. John Norton, Randall Reynolds, William Wetsel, Ramona Rodriguiz, Roger McLendon, Neil Petry, Michael Zalutsky, Bruce Burnett, Ira Pastan and research teams from Division of Laboratory Animal Resources (DLAR) and Mouse Behavioral and Neuroendocrine Analysis Core Facility for their collaboration and intensive work studying the preclinical toxicity of D2C7 immunotoxin.

Drs. Stephen Keir, Vidyalakshmi Chandramohan, Smita Nair, Matthias Gromeier, and Dani Bolognesi for their guidance, collaboration, and instructions in the immunotoxin monotherapy and immunotoxin and immune checkpoint inhibitors combinatorial study.

Drs. M. Dee Gunn and Yen-Rei Andrea Yu for the collaboration, instructions, and training in the flow cytometry analysis for the tumor infiltrative immune cells.

My lab-mates (present and previous): who both technically and intellectually helped me during my training: Drs. Hailan Piao, Chien-tsun Kuan, Liang Qu, Jianjun Li; Charles Pegram, Scott Szafranski, Steven Clayton, Huishan Zhu, Jenna Lewis, Timothy Lee, Carol Porterfield, and Heather Rabalais.

Pamela Harris, Margaret Atchison, and Dr. Soman Abraham (Pathology Graduate Program) for their guidance, suggestions, and instructions during my PhD training.

Keith St. Pierre and his team (Cancer Center Isolation Facility) for all the great help for my animal experiments there.

Diane Satterfield, Merrie Burnett, and Elizabeth Thomas (Brain Tumor Tissue Biorepository) for their help and instructions with tissue processing and sectioning.

Drs. Michael Brown, Wei Huang, and Christopher Pirozzi for their great help and precious instructions during the preparation of this dissertation.

My whole family for providing such a generous and endless support network throughout my life.

1. Introduction

1.1 Malignant brain tumors

1.1.1 EGFR/EGFRvIII in glioblastomas

Glioblastomas account for 45%-50% of all primary malignant brain tumors (**Figure 1**) and for 82% of malignant glioma cases. They are the most aggressive malignant brain tumors among all primary brain and central nervous system (CNS) tumors diagnosed in the United States [1, 2].

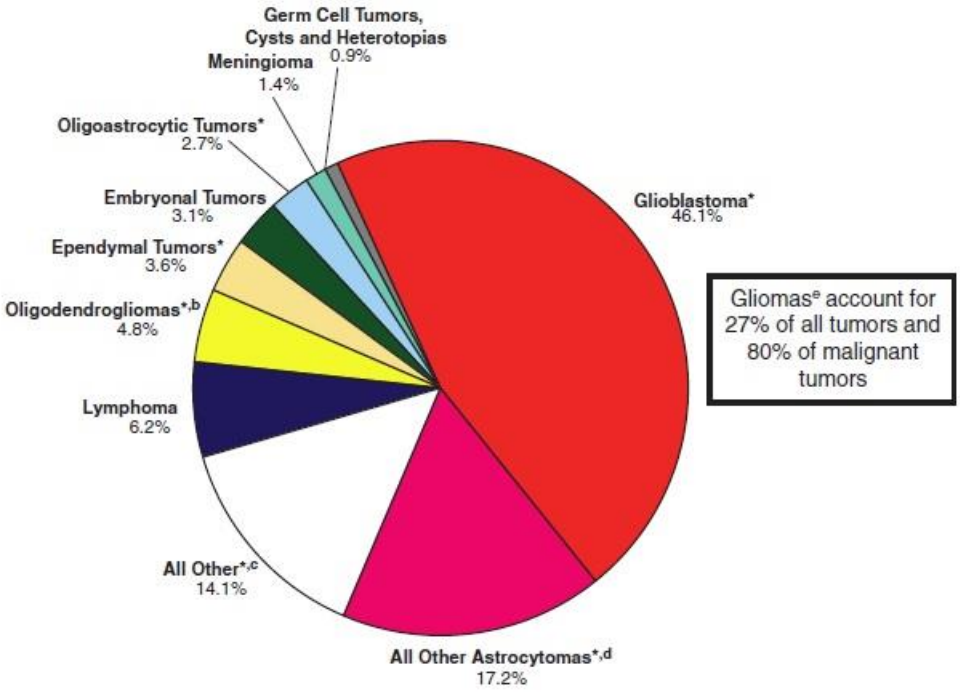

Figure 1: Distribution of Malignant Primary Brain and CNS Tumors by CBTRUS Histology Groupings and Histology (N = 117,023).

Central Brain Tumor Registry of the United States (CBTRUS) Statistical Report: the National Program of Cancer Registries (NPCR) and the Surveillance, Epidemiology, and

End Results program (SEER), 2008-2012. From [2] with permission from publisher, see appendix for license.

Although glioblastomas typically grow in the CNS and rarely metastasize, they do infiltrate the surrounding brain tissue and are highly invasive [3]. The median survival time for glioblastoma patients undergoing the current standard of care treatment of surgery, followed by radiation and chemotherapy, is less than 15 months [2, 4]. Thus, more effective therapeutic approaches are desperately needed to improve the poor survival rates of patients with glioblastoma.

Epidermal growth factor receptor (EGFR), a 170 kDa, transmembrane receptor tyrosine kinase (RTK), has been associated with a large number of human malignancies, including glioblastomas [5]. In 1985, Libermann et al. were the first to describe *EGFR* gene amplification in malignant brain tumors [6], and subsequent studies have confirmed that approximately 37%-58% of glioblastomas have an amplification of the *EGFR* gene [7]. Amplification of the *EGFR* gene is related to high EGFR mRNA or protein levels [7]. Even without the gene amplification, EGFR overexpression has been detected in 12% to 38% of glioblastoma patients [8], which may be caused by some aberrant translational and posttranslational mechanisms. In addition, the rearrangement of the *EGFR* gene often occurs together with its amplification. Extensive deletions in the *EGFR* gene's coding sequence is the most frequent rearrangement in glioblastomas [7].

Hence, the *EGFR* gene amplification, along with its deletions/mutations that lead to the generation of constitutively active mutant receptors, are two important mechanisms for the EGFR-related oncogenicity [9].

Among the genomic variants of EGFR, the class III mutant *EGFRvIII* is the most frequently detected deletion, which is present in 67% of glioblastomas with the wild-type *EGFR* (*EGFRwt*) amplification [10]. *EGFRvIII* contains a deletion of exons 2–7 of the *EGFR* gene, by which a novel glycine residue is created at the fusion junction at position 6, between amino acid residues 5 and 274 [11-17]. The mutant EGFRvIII protein is approximately 145 kD and has a tumor-specific sequence represented by that novel glycine residue to generate a tumor-specific epitope that is solely expressed on cancer cells instead of normal tissues (**Figure 2**) [18]. The *EGFRvIII* gene/transcript is found in more than 50% of glioblastomas exhibiting *EGFR* gene amplification [19, 20]. EGFRvIII is a constitutively active RTK that cannot be further activated by EGFR ligands [21]. Like EGFRwt, EGFRvIII is also widely expressed in glioblastomas [16]. Resistance to radiation and chemotherapy can be induced by the overexpression of EGFRvIII in glioma cells [22].

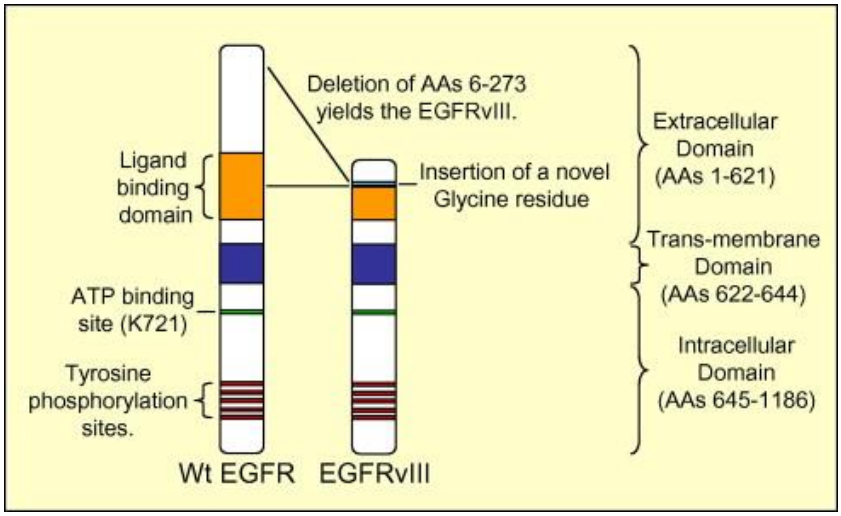

Figure 2: Schematic of EGFRwt and EGFRvIII.

From [18] with permission from publisher, see appendix for license.

The *EGFRvIII* mutation is highly prevalent in glioblastomas with *EGFRwt* amplification, while the EGFR protein is nearly undetectable in the normal brain [5]. Therefore, the development of a therapeutic agent that can target both forms of the receptor—rather than only targeting a single antigen—would be advantageous for glioblastoma treatment.

1.1.2 Podoplanin in glioblastomas and medulloblastomas

Medulloblastoma, an embryonal tumor of the cerebellum, is one of the most common childhood malignant brain tumors. While it occurs at all ages, medulloblastoma peaks in 9-year old children and younger, and is rarely diagnosed in adults [2]. The 10-year survival rate of medulloblastoma patients has increased to 63.3%

due to recent advances in surgery, radiotherapy, and chemotherapy. [2]. However, the aggressive nature of these therapies results in long-term adverse effects, including cerebellar mutism, cognitive and endocrine impairments, hearing loss, infertility, and neuropathies [23, 24]. To overcome these difficulties, there is a need to develop novel and effective therapies specifically destroying the tumor cells whereas preserving the surrounding normal tissues in the CNS.

Podoplanin (PDPN) is a 162-amino acid type I transmembrane sialomucin-like glycoprotein consisting of a serine- and threonine-rich extracellular domain, a single transmembrane domain, and a short cytoplasmic domain containing phosphorylation sites of cyclic adenosine monophosphate (cAMP) and protein kinase C (**Figure 3**) [25, 26].

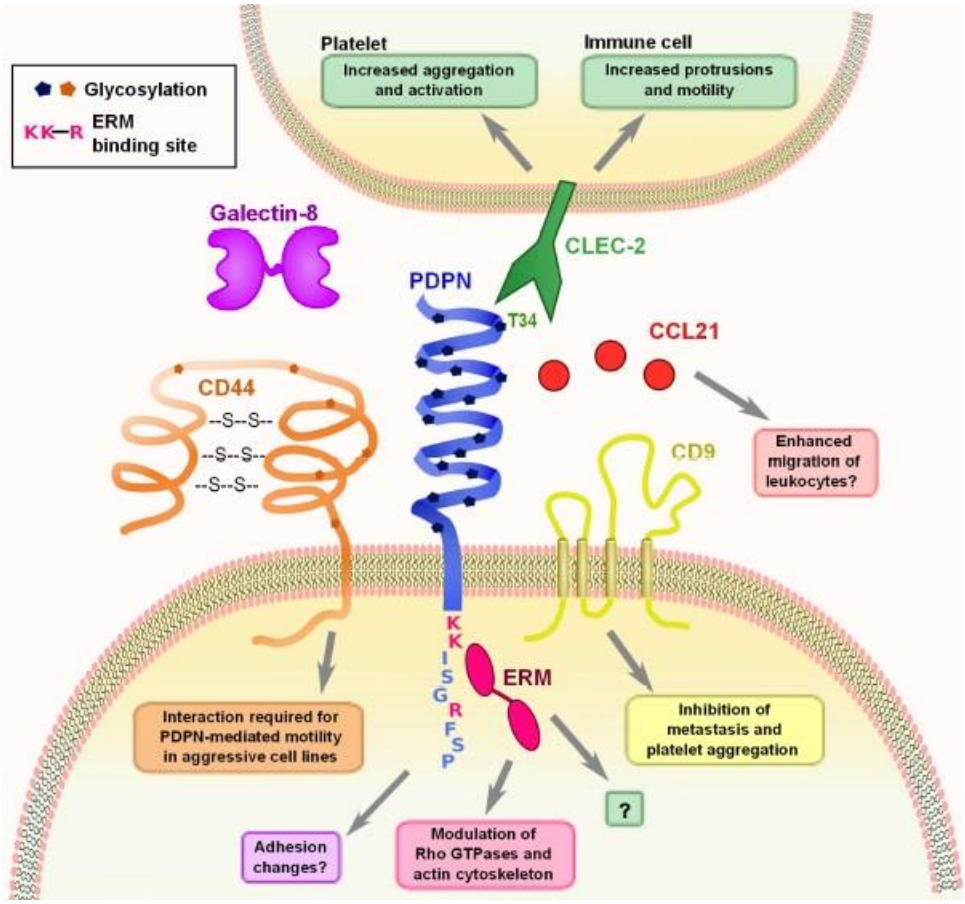

Figure 3: PDPN interacts with a variety of intracellular and transmembrane proteins to mediate effects on cell migration and adhesion.

From [26] with permission from publisher, see appendix for license.

PDPN is highly expressed by cultured human lymphatic endothelial cells, and PDPN$^{-/-}$ mice die at birth due to impaired lymphatic vessel pattern formation and respiratory failure [27]. PDPN expression has been described in several tumors, including brain tumors [25, 28, 29], and is associated with malignant progression

involving epithelial–mesenchymal transition, metastasis, and invasion [30-33]. Among the CNS tumors, PDPN expression is observed in 83% and 27% of glioblastoma and medulloblastoma cases, respectively, making it an attractive target for brain tumor therapy [28].

1.2 Immunotoxin therapy for malignant brain tumors

Current advances in brain tumor biology have identified unique molecular abnormalities that are specifically associated with malignant brain tumors but absent in the normal CNS [34]. Molecular characterization of malignant brain tumors has resulted in the recognition of tumor-specific proteins, which are becoming potential candidates for the development of targeted therapies for malignant brain tumors [35]. To this end, several monoclonal antibodies (mAbs) against specific brain tumor antigens have been generated in previous studies [36].

Developed from mAbs, immunotoxins (ITs) classically advert to those molecules that are generated by a protein toxin fused with a specific binding part originated from the immune system (e.g., a mAb or its fragment). More than a century ago, Paul Ehrlich was the first to introduce the concept of an immunotoxin that has a unique binding capacity to a disorder-related target and the ability to avoid interaction with normal body tissue [37]. The most frequently used toxins to form ITs include two bacterial toxins—*Pseudomonas* exotoxin A (PE) and diphtheria toxin (DT)—and ricin, which is a

plant toxin [38]. All three toxins, PE, DT, and ricin, are engineered into single-polypeptide chains containing binding, translocation, and catalytic domains (**Figure 4**) [37]. All three toxins are characterized as the A-B toxin, which needs cellular internalization via the endocytosis mediated by surface receptors to function [39]. Generally, a binding domain was encoded by the B subunit of these toxins to combine with the catalytic domain (A subunit) conferring cytotoxicity [37, 39]. In spite of their molecular size, domain composition, binding specificity, and catalytic activity, those toxins have a similar cell killing mechanism that inhibits protein synthesis by suppressing the elongation factor 2 (EF2) or 60S ribosome [37]. It is reported that up to 300 ribosomes can be irrecoverably inhibited in 35 minutes, even by a single toxin molecule, which is toxic enough to destroy a cancer cell [39-42]. However, ITs were not shown to kill tumor cells until the 1970s [43, 44].

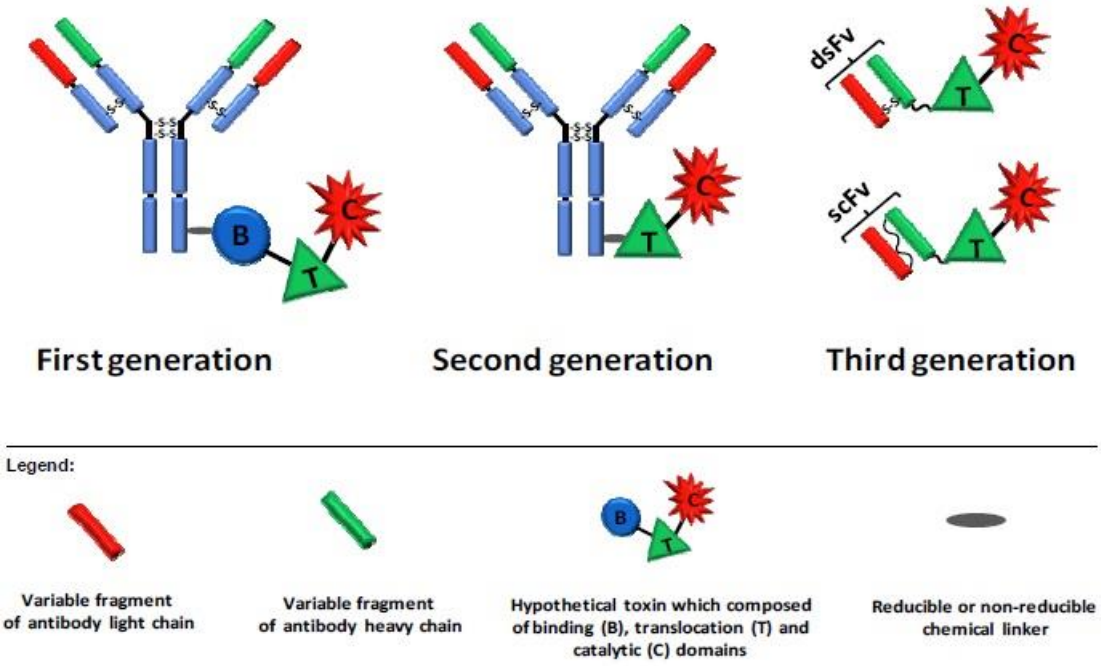

Figure 4: Three generations of immunotoxins.

First-generation immunotoxins were prepared by chemically conjugating antibodies to intact toxin units. In second-generation immunotoxins, truncated toxins that lacked a cell-binding domain were chemically conjugated to a targeting moiety. In third-generation immunotoxins, the cell binding domain of the toxin is genetically replaced with the variable fragment portion of an antibody, in which the light and heavy chain variable fragments are either genetically linked (single chain variable fragment, scFv) or held together by a disulfide bond (disulfide stabilized single chain variable fragment, scdsFv). From [37] with permission from publisher, see appendix for license.

Over the past two decades, the third-generation recombinant single-chain variable-region antibody fragment (scFv)-based ITs, composed of the heavy-chain and light-chain variable regions (V_H and V_L) of a mAb-targeting tumor antigen fused to a toxin molecule, have been widely investigated to treat several cancers, including

malignant brain tumors [38]. Since the scFv-IT fusion protein is smaller than the original mAb, it has a superior capacity for tumor penetration, which can lead to enhanced anti-tumor efficacy when it is delivered intrathecally or intratumorally [37, 38, 45, 46].

1.2.1 EGFR/EGFRvIII-targeted immunotoxin

D2C7 is a unique mAb that reacts with both EGFRwt and EGFRvIII proteins [47]. In comparison with other established specific mAbs (anti-EGFRwt mAb, EGFR1, or anti-EGFRvIII mAb, L8A4), D2C7 showed a significantly higher tumor localization in tumors expressing EGFRwt and/or EGFRvIII proteins [47]. Significantly, in an immunohistochemistry analysis of 101 adult glioblastoma samples, the D2C7 mAb positively stained virtually all cells in 100% (50/50) of the samples that had amplification of the *EGFRwt* gene and in 76% (39/51) of the cases without this amplification [47]. The D2C7 mAb is reactive with a 55-amino acid (AA) region present in the extracellular domain of both EGFRwt (583-637 AAs) and EGFRvIII (292-346 AAs) proteins (**Figure 5**). Based on this D2C7 mAb, a novel IT, D2C7-(scdsFv)-PE38KDEL (D2C7-IT), was developed by fusing the scFv of the D2C7 mAb with domains II and III of *Pseudomonas* exotoxin A (PE38KDEL) [48]. The antigen-binding capacity of D2C7-IT was first assessed by surface plasmon resonance, which showed that the K_D of D2C7-IT on the EGFRwt- and EGFRvIII-coated chips was 1.6×10^{-9} and 1.3×10^{-9} mol/L, respectively, indicating a robust binding affinity to the specific targets [48].

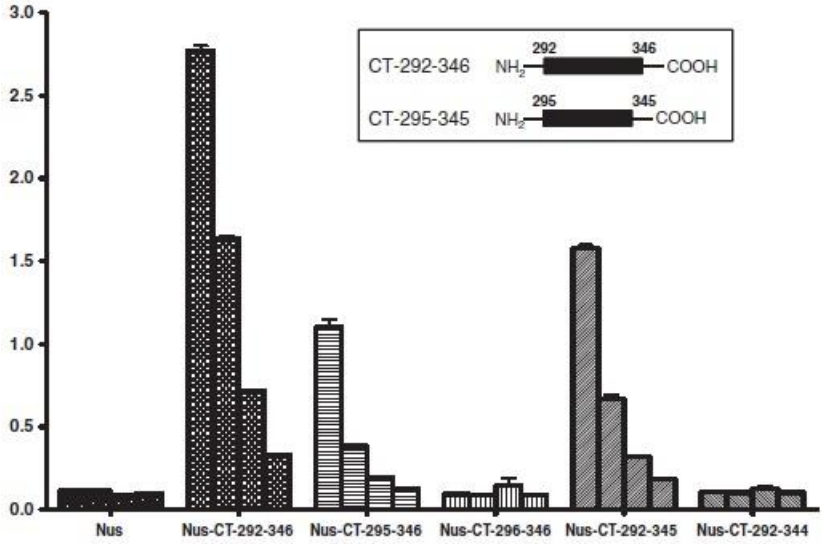

Figure 5: Determination of the epitope of D2C7 on the EGFRvIII extracellular domain (ECD).

Different concentrations (0.5, 0.25, 0.125, and 0.0625 mg) of Nus-Tag alone or Nus-Tag conjugated to EGFRvIII ECD deletion mutants (CT 292-346, CT 295-346, CT 296-346, CT 292-345, and CT 292-344) were immobilized on 96-well plates. The wells were blocked with superblock and incubated with D2C7 mAb followed by peroxidase conjugated anti-mouse IgG antibody. Following the addition of TMB substrate solution, and stop solution, the optical density was measured at 450 nm. The ELISA assay with different concentrations of Nus-Tag alone or Nus-Tag conjugated to EGFRvIII ECD deletion mutants was conducted in triplicate for each epitope. Results are presented as mean ± SD where n > 2. Inset represents the EGFRvIII ECD peptides essential for minimum (CT 295-345) and strong binding (CT 292-346) of D2C7 [48].

1.2.2 PDPN-targeted immunotoxin

Previous studies have shown that several anti-PDPN antibodies (NZ-1, D2-40, AB3 and 18H5) had already been developed and well characterized [49, 50]. A functional immunotherapeutic agent should be able to bind to the target tumor cells with high

affinity and be internalized. The radiolabeled NZ-1 mAb has been previously demonstrated to bind avidly by D397MG cells and be rapidly internalized by D2159MG xenograft cells [51]. Furthermore, the [^{131}I] SGMIB-NZ-1 mAb exhibited significant tumor accumulation in D2159MG tumor-bearing mice, which thereby established the potential utilization of NZ-1 as an immunotherapeutic agent against malignant brain tumors [51]. Based on the NZ-1 mAb, a novel IT, NZ-1-(scdsFv)-PE38KDEL (NZ-1-IT), was developed by fusing the scFv of the NZ-1 mAb with domains II and III of *Pseudomonas* exotoxin A (PE38KDEL) [52]. The antigen-binding kinetics of NZ-1-IT was then assessed by surface plasmon resonance, which showed that the K_D of NZ-1-IT on the PDPN-coated chips was 8.0×10^{-8} mol/L, indicating a robust binding affinity to the specific target [52].

1.3 Immune checkpoint inhibitors for the treatment of malignant brain tumors

1.3.1 Immune checkpoint system

It is known that genetic and epigenetic alterations of cancers can provide emerging antigens that can be recognized by the immune system to differentiate tumor cells from the normal tissue, in which T cells play a major role to therapeutically regulate endogenous anti-tumor immune responses. T cells can selectively recognize the peptides generated from proteins inside the cell, and can directly detect and destroy those cells

expressing specific antigens by $CD8^+$ T effector cells (cytotoxic T lymphocytes, CTLs). T cells can also regulate immune responses by $CD4^+$ T helper cells to coordinate innate and adaptive immunity [53]. The T-cell-mediated immune response is initiated from the primary antigen recognition by the T cell receptor (TCR), and then determined by a second signal that is harmonized by the delicate balance between co-stimulatory and co-inhibitory pathways (immune checkpoints) [54, 55] (**Figure 6**). These two signals are crucial to activate or inhibit the T-cell immune response. The primary signal is triggered once antigens are presented with the major histocompatibility complex (MHC) to the TCR, whereas the secondary signal, which can be co-stimulatory or co-inhibitory, decides the activation or inhibition of T cells [56]. Immune checkpoint molecules are critical to release the co-stimulatory or co-inhibitory secondary signal. Among them, CD28, CD40L, CD58, CD80, CD86, CD137, and OX40 can stimulate T cell activation, while cytotoxic T-lymphocyte-associated antigen 4 (CTLA4), Programmed cell death protein 1(PD1), lymphocyte activation gene 3 (LAG-3), and T-cell immunoglobulin and mucin domain-3 (TIM3) inhibit the immune activation [53, 56, 57].

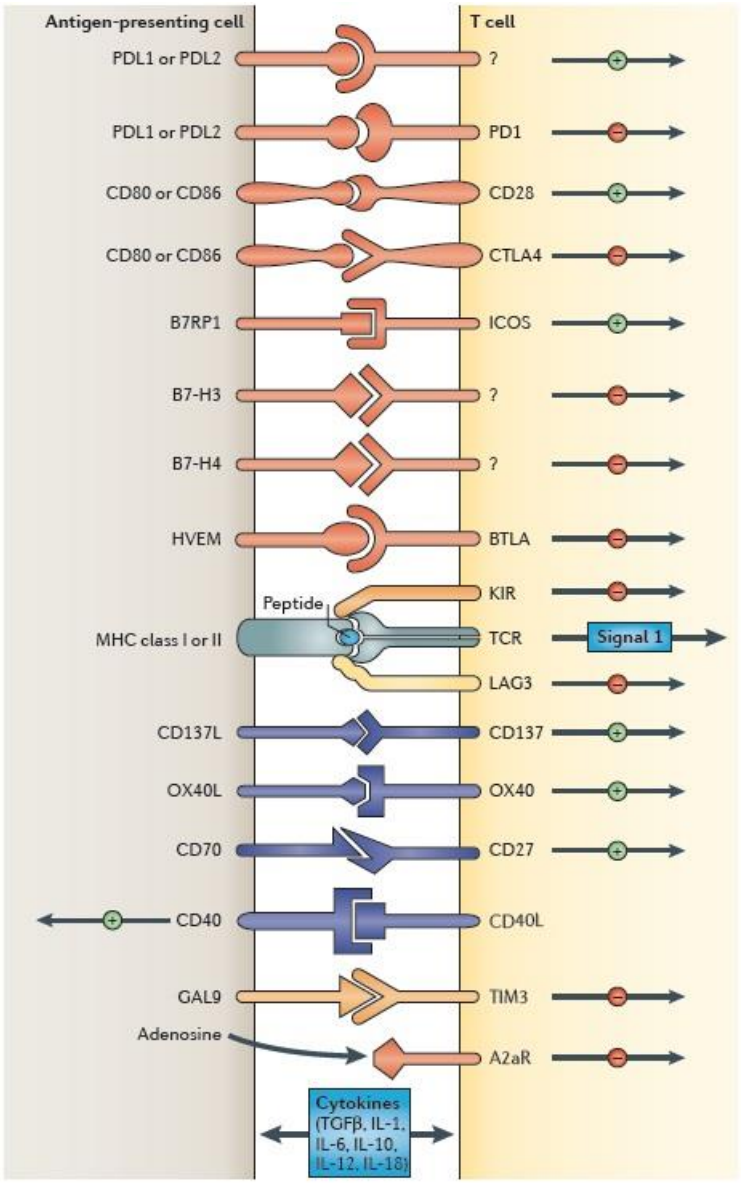

Figure 6: Multiple co-stimulatory and inhibitory interactions regulate T cell responses.

Depicted are various ligand–receptor interactions between T cells and antigen-presenting cells (APCs) that regulate the T cell's response to the antigen (which is mediated by peptide–MHC that are recognized by the TCR). These responses can occur at the initiation of T cell responses in lymph nodes (where the major APCs are dendritic

cells) or in peripheral tissues or tumors (where effector responses are regulated). From [53] with permission from publisher, see appendix for license.

In fact, immune checkpoints are crucial under normal conditions to maintain the self-tolerance to prevent autoimmunity, and also to prevent the damage of normal tissues during the immune response against pathogenic infection. However, many tumors can dysregulate the expression of immune checkpoint molecules to resist the anti-tumor immunity by inhibiting T cell activation, which can be potential targets for further anti-tumor therapies [58, 59].

1.3.2 Immune checkpoint inhibitors for anti-tumor therapies

Immune checkpoint inhibitors that specifically suppress co-inhibitory checkpoint pathways have achieved a great success in the treatment of several advanced tumors, for example, melanomas and non-small-cell lung cancers (NSCLCs). Among many immune checkpoint inhibitors, the inhibitor of CTLA4 is the first therapeutic agent that has displayed significant clinical profit [58, 60]. Ipilimumab, a fully humanized anti-CTLA4 mAb, was approved by the U.S. Food and Drug Administration (FDA) in 2011 to treat unresectable or metastatic melanomas. Ipilimumab has also shown a therapeutic effect for the melanoma brain metastases [61-64].

Another effective therapeutic method is to target the pathway involving PD1 and its ligands [58, 65]. Nivolumab and pembrolizumab are two anti-PD1 mAbs that block

the interaction between the PD1 protein and its ligands, programmed cell death protein ligand 1 (PDL1) and PDL2, to overcome the inactivation of CTLs mediated by PD1 pathway. Both anti-PD1 inhibitors were approved by the FDA in 2014 to treat unresectable or metastatic melanomas as well as disease progression after ipilimumab treatment [56, 58]. Furthermore, nivolumab was subsequently approved by the FDA as a new therapeutic approach for NSCLC in 2015. However, the function and mechanism of immune checkpoint pathways in brain tumors are not well known because all the current clinical data of these immune checkpoint inhibitors have originated from melanomas, NSCLC, and other tumor types (**Table 1**). Therefore, more preclinical and clinical studies need to be organized to investigate the anti-tumor mechanism and efficacy of immune checkpoint inhibitors in malignant brain tumor models and clinical trials.

Table 1: Examples of immune checkpoint inhibitors in development.

From [56] with permission from publisher, see appendix for license.

Agent	Target	Tumour type(s)	Highest phase trial	Indication in the highest-phase trial
Ipilimumab	CTLA4	Glioblastoma, NSCLC, SCLC, gastric cancer, melanoma, ovarian, pancreatic cancer, renal cancer, multiple myeloma, lymphomas	Marketed	Advanced melanoma
Tremelimumab	CTLA4	NSCLC, mesothelioma, squamous cell cancer of the head and neck, other solid tumours	III	Mesothelioma
Nivolumab	PD1	Colorectal cancer, glioblastoma, hepatocellular carcinoma, NSCLC, SCLC, squamous cell cancer of the head and neck, breast cancer, bladder cancer, gastric cancer, melanoma, ovarian cancer, pancreatic cancer, renal cancer, multiple myeloma, lymphomas	Marketed	Metastatic melanoma, non-small cell lung cancer
Pembrolizumab	PD1	NSCLC, glioblastoma, squamous cell cancer of the head and neck, pancreatic cancer, renal cell cancer, other advanced solid tumours, lymphoma	Marketed	Metastatic melanoma
Pidilizumab	PD1	Multiple myeloma, glioblastoma, lymphoma	III	Lymphoma
AMP224	PD1	Advanced solid tumours, colorectal cancer	I	Advanced solid tumours, colorectal cancer
AMP514/ MEDI0680	PD1	Advanced malignancies, aggressive B-cell lymphomas	II	Aggressive B-cell lymphomas
BMS936559	PDL1	Advanced solid tumours	I	Several
MEDI4736	PDL1	NSCLC, squamous cell cancer of the head and neck, glioblastoma, and other advanced solid tumours	III	Non-small cell lung cancer
MPDL3280A	PDL1	Bladder cancer, NSCLC, renal cell carcinoma, and other advanced solid tumours	III	Non-small cell lung cancer
MSB0010718C	PDL1	Advanced solid tumours	II	Merkel cell carcinoma
BMS986016	LAG-3	Advanced solid tumours, chronic lymphocytic leukaemia, Hodgkin lymphoma, non-Hodgkin lymphoma, multiple myeloma	I	Advanced solid tumours, chronic lymphocytic leukaemia, Hodgkin lymphoma, non-Hodgkin lymphoma, multiple myeloma
IMP321	LAG-3	Advanced pancreatic cancer, metastatic breast cancer, metastatic kidney cancer, metastatic melanoma	I/II	Melanoma
Lirilumab	KIR	Advanced solid tumours, multiple myeloma, Hodgkin lymphoma, non-Hodgkin lymphoma, acute myeloid leukaemia	II	Acute myeloid leukaemia
IPH2101	KIR	Squamous cell cancer of the head and neck, multiple myeloma	II	Multiple myeloma
1-7F9	KIR	Multiple myeloma, acute myeloid leukemia	II	Multiple myeloma
KW-6002	A2aR	Preclinical	Preclinical	Not applicable

Abbreviations: A2aR, adenosine A2a receptor; CTLA4, cytotoxic T-lymphocyte associated protein 4; KIR, killer-cell immunoglobulin-like receptors; LAG-3, lymphocyte activation gene 3; NSCLC, non-SCLC; PD1, programmed cell death protein 1; PDL1, programmed cell death 1 ligand 1; SCLC, small-cell lung cancer.

1.4 Convection-enhanced delivery of the tumor-targeted immunotoxin

Current glioblastoma therapeutics are limited because they are rarely able to efficiently overcome the restrictive nature of the blood-brain barrier (BBB). The non-targeted intrathecal or systemic administration can result in systemic toxicity to surrounding normal tissues and suboptimal dosage to the tumor, especially for large soluble molecules such as antibodies or ITs [66]. In 1994, Bobo et al. reported that the convection-enhanced delivery (CED) of macromolecules could enhance the administration and distribution of large molecules into the brain, and achieve greater magnitudes of their concentration levels [67]. CED continues to be a novel technique that bypasses the BBB but takes advantage of its restrictive nature to prevent the drug leakage from the brain, therefore allowing targeted localized delivery and significantly increasing the therapeutic dosage that can be administered into the brain tumor [68, 69]. In the clinic, co-infusion of gadolinium-diethylene triamine pentaacetic acid (Gd-DTPA, a small-molecule contrast agent) and ^{124}I-labeled human serum albumin (^{124}I-HSA) has enabled the use of magnetic resonance imaging (MRI) and positron emission tomography (PET) scanning to accurately trace the intracerebral distribution of an infused IT administered by the CED (**Figure 7**) [70]. Co-infusion of Gd-DTPA and ^{124}I-HSA has been demonstrated to be a safe and minimally invasive technique for patients [70].

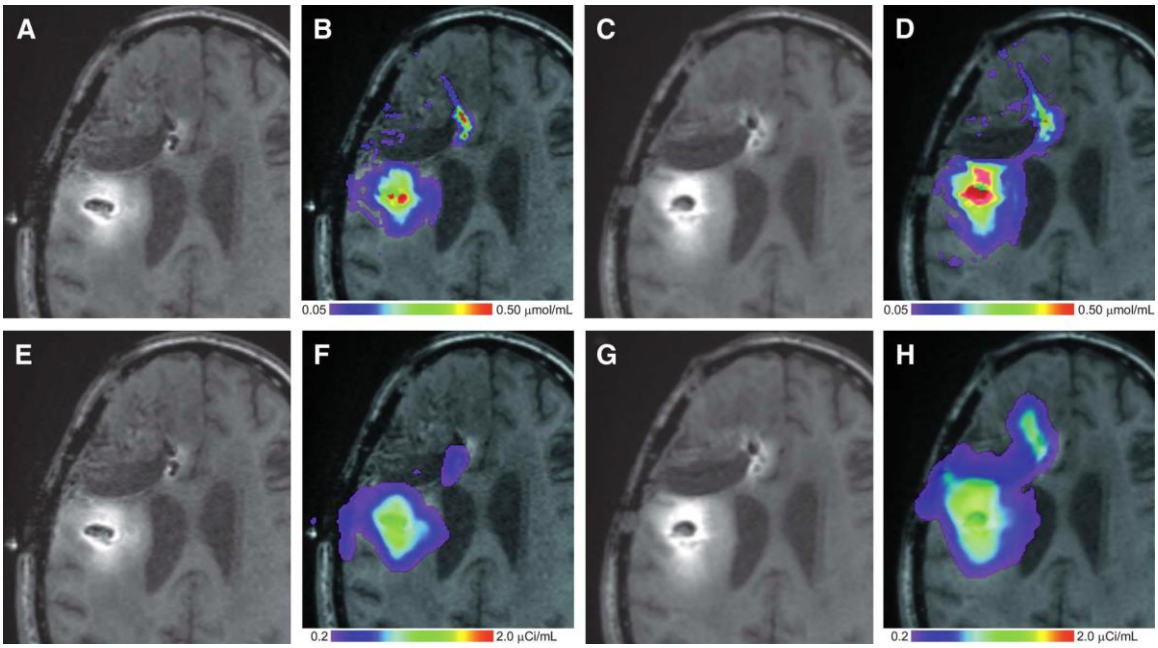

Figure 7: A-D, T1-weighted MRI signal (A and C) compared with measured Gd-DTPA concentration profile (B and D). E-H, T1-weighted MRI signal (E and G) with overlaid ^{124}I-HSA concentration (F and H).

(A) T1-weighted signal at 24 hours. (B) Gd concentration at 24 hours. (C) T1-weighted signal at 72 hours. (D) Gd concentration at 72 hours. (E) T1-weighted signal at 24 hours. (F) ^{124}I-HSA activity at 24 hours. (G) T1 weighted signal at 72 hours. (H) ^{124}I-HSA activity at 72 hours. From [70] with permission from publisher, see appendix for license.

Since intracerebral CED for IT administration has been well established and has shown promising benefits [52, 71-73], the intracerebral administration of ITs was then performed in many orthotopic glioma rodent models via CED, in which an osmotic pump was used to deliver the ITs directly into the brain tumor site (**Figure 8**) [48, 74, 75].

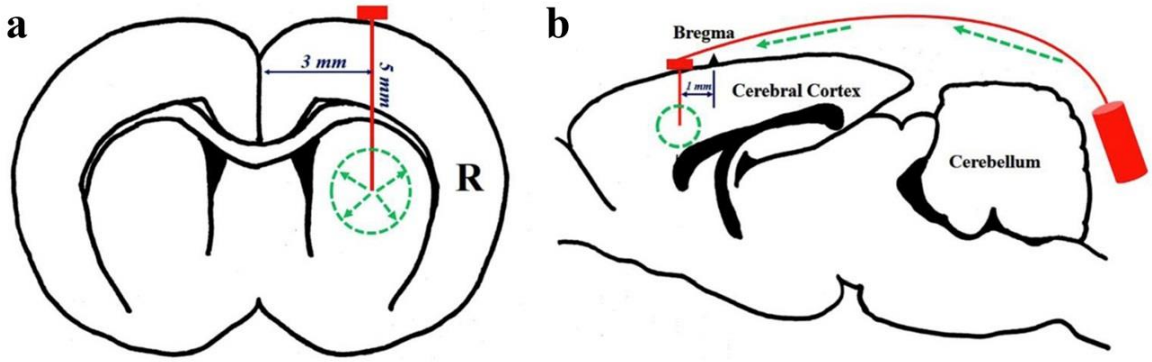

Figure 8: Intracerebral CED in the rat model.

(a) The coordinates of the cannula in the rat brain (the coronary view). (b) The diagram of the CED pump system used in the intracerebral infusion (the sagittal view). From [76] with permission from publisher, see appendix for license.

1.5 Preclinical toxicity study in rats under Good Laboratory Practice regulations

According to our discussion with the FDA, and based on the sequence similarity between human and rat EGFR proteins (90% amino acid identity), Sprague-Dawley (SD) rats were chosen as an appropriate animal model for the preclinical toxicity evaluation of D2C7-IT. A preclinical study was performed under Good Laboratory Practice (GLP) regulations to evaluate the systemic toxicity of D2C7-IT administered via intracerebral CED using an osmotic pump in rats to support an initial US FDA Investigational New Drug (IND) application for a Phase I/II clinical trial in patients with glioblastoma. In patients, the distribution of ITs by intracerebral CED can be monitored by co-infusion with a low-molecular-weight tracer, Gd-DTPA, and ^{124}I-HSA. Thus, the IT was co-

infused with Gd-DTPA and ^{124}I-HSA in the rat GLP study with the aim of replicating this formulation in the future D2C7-IT clinical trial.

1.6 Introduction to the thesis chapters

Based on the novel and robust immunotoxins developed in our laboratory, and considering the findings in previous melanoma studies and immunotoxin clinical trials, it is probable that tumor-targeted immunotoxin therapy can not only specifically target and destroy tumor cells in the CNS, but can also stimulate a secondary immune response that may eliminate remaining and recurrent tumor cells. While chapter two focuses on the materials and methods of the various experiments performed, chapters 3.1, 3.2, and 3.3 will address the following issues to demonstrate the therapeutic mechanisms involved:

Chapter 3.1: To determine the direct therapeutic efficacy of ITs in orthotopic immunocompromised mouse glioma models, I established orthotopic mouse glioma models using human xenograft glioblastoma and medulloblastoma cells, and modified murine fibroblast cells in immunocompromised mice. I utilized the intracerebral CED to administer ITs to treat the tumor-bearing mice, which mimics what is applied in the clinic to treat patients.

Chapter 3.2: To evaluate the preclinical toxicity of D2C7-IT in an intracerebral rat model, I utilized the same CED method to administer D2C7-IT intracerebrally in normal

SD rats for toxicity evaluation. The toxicity of intracranial D2C7-IT infusion was evaluated by clinical observations, body weight changes, behavioral tests, clinical laboratory tests, gross pathology, and histopathology. The maximum tolerated dose (MTD) and no-observed-adverse-effect level (NOAEL) were established for future clinical use.

Chapter 3.3: To investigate the secondary anti-tumor immune response induced by the D2C7-IT therapy in immunocompetent mouse glioma models, I first validated the anti-tumor efficacy of D2C7-IT. Then, distal tumor rechallenging was performed to confirm the secondary immune response. Moreover, immune checkpoint inhibitors were combined with D2C7-IT to augment anti-tumor response to distal tumors.

Finally, in chapter four, I elaborate on the significance of my studies and discuss future endeavors.

2. Materials and Methods

2.1 Cell lines and dissociation of xenografts

The medulloblastoma cell line DAOY (ATCC No. HTB-186) was cultured in complete zinc option (ZO)–10% fetal bovine serum (FBS) [Improved Modified Eagle Medium ZO (Richter's Modification, Cat. No. 10373-017) liquid; Invitrogen, San Diego, CA] and passed at confluence with 0.05% Trypsin–Ethylenediaminetetraacetic acid (EDTA) (Invitrogen). The other cell lines used were, the human epidermoid-carcinoma cell line, A43l (expressing EGFRwt), the murine Swiss 3T3 fibroblast cell line NR6 transfected with human EGFRwt (NR6W) [21], and human EGFRvIII (NR6M) [21]. The parental murine Swiss 3T3 fibroblast cell line, NR6 (kindly provided by Dr. Harvey Herschman, University of California, Los Angeles, CA), which lacks expression of murine or human EGFRwt and EGFRvIII, was used as control. All cell lines were cultured in complete 10% FBS-ZO medium and passed at confluence with 0.05% trypsin-EDTA. Mouse glioma cell lines SMA560-mD2C7, CT2A-mD2C7, and their parental cell lines SMA560 and CT2A were cultured in ZO and DMEM with high glucose and pyruvate (Cat. No. 11995, Invitrogen)-10% FBS, respectively, and passed at confluence with non-enzymatic cell dissociation solution (Corning).All cell lines were authenticated by periodic morphologic assessment and by testing for mycoplasma infection.

Human-biopsy-derived xenograft tissue from glioblastomas and malignant gliomas samples D270MG (expressing EGFRwt and EGFRvIII), D2159MG (expressing

EGFRwt and EGFRvIII), 43 (expressing EGFRwt; kindly provided by Dr. C. David James, University of California, San Francisco, CA), D08-0493MG (expressing EGFRwt), D08-0308MG, D08-0695MG and D08-0537MG, and medulloblastoma lines, D283MED and D425MED, obtained under sterile conditions from Duke animal facility, were prepared for cell culture in a laminar flow hood with a sterile technique. Tumor material was finely minced and digested with 100 μg liberase (Roche, Indianapolis, IN). This mixture was stirred at 37°C for 10 min, and a cell-rich supernatant was obtained. The cells were washed with complete ZO medium, further treated with Ficoll-Hypaque (GE Healthcare) to remove any red blood cells and then washed once in ZO medium.

2.2 Flow cytometry analysis

2.2.1 Indirect fluorescence-activated cell sorting (FACS)

Indirect FACS analysis was carried out with the D2C7-IT and NZ-1-IT immunotoxin. Briefly, 1×10^6 cells were suspended in 500 μl of phosphate-buffered saline (PBS) pH 7.4 (Invitrogen) containing 5% FBS (5% FBS-PBS; Invitrogen). The D2C7-IT or NZ-1-IT or negative control, P588-(scdsFv)-PE38KDEL (P588-IT), was added to the cells at a concentration of 10 μg/mL, and the samples were incubated for 40 minutes at 4°C. After washing, cells were incubated with rabbit anti-*Pseudomonas* exotoxin A antibody (Sigma) followed by goat anti-rabbit-IgG-FITC antibody (Zymed). Stained cells were washed with 1 × PBS and analyzed on a Becton Dickinson FACSort instrument equipped with Cell-Quest software (BD Biosciences).

2.2.2 Direct FACS

Direct FACS analysis was carried out with AF488-labeled (Pierce) D2C7 mAb (D2C7-AF488), anti-Mouse MHC Class I (H-2K^b) mAb-PE (eBioScience), anti-Mouse MHC Class I (H-2D^b) mAb-PE (eBioScience), and anti-mouse PDL1 mAb-APC (BioLegend). P588-AF488, mouse IgG2a-PE κ isotype control (BD Pharmingin), and rat IgG2b-APC κ isotype control (BioLegend) were used as negative controls. 1×10^6 cells were suspended in 500 μl of 5% FBS-PBS. The fluorescence-labeled antibodies were added to the cells at a concentration recommended by the manufacturer, and the samples were incubated for 1 hour on ice. Stained cells were then washed with 1 × PBS and analyzed on a Becton Dickinson FACSort instrument equipped with Cell-Quest software.

2.3 In vitro cytotoxicity assay

2.3.1 Protein synthesis inhibition assay

The cytotoxicity of immunotoxins on cultured cell lines and cells freshly isolated from malignant brain tumor xenografts was first assayed by inhibition of protein synthesis. P588-IT was used as negative control immunotoxin. Cells were seeded in 96-well plates at a density of 2×10^4 cells per well in 200 μl of complete ZO medium 24 hours before the assay. Immunotoxins were serially diluted to achieve a final concentration of 0.01–1,000 ng/ml in PBS containing 0.2% bovine serum albumin (BSA; 0.2% BSA-PBS), and 10 μl of diluted immunotoxin was added to each well. Plates were

incubated for 20 hours at 37°C and then pulsed with 1 μCi per well of L-[4,5-^{3}H]leucine (PerkinElmer) in 25 μl of 0.2% BSA-PBS for 3 hours at 37°C. Radiolabeled cells were captured on filter-mats and counted in a MicroBeta scintillation counter (PerkinElmer). The cytotoxic activity of immunotoxins was defined by 50% inhibitory concentration (IC_{50}), which was the immunotoxin concentration that inhibited radioactivity incorporation by 50% when compared to the radioactivity measured in untreated cells. All the assays were performed in triplicate for each cell line. Results are presented as mean ± standard deviation (SD) where $n \geq 3$.

2.3.2 WST-1 cell proliferation assay

The cytotoxicity of immunotoxins on cultured cell lines and cells freshly isolated from malignant brain tumor xenografts was also assayed by WST-1 cell proliferation assay. Cells were seeded in 96-well plates at a density of 10^4 cells per well in 100 μl of complete ZO medium or DMEM over night before the assay. Immunotoxins were serially diluted to achieve a final concentration of 0.01–1,000 ng/ml in PBS containing 0.2% bovine serum albumin or human serum albumin (BSA/HSA; 0.2% BSA/HSA-PBS), and 10 μl of diluted immunotoxin was added to each well. Plates were incubated for 48 hours at 37°C and then added 10 μl WST-1 reagent (Roche) for 0.5-4 hours at 37°C. Measure the absorbance of each well against a background control as blank using a microplate reader (TECAN) at 420-480 nm wavelength. The reference wavelength was 650 nm. The cytotoxic activity of immunotoxins was defined by IC_{50}, which was the

immunotoxin concentration that inhibited cell proliferation by 50% when compared to that of untreated cells. All the assays were performed in triplicate for each cell line. Results are presented as mean ± SD where n ≥ 3.

2.4 Animal care

2.4.1 Mouse study

Male immunocompromised NOD SCID gamma (NSG) mice (20–30 g; 8-12 weeks old) were received from the Division of Laboratory Animal Resources (DLAR) at Duke University Medical Center (DUMC). Female immunocompetent C57BL/6 mice (around 20 g; 7-8 weeks old) were received from Charles River Laboratories, Inc. (Portage, MI, USA). Immunocompetent VM/Dk mice (around 20-30g; 6-12 weeks old) were bred in the Cancer Center Isolation Facility (CCIF) at DUMC under the animal protocol. Upon arrival, the mice were visually inspected for general health and acceptability for use in this study, and the numbers of mice and sex were verified. Each mouse then received a unique identification number following randomization into the different groups before the treatment. The animal study protocol was approved by the Institutional Animal Care and Use Committee (IACUC) at DUMC.

2.4.2 Rat study

Equal numbers of adult male and female Sprague–Dawley (SD) rats were selected for use in this study, and all rats were received from Charles River Laboratories, Inc. Upon arrival, the rats were visually inspected for general health and acceptability

for use in this study, and the numbers of rats and sex were verified. Each rat received a unique identification number following randomization into the different groups. The rats were approximately 13 to 17 weeks of age at the initiation of the study. At the beginning of treatment, the body weights of the rats were 360–460 g for the males and 210–290 g for the females. The animal housing and care, study protocol, and standard operating procedures (SOPs) were approved by the IACUC and DLAR at DUMC.

2.5 In vivo intracranial tumor model and CED in mice

2.5.1 Intracranial human cell line and xenograft glioma model and CED in immunocompromised mice

Male NSG mice were anesthetized by an intraperitoneal injection of a solution of ketamine 50 mg/kg (Fort Dodge Animal Health) and xylazine 10 mg/kg (Akorn, Inc). The anterior cranial region was shaved under sterile conditions and an incision approximately 1 cm in length was made in the skin over the skull, and a small burr hole was drilled at coordinates 2.5 mm left lateral of the sagittal and 1 mm anterior to the bregma. A 25-gauge 10-μL Hamilton needle was inserted vertically to a depth of 2.5 mm from the dura mater. For D2C7-IT study, all mice were implanted with 10^5 43 or D270MG xenograft cells in 3 μL of 1 × PBS or NR6M cells in 3 μL of BD PuraMatrix peptide hydrogel (BD Biosciences) into the cortex. Six (43 xenograft), 5 (NR6M), or 11 (D270MG) days after tumor implantation, animals were randomized into 4 groups (sham n = 4/5, others n = 8–10), Sham (no pump), 0.2% HSA-PBS, P588-IT, and D2C7-IT. One microgram of D2C7-IT or P588-IT diluted in 100 μL of 0.2% HSA-PBS was delivered

via Alzet osmotic mini pumps (Durect Corporation) over a 3-day (43 xenograft) or 7-day (NR6M and D270MG) period. For NZ-1-IT study, all mice were implanted with 10^5 D425MED cells in 5 μL of 1 × PBS into the cortex. Four days post-tumor implantation, a 3-day Alzet mini pump (Durect Corporation, Cupertino, CA) containing 0.3 μg of the P588-IT or NZ-1-IT diluted in 100 μl of 0.2% HSA-PBS was implanted subcutaneously on the back of the anesthetized mice slightly posterior to the scapulas. The pump was connected to the cannula (Durect Corporation) through a catheter passing through a tunnel created under the skin of mice, and the IT was infused through the cannula into the tumor site over a 3-day period. The control animals were handled in the same manner, but were either left untreated (sham) or treated with 0.2% HSA-PBS alone. The mice were followed to assess tumor development and death. The response of intracranial xenografts to treatment was assessed by percentage increase in time to a specific neurologic endpoint (seizure-like activity, repetitive circling, or other subtle changes such as grooming or decrease in appetite), body weight loss, or to death. Animals were observed for signs of distress or development of neurologic symptoms, at which time, the mice were euthanized according to the animal protocol. Wilcoxon rank order test and log-rank test were used to compare survival curves.

2.5.2 Intracranial syngeneic mouse glioma model in immunocompetent mice

C57BL/6 mice (female) or VM/Dk mice (either gender) were anesthetized by isoflurane (Henry Schein Animal Health, Dublin, OH, USA). The anterior cranial region

was shaved under sterile conditions and an incision approximately 1 cm in length was made in the skin over the skull, and a small burr hole was drilled at coordinates 2.5 mm right lateral of the sagittal and 1 mm anterior to the bregma. A 25-gauge 10-μL Hamilton needle was inserted vertically to a depth of 2.5 mm from the dura mater. Mice were implanted with 3×10^5 CT2A-mD2C7 or 10^5 SMA560-mD2C7 cells in 3 μL injection methocellulose media (Sigma) into the cortex. The mice were followed to assess tumor development and death. The response of intracranial xenografts to treatment was assessed by percentage increase in time to a specific neurologic endpoint (seizure-like activity, repetitive circling, or other subtle changes such as grooming or decrease in appetite), body weight loss, or to death. Animals were observed for signs of distress or development of neurologic symptoms, at which time, the mice were euthanized according to the animal protocol. Wilcoxon rank order test and log-rank test were used to compare survival curves.

2.6 In vivo subcutaneous tumor model in mice

Female immunocompetent C57BL/6 mice (around 20 g; 7-8 weeks old) were anesthetized by isoflurane inhalation and shaved. 3×10^6 CT2A-mD2C7 mouse glioma cells in 100 μL 1 × PBS were subcutaneously (SC) implanted in the right flank of C57BL/6 mice for the single-side SC tumor model. For the bilateral tumor model, 3×10^6 CT2A-mD2C7 mouse glioma cells in 100 μL 1 × PBS were subcutaneously implanted in the right flank of C57BL/6 mice, whereas 10^6 CT2A-mD2C7 mouse glioma cells in 100 μL 1 ×

PBS were subcutaneously implanted in the left flank at the same time. When the right implanted tumors reached approximately 100 mm^3, ten mice per arm were randomly selected for treatment. The test mice were treated by intratumoral (i.t.) injection every 2 or 3 days with a total of 4 doses of D2C7-IT or P588-IT [1.5 or 4.5 μg in 100 μL PBS with 0.1% mouse serum albumin (MSA) per mouse per dose] combined with or without intraperitoneal (i.p.) injection of immune checkpoint inhibitors such as anti-PD1 mAb (clone RMP1-14, BioXcell, 250 μg in 100 μL PBS per mouse per dose) or anti-CTLA4 mAb (clone 9H10, BioXcell, 100 μg in 100 μL PBS per mouse per dose). Tumors were measured twice weekly with a handheld vernier caliper, and the tumor volumes were calculated in cubic millimeters by using the formula: ([length] × [$width^2$])/2. When tumor volume met both of the following criteria: (i) >1,000 mm^3 and (ii) five times its original treatment size, animals were tested out of the study. Nonparametric Wilcoxon each pair multiple comparison method was used to analyze the data.

2.7 Immunohistochemistry of frozen brain tumor tissue

Eleven days post D270MG tumor implantation, animals (n=4) were treated with 1 μg of D2C7-IT delivered via Alzet osmotic mini pumps (Durect Corporation) over a seven-day period. After treatment, pumps were removed and frozen brain tumor tissues were obtained from all the euthanized animals. Brain tumor tissues were also obtained from the D270MG-sham group. A Ventana Discovery XT Automated System (Ventana Medical Systems, Tucson, AZ) with DAB Map kit was used to test the frozen tissue

applying an optimized protocol. Briefly, frozen tissue sections from the D270MG-sham group (negative control) and the D270MG-D2C7-IT group (test) were thawed at room temperature (RT) for 20 minutes and then loaded onto the system. Mouse-anti-PE38KDEL antibodies (generated by Dr. Ira Pastan) at a final concentration of 1 μg/ml in antibody diluent (Ventana) were incubated at RT for 20 min. Monoclonal antibodies were visualized by addition of anti-mouse-IgG(H+L)-horseradish peroxidase conjugate (Invitrogen) (1:200 dilution) at RT for 20 min. Treated slides were incubated with DAB substrate (Ventana), dehydrated in 95%(v/v) ethanol followed by 100%(v/v) ethanol and, finally, 100% (v/v) xylene. Sections were mounted with coverslips for observation. Tumor sections from the D270MG-D2C7-IT group, pre-stained with D2C7-IT, were run as the positive control.

2.8 Preclinical toxicity of D2C7-IT via intracerebral CED in SD rats

2.8.1 Test/control article preparation and quality control

A stock formulation of D2C7-IT was diluted in a control formulation, which consisted of phosphate buffer, saline, HSA (USP; Grifols, Clayton, NC, USA) or rat serum albumin (RSA) (catalog # RTSA62-1256; Equitech-Bio, Inc., Kerrville, TX, USA), 1 mM gadolinium [Gd-DTPA; Magnevist (gadopentetate dimeglumine); Bayer Health Care, Whippany NJ, USA], and 2 μCi ^{124}I-labeled (IBA Molecular, Dulles, VA, USA) HSA (Talecris Biotherapeutics, Research Triangle Park, NC, USA) [^{124}I-HSA, labeled in house and evaluated by size exclusion high performance liquid chromatography (HPLC)], on

each day of use to yield formulations containing D2C7-IT at different concentrations. Before the initiation of the study, biochemical analysis was performed to ensure the strength, purity, and identity of the active ingredients in the test article formulation. Aliquots were immediately collected for each group after formulation and tested for the potency measurement, sterility, and endotoxin level. As for the potency measurement, formulated D2C7-IT samples for each set were either transferred to 15-ml sterile tubes (the bulk test article) or used to fill the osmotic pumps (the pump test article). The filled osmotic pumps were then placed into sterile 50-ml tubes containing sterile saline, which covered the pumps. The bulk test article and pump test article were incubated at 37 °C for the subsequent measurements of the inhibition (the half maximal inhibitory concentration, IC_{50}) of A431P (EGFRwt expressing) and/or NR6M (EGFRvIII expressing) cell proliferation. A cytotoxicity assay was performed following the CellTiter-Fluor Cell Viability Assay protocol (Promega, Madison, WI, USA). The cytotoxic activities of the pump samples were compared to those of the bulk samples that were used as reference standard controls in this assay. In addition, trypticase soy broth (BD, Sparks, MD, USA) and fluid thioglycollate medium (BD, Sparks, MD, USA) were utilized to test the sterility of each formulation sample, whereas the limulus amebocyte lysate (LAL) test (Endosafe®; Charles River, Charleston, SC, USA) was used to determine the endotoxin level of the formulation samples.

2.8.2 Intracerebral CED by osmotic pump in rats

An osmotic pump (Alzet Osmotic Pumps 2ML1 or 2001; Durect Corporation, Cupertino, CA) was connected to a brain infusion cannula (Alzet Brain Infusion Kit 2; Durect Corporation, Cupertino, CA) to form a pump assembly. The control or test article formulations were prepared fresh each day, loaded into the pump assembly, maintained at 37 °C overnight to facilitate pump priming, and implanted into each rat for intracerebral infusion over approximately 72 hours. The implantation procedure for the osmotic pump assembly was as follows: anesthesia was induced and maintained with isoflurane (Henry Schein Animal Health, Dublin, OH, USA); the hair over the surgical site was clipped, cleaned with alcohol (70 % isopropyl alcohol; Priority Care, Inc., Elgin, IL, USA) and scrubbed with Avagard (Avagard Surgical and Health Care; 3 M, St. Paul, MN, USA); while anesthetized, the animals were placed into a stereotaxic frame; the intracerebral cannula was placed 1 mm anterior to the bregma, 3 mm to the right of the cranium midline, and 5 mm into the caudate nucleus (**Figure. 8**), which was held in place using cyanoacrylate adhesive (3M Vetbond Tissue Adhesive; 3M Animal Care Products, St. Paul, MN, USA); the primed pump was implanted subcutaneously into the mid-scapular region of each animal; and the incision was closed with sterile wound clips (MikRon Precision Inc., Gardena, GA, USA). The beginning of the infusion period was designated as the time when the cannula/pump assembly was placed into the brain. The

infusion pump was removed from each animal approximately 72 hours after the start of the infusion, and the cannula was left in the brain.

2.8.3 One-month toxicity study of SD rats

Two cohorts of SD rats were evaluated for systemic toxicity (acute cohort: necropsy on study day 5, and chronic cohort: necropsy on study day 34). Each cohort consisted of four groups (control, low, medium, and high dose of D2C7-IT) consisting of five male rats and five female rats per dose group. All animals were observed upon receipt into the facility, and daily observations of each animal were performed and recorded throughout the study for moribundity, mortality, and general well-being. In addition, the animals were thoroughly examined for pharmacotoxic signs, pain, or gross abnormalities on the day before pump implantation and then once weekly throughout the study until the surviving animals were humanely euthanized. The rats in both cohorts (acute and chronic) were weighed on study day 1 (before implantation), study day 5, weekly thereafter (for surviving animals in the chronic cohort), and before euthanasia. Blood was collected from each rat for the clinical laboratory tests, including hematology, serum chemistry, and blood cell morphology (ANTECH Diagnostics, Morrisville, NC, USA) before euthanasia on days 5 or 34, or before unscheduled euthanization of moribund rats. On the scheduled study termination dates and following the unscheduled euthanization of moribund rats, the animals were euthanized for complete necropsy. The animals found dead were necropsied upon discovery. At

necropsy, major organ systems and tissues were collected, weighed, and then examined for gross lesions as well as for histopathologic changes.

2.8.4 Functional observational battery (FOB)

The FOB parameters were measured within one week before randomization into the study groups and for the surviving animals on study days 4, 15, and 31 (days 15 and 31 for the rats scheduled for necropsy on day 34 only) at the Mouse Behavioral and Neuroendocrine Analysis Core Facility at DUMC, led by Drs. William Wetsel and Ramona Rodriguiz. The FOB was designed and validated for sensitive determination of neurobehavioral toxicity [77]. The FOB components included observations of home cage behaviors [convulsions (tonic and clonic) and vocalizations], and reactivity of the animals to handling by the investigator (ratings of the ease of removal of animals from cages (including aggressiveness), coordination of the rat during handling, lacrimation, piloerection, and salivation). Open field activity measurements included the distance moved during testing and the time spent in mobility. Assessment of gait was performed in Clever Sys Free Walk automated test arenas with behavioral recognition software (Clever Sys Inc., Reston, VA, USA). Stimulus reactivity measurements to an auditory "click" and the core body temperature were also assessed. Behavioral data were analyzed by repeated measures ANOVA (RMANOVA) and chi-square analysis (χ^2) using IBM SPSS 21 statistical software (IBM, Chicago, IL, USA). In all cases, $P < 0.05$ was considered to be statistically significant.

2.9 Statistical analysis

GraphPad Prism 6.0 (GraphPad Software, Inc., CA, USA) and JMP Pro 12 (SAS Institute, Inc., NC, USA) were utilized for the statistical analysis. $P < 0.05$ was considered to be statistically significant.

3. Results

3.1 The direct therapeutic efficacy of ITs in orthotopic immunocompromised mouse glioma models.

3.1.1 Introduction

Because of the high prevalence of EGFRvIII mutation in tumors that have *EGFRwt* amplification [10], it would be advantageous to have antibodies that could target both antigens for glioblastoma therapy. Co-targeting these two antigens could promote greater killing of tumor cells than that which is achieved by antibodies specific for a single antigen. Cetuximab, an unarmed EGFRwt- and EGFRvIII-reactive antibody, has shown limited activity (progression free survival of <6 months) in a phase II trial in recurrent, high-grade glioma in patients with *EGFRwt* amplification [78]. Our study focuses on D2C7, a novel mAb that reacts with both EGFRwt and EGFRvIII proteins. D2C7 mAb showed a significantly higher tumor localization in tumors expressing EGFRwt or EGFRvIII proteins [47]. Made from D2C7 mAb, D2C7-IT is reactive with a 55-amino acid (AA) region present in the extracellular domain of both EGFRwt (583-637 AAs) and EGFRvIII (292-346 AAs) proteins.

Among the CNS tumors, PDPN expression is observed in 83% and 27% of glioblastoma and medulloblastoma cases [28], respectively, making it another attractive target for brain tumor therapy. Several anti-PDPN antibodies (NZ-1, D2-40, AB3 and 18H5) have been developed and well characterized [49, 50]. The radiolabeled NZ-1 mAb has been previously demonstrated to bind avidly by D397MG cells and rapidly

internalized by D2159MG xenograft cells. Further, the [^{131}I]SGMIB-NZ-1 mAb exhibited significant tumor accumulation in D2159MG tumor-bearing mice, which thereby established the potential utility of NZ-1 as an immunotherapeutic agent against malignant brain tumors [51]. NZ-1-IT was developed from NZ-1 mAb, which robustly reacts with PDPN on the tumor cell surface.

Since both D2C7-IT and NZ-1-IT showed great binding affinity in surface plasmon resonance analysis, we then examined their anti-tumor efficacy for malignant brain tumors *in vitro* and *in vivo* at the preclinical level, in order to establish both ITs as potential promising candidates for the future therapies of malignant brain tumors. In this work, flow cytometry analysis was first used to determine their specific binding capacity to epitope-expressing tumor cells. *In vitro* cytotoxicity assay was utilized to examine their specific tumor killing ability and stability over the time. In addition, orthotopic brain tumor models were established in immunocompromised NSG mice to test the preclinical anti-tumor efficacy of both ITs in several brain tumor cell lines.

3.1.2 Results

3.1.2.1 Antigen-binding specificity of D2C7-IT to epitope-expressing cells

To determine whether the D2C7-IT binds to native EGFRwt and EGFRvIII proteins expressed on the cell surface, indirect flow cytometric analysis was conducted (**Figure 9**). FACS analysis revealed that D2C7-IT bound to both the EGFRwt-expressing NR6W cells (**Figure 9B**) and the EGFRvIII-expressing NR6M cells (**Figure 9C**). The

parental NR6 cells (**Figure 9A**) and the non-specific immunotoxin P588-IT were used as negative controls, which confirmed the binding specificity of D2C7-IT. These results show that D2C7-IT can bind to not only purified EGFRwt and EGFRvIII proteins on a chip, but also to native protein molecules expressed on live transfected cells.

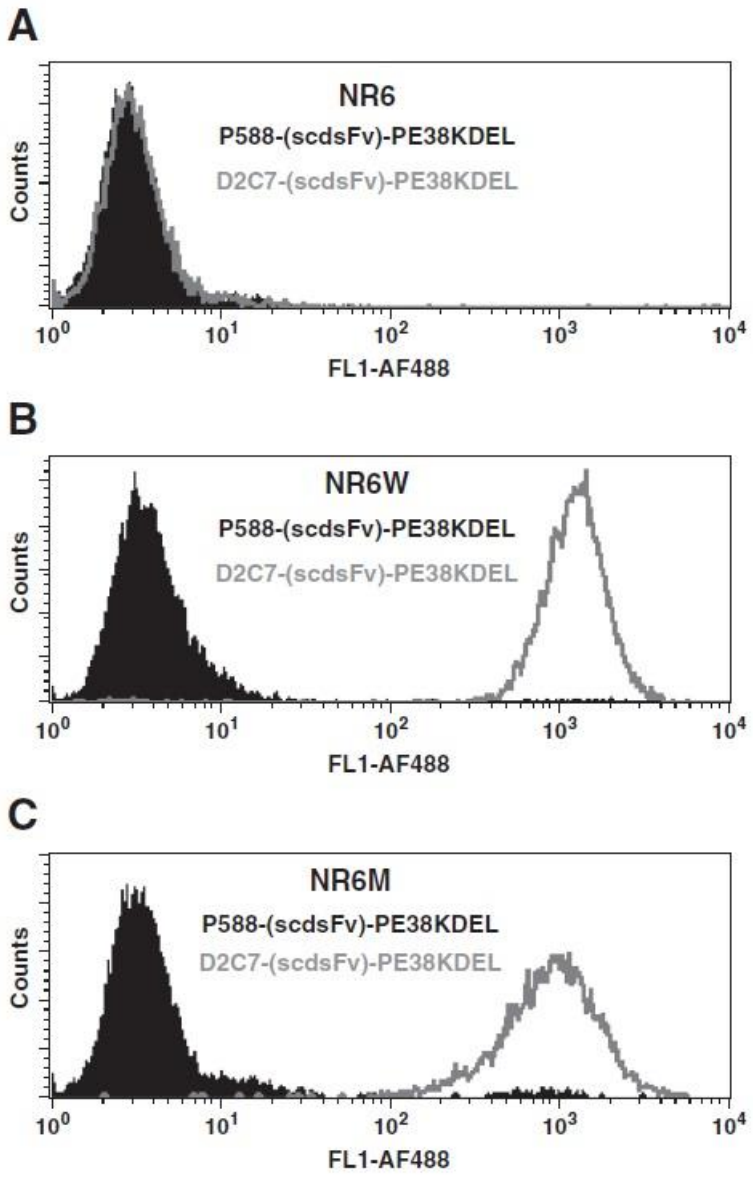

Figure 9: Flow cytometric analysis of D2C7-IT to determine its reactivity.

(A) Parental NR6 cells were used as control. Indirect FACS analysis shows the reactivity of D2C7-IT with cells expressing EGFRwt (NR6W) (B) or EGFRvIII (NR6M) (C). Cells were stained with D2C7-IT (gray open peaks) or a non-specific P588-IT control (filled black peaks).

3.1.2.2 Antigen-binding specificity of NZ-1-IT to epitope-expressing cells

To determine whether the NZ-1-IT binds to PDPN expressed on the cell surface, indirect flow cytometric analysis was performed (**Figure 10**). FACS analysis revealed significant NZ-1-IT binding to both glioblastomas (D2159MG, D08-0308MG and D08-0493MG) and medulloblastomas (D283MED, D425MED and DAOY).

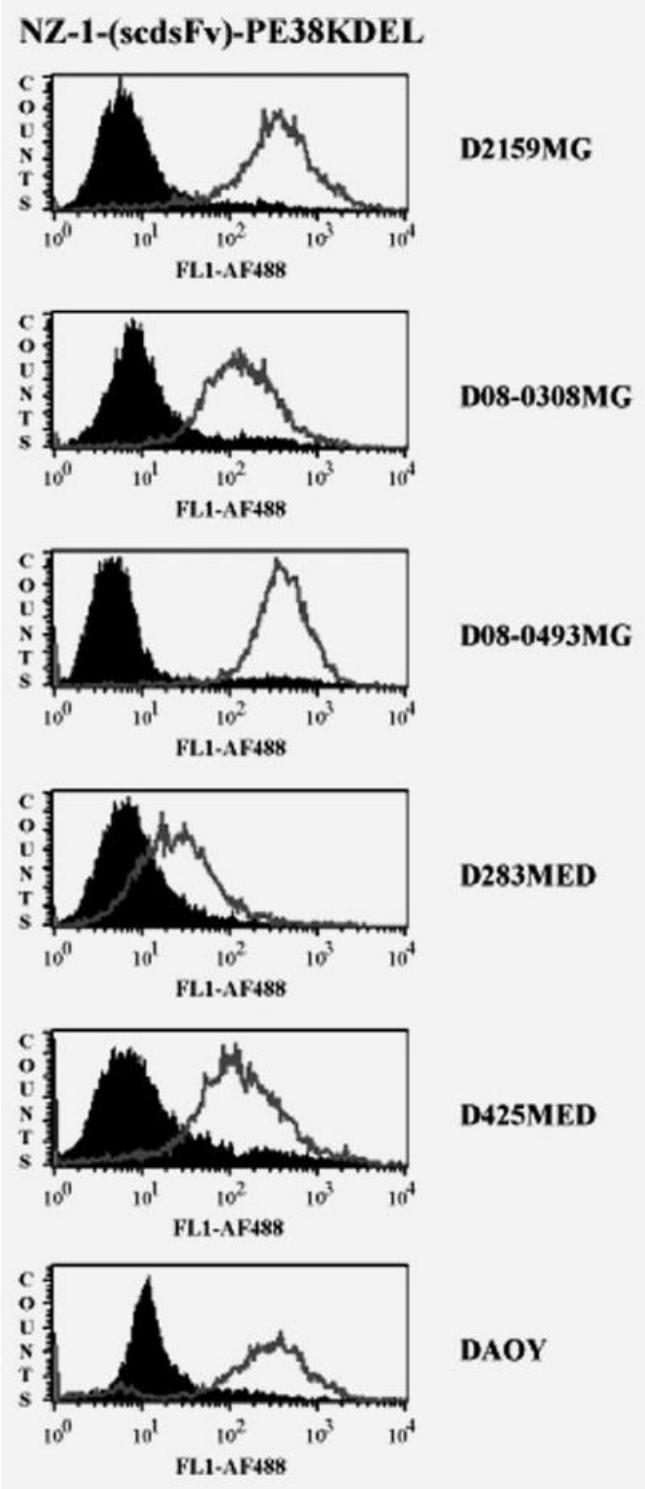
NZ-1-(scdsFv)-PE38KDEL
COUNTS
FL1-AF488
D2159MG
D08-0308MG
D08-0493MG
D283MED
D425MED
DAOY

Figure 10: Flow cytometric analysis of brain tumor xenografts to determine reactivity of the NZ-1-IT.

Cells isolated from brain tumor xenografts D2159MG, D08-0308MG, D08-0493MG, D283MED, D425MED and DAOY cell line were stained with NZ-1-IT (gray open peaks) or P588-IT (filled black peaks). From [52] with permission from publisher, see appendix for license.

3.1.2.3 *In vitro* cytotoxicity of D2C7-IT on transfected cells and cancer cells

We next examined the effects of the D2C7-IT on EGFRwt- or EGFRvIII-transfected NR6W and NR6M cell lines, respectively. The ability of the D2C7-IT to inhibit protein synthesis was used as a measure of its cytotoxic effect. The cytotoxicity of the D2C7-IT was compared with that of a known EGFRwt-specific immunotoxin, TP-38 [79], and that of a known EGFRvIII-specific immunotoxin, MR1-1 [80]. We initially evaluated the cytotoxicity of the various immunotoxins to the EGFRwt-expressing NR6W cells. The IC_{50} of the D2C7-IT on NR6W cells was 10 times lower than that of the EGFRwt-specific immunotoxin, TP-38 (0.467 vs. 4.6; **Table 2**). Even on the NR6M cells, D2C7-IT had an IC_{50} value 1.6 times lower than that of the EGFRvIII-specific immunotoxin, MR1-1 (0.253 vs. 0.413; **Table 2**).

The cytotoxic effects of D2C7-IT were also tested on various EGFRwt- and EGFRvIII-positive human cancer cells. The A431-epidermoid-carcinoma cell line overexpresses wild-type EGFR protein. Freshly isolated cells from glioblastoma xenografts, 43 and D08-0493MG express EGFRwt protein, and D2159MG and D270MG

express both EGFRwt and EGFRvIII proteins. As shown in **Table 3**, D2C7-IT was highly effective, with an IC_{50} of 0.18 to 2.5 ng/mL, in killing the A431 human cancer cell line and all of the glioblastoma xenograft cells tested.

Table 2: Cytotoxicity of D2C7 (EGFRwt and EGFRvIII), TP-38 (EGFRwt), and MR1-1 (EGFRvIII) immunotoxins toward EGFRwt / EGFRvIII-transfected cell lines*.

Cell line	D2C7 IC_{50} (ng/ml)	TP-38 IC_{50} (ng/ml)	MR1-1 IC_{50} (ng/ml)
NR6W	0.467 ± 0.18	4.6 ± 2.2	74.7 ± 17.9
NR6M	0.253 ± 0.04	101.7 ± 14.4	0.413 ± 0.03

*Cytotoxicity data are given as an IC_{50} value, the concentration of immunotoxin that causes a 50% inhibition of protein synthesis after a 20-hour incubation with immunotoxin. All the assays were conducted in triplicate for each cell line. Results are presented as mean ± standard deviation (SD) where $n \geq 2$.

Table 3: Cytotoxicity of D2C7 immunotoxin toward various cancer cells*.

Cell line	Cancer type	D2C7-IT IC_{50} (ng/ml)
A431 (EGFRwt)	Epidermoid Carcinoma	0.180 ± 0.014
43 (EGFRwt)	Glioblastoma	2.28 ± 0.85
D08-0493MG (EGFRwt)	Glioblastoma	2.5 ± 0.99
D2159MG (EGFRwt and EGFRvIII)	Glioblastoma	0.204 ± 0.220
D270MG (EGFRwt and EGFRvIII)	Glioblastoma	0.265 ± 0.134

*All the cells are of human origin. Cytotoxicity data are given as an IC_{50} value, the concentration of immunotoxin that causes a 50% inhibition of protein synthesis after a 20-hour incubation with immunotoxin. All the assays were conducted in triplicate for each cell line. Results are presented as mean ± SD where $n \geq 2$.

3.1.2.4 *In vitro* cytotoxicity of NZ-1-IT toward PDPN-expressing brain tumor cells

The cytotoxic activity of NZ-1-IT was assessed on three PDPN-positive (D2159MG, D08-0308MG and D08-0493MG) and two PDPN-negative glioblastoma xenograft cells (D08-0695MG and D08-0537MG), and two medulloblastoma xenograft cells (D283MED and D425MED) and a medulloblastoma cell line (DAOY) (**Table 4**). Inhibition of protein synthesis by NZ-1-IT was used as a measure of its cytotoxic effect. The NZ-1-IT was highly cytotoxic, with IC_{50} in the range of 1.6–3.3 and 9.7-29 ng/ml on the glioblastoma and medulloblastoma cells, respectively (**Table 4**).

Table 4: Cytotoxicity of NZ-1-IT on brain tumor cells*

Xenograft	NZ-1-IT IC_{50} (ng/ml)
D08-0695MG	>1,000
D08-0537MG	>1,000
D2159MG	1.6 ± 1.2
D08-0308MG	3.3 ± 2.0
D08-0493MG	2.7 ± 1.7
D283MED	9.7 ± 4.0
D425MED	26.7 ± 4.0
DAOY	29 ± 14.4

*Cytotoxicity data are given as an IC_{50} value, the concentration of immunotoxin that causes a 50% inhibition of protein synthesis after a 20-hour incubation with immunotoxin. Results are presented as mean ± SD where n ≥ 2. From [52] with permission from publisher, see appendix for license.

3.1.2.5 Stability of D2C7-IT

The therapeutic efficacy of an immunotoxin is greatly influenced by its stability. Hence, the stability of D2C7-IT was determined at two different concentrations over a 7-day period at 37°C by measuring its cytotoxic activity against NR6M cells. A solution of D2C7-IT, either at 40 µg/ml or 7.5 µg/ml in 0.2 % BSA-PBS, was incubated at 37°C in a humidified CO_2 incubator. A small aliquot of the immunotoxin was periodically removed and assayed for its ability to inhibit protein synthesis in NR6M cells. The cytotoxicity of the aliquots was compared to that of the untreated immunotoxin. Statistical analysis (P = 0.103, analyzed by a nonlinear regression module within SAS statistical software) of the 7-day IC_{50} values established D2C7-IT to be highly stable throughout the assay period (**Figure 11**).

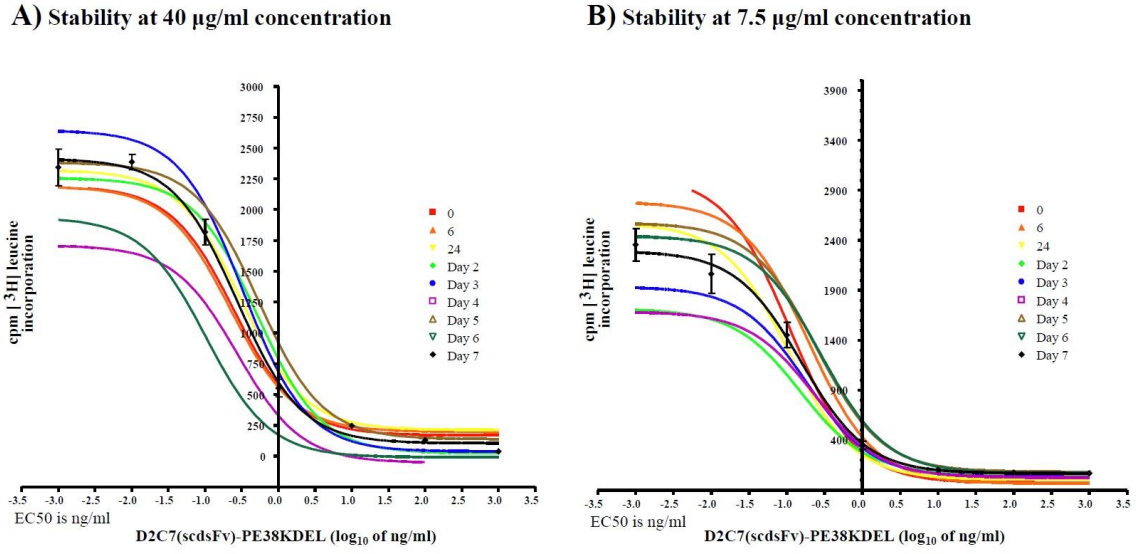

Figure 11: Stability of D2C7-IT.

D2C7-IT was incubated with 0.2% BSA-PBS at 40 μg/mL (A) and 7.5 μg/mL (B), over a 7-day period at 37°C and then assayed for cytotoxic activity on NR6M cells. Cytotoxicity data are given as IC_{50} value versus radioactive leucine incorporation.

3.1.2.6 Stability of NZ-1-(scdsFv)-PE38KDEL (NZ-1-IT)

The stability of an IT plays a significant role in determining its therapeutic efficacy. Earlier studies indicated scdsFvs might be more stable than scFvs [81]. Hence, the stability of NZ-1-(scFv)-PE38KDEL was compared to that of NZ-1-(scdsFv)-PE38KDEL over a 6- or 7-day period at 37°C by measuring its cytotoxic activity against D2159MG xenograft cells (**Table 5**) and DAOY cells (**Table 6**). Although the IC_{50} value of NZ-1-(scdsFv)-PE38KDEL increased eightfold from day 0 to day 7, the IC_{50} value of NZ-1-(scFv)-PE38KDEL increased 33.3-fold over the same time period on D2159MG xenograft cells (**Table 5**). Similarly, on the medulloblastoma cells DAOY, the IC_{50} value of NZ-1-(scdsFv)-PE38KDEL increased 1.3-fold from day 0 to day 6; however, there was a much higher increase in the IC_{50} value of NZ-1-(scFv)-PE38KDEL, 21.4-fold over the same time period (**Table 6**), demonstrating that NZ-1-(scdsFv)-PE38KDEL (NZ-1-IT) was more stable than NZ-1-(scFv)-PE38KDEL.

Table 5: Stability of NZ-1-(scFv)-PE38KDEL vs. NZ-1-(scdsFv)-PE38KDEL on D2159 MG*

Sample	IC_{50} (ng/ml)						
	0	2	3	4	5	6	7 (days)
NZ-1-(scFv)-PE38KDEL	0.6	3	4.5	5.5	6	7	20
NZ-1-(scdsFv)-PE38KDEL	0.5	1	1.5	1.5	3.5	2.5	4

*NZ-1-(scFv)-PE38KDEL and NZ-1-(scdsFv)-PE38KDEL were incubated with 0.2% BSA-PBS at 7.5 μg/ml over a 7-day period at 37°C and then assayed for cytotoxic activity on D2159MG xenograft cells. Cytotoxicity data are given as an IC_{50} value, the concentration of immunotoxin that causes a 50% inhibition of protein synthesis after a 20-hour incubation with immunotoxin. From [52] with permission from publisher, see appendix for license.

Table 6: Stability of NZ-1-(scFv)-PE38KDEL vs. NZ-1-(scdsFv)-PE38KDEL on DAOY*

Sample	IC_{50} (ng/ml)						
	0	1	2	3	4	5	6 (days)
NZ-1-(scFv)-PE38KDEL	28	81	220	220	380	400	600
NZ-1-(scdsFv)-PE38KDEL	40	42	41	41	48	48	51

*NZ-1-(scFv)-PE38KDEL and NZ-1-(scdsFv)-PE38KDEL were incubated with 0.2% BSA-PBS at 7.5 μg/ml over a 6-day period at 37°C and then assayed for cytotoxic activity on DAOY medulloblastoma cell line. Cytotoxicity data are given as an IC_{50} value, the concentration of immunotoxin that causes a 50% inhibition of protein synthesis after a 20-hour incubation with immunotoxin. From [52] with permission from publisher, see appendix for license.

3.1.2.7 Efficacy of D2C7-IT in intracranial tumor models

The D2C7-IT is human specific and does not react with murine EGFR. As a model for tumors expressing EGFRwt, the glioblastoma xenograft 43 was chosen; as a model for tumors expressing both EGFRwt and EGFRvIII, the glioblastoma xenograft D270MG was chosen. As the EGFRvIII mutation is most frequently reported in glioblastomas with *EGFR* amplification (19), there is no true glioblastoma xenograft that expresses EGFRvIII only. Therefore, we selected the murine fibroblast cell line NR6M, transfected with the human EGFRvIII as a model for EGFRvIII-expressing tumor. The survival curves for 43, NR6M, and D270MG (**Figure 12**) showed that 100% death occurred at day 18, day 15, and day 36 post tumor implantation for 43, NR6M, and D270MG, respectively. Therefore, day 6 (43 xenograft), day 5 (NR6M), and day 11 (D270MG) post tumor implantation were chosen as the optimal days to study the efficacy of D2C7-IT. Furthermore, toxicity studies in NSG mice with different concentrations of the D2C7-IT (1–10 μg/100 μL) showed that 1 μg of D2C7-IT had no toxicity-associated mortality (**Figure 13**).

In the 43 intracranial tumor model overexpressing EGFRwt protein in the absence of *EGFRwt* amplification, orthotopic delivery of D2C7-IT prolonged the survival by 310% ($P = 0.006$; **Figure 14A**). The group treated with the control immunotoxin, P588-IT, showed only a 7% increase in survival with a P value of 0.264. Four of ten 43 tumor-bearing mice in the D2C7-IT treatment group were still alive at the termination of the

study. Similarly, in the EGFRvIII-expressing NR6M orthotopic tumor model, the control immunotoxin, P588-IT, failed to show any response whereas D2C7-IT treatment showed a statistically significant (P = 0.002) increase in survival by 28% (**Figure 14B**). Likewise, in the D270MG intracranial tumor model expressing both EGFRwt and EGFRvIII, delivery of D2C7-IT by CED improved the survival by 166% (P = 0.001; **Figure 14C**). Notably, 8 of 10 of the D270MG tumor bearing mice in the D2C7-IT treatment group were still healthy and alive at the termination of the study. In sum, in the orthotopic brain tumor models of 43, NR6M, and D270MG, D2C7-IT therapy via CED significantly prolonged the median survival time of the treatment group by about 1 month (log-rank test P=0.0010), 1 week (log-rank test P=0.0074), and over 1 month (log-rank test P=0.0061), respectively, compared with that of vehicle or negative control groups.

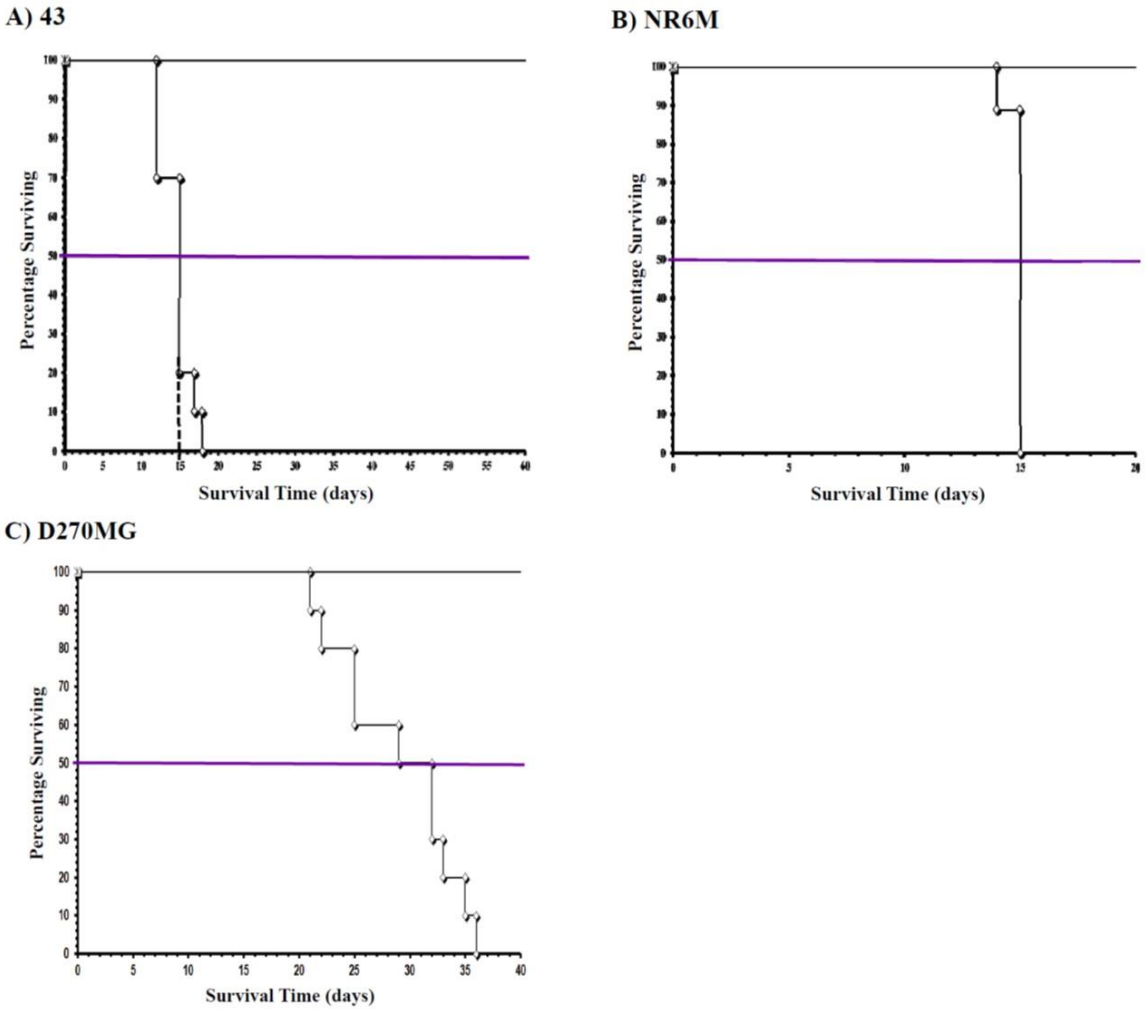

Figure 12: Survival of mice injected intracranially with 43 xenograft cells (A), NR6M cells (B), or D270MG xenograft cells (C).

Mice were injected intracranially with 1 x 10^5 43, NR6M, or D270MG cells and were checked daily for survival. Data are presented as the survival time in days versus percentage of mice surviving.

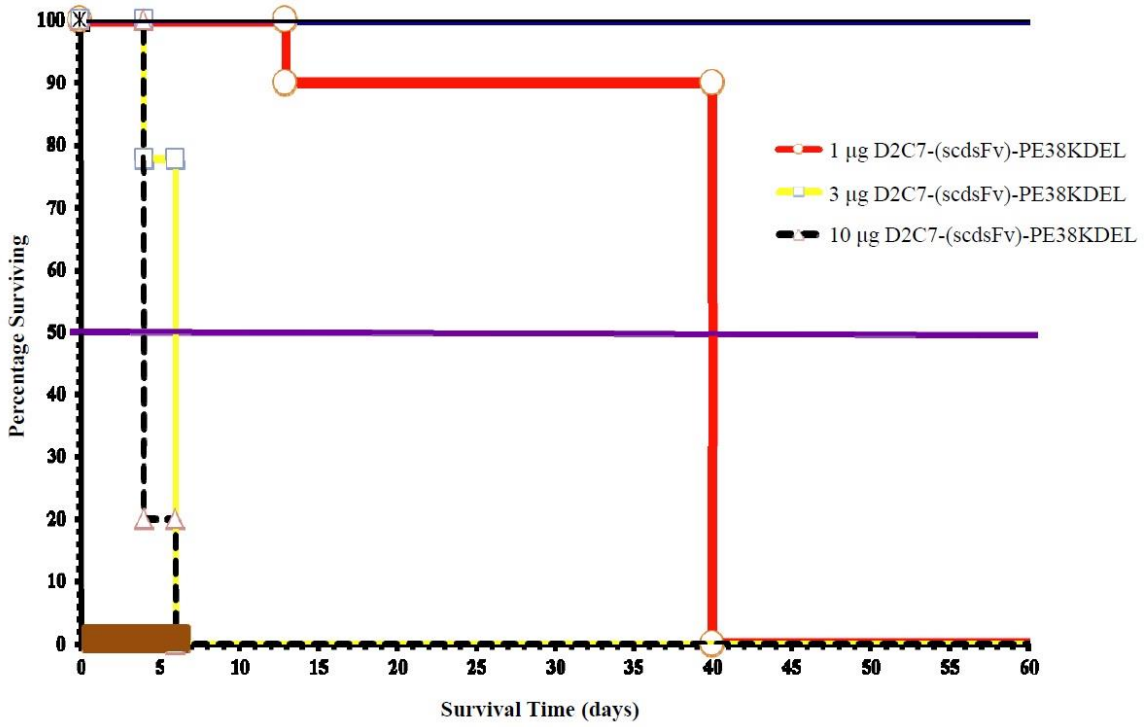

Figure 13: Toxicity of D2C7-IT administered to NSG mice.

Different doses of D2C7-IT were delivered intracranially over a 7-day period to NSG mice (5 mice/group). Animals were monitored for toxicity related death. Data are expressed as percentage of mice surviving versus time.

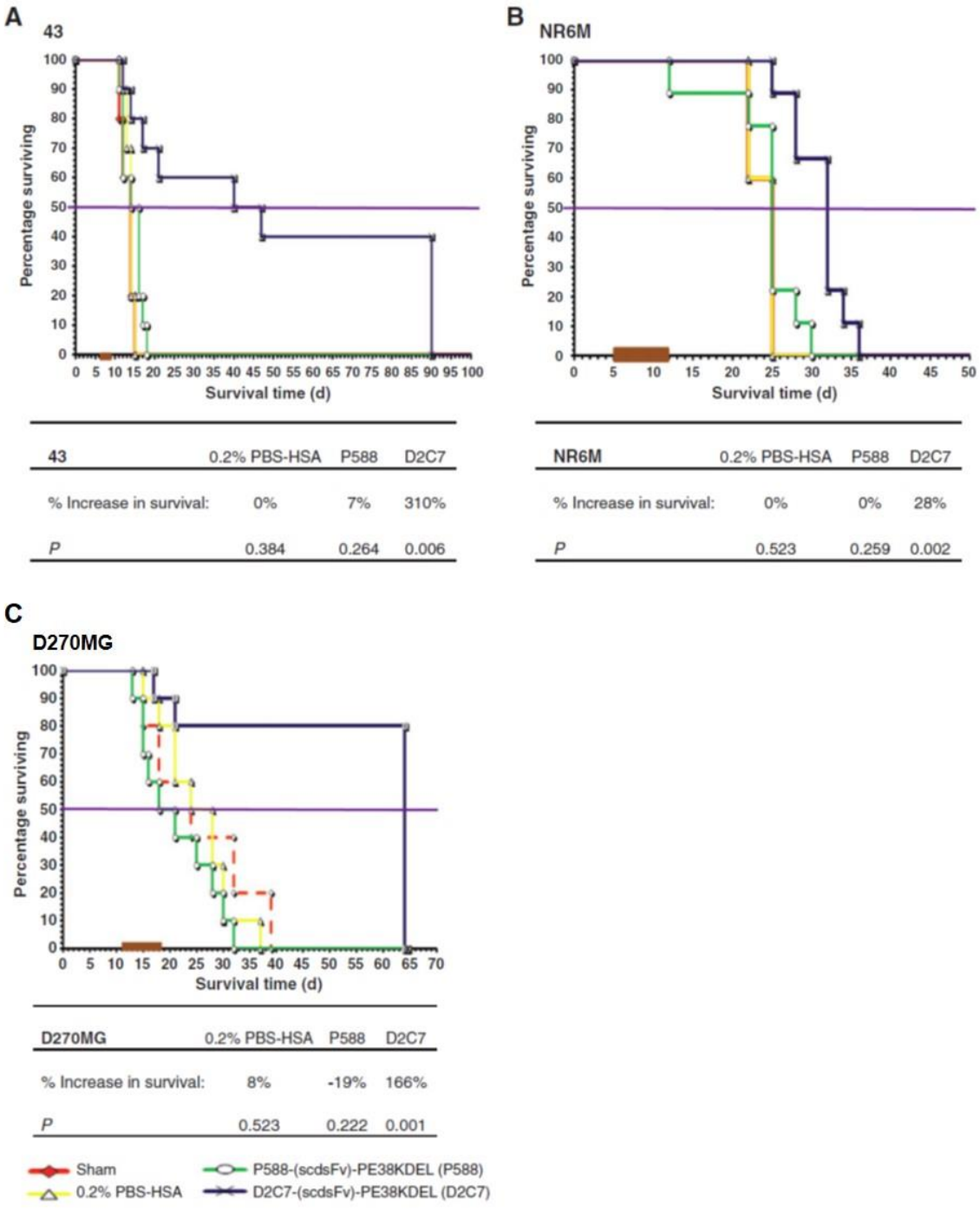

43	0.2% PBS-HSA	P588	D2C7
% Increase in survival:	0%	7%	310%
P	0.384	0.264	0.006

NR6M	0.2% PBS-HSA	P588	D2C7
% Increase in survival:	0%	0%	28%
P	0.523	0.259	0.002

D270MG	0.2% PBS-HSA	P588	D2C7
% Increase in survival:	8%	-19%	166%
P	0.523	0.222	0.001

Figure 14: Effect of D2C7-IT on 43, NR6M, and D270MG intracranial tumors in NSG mice.

Male NSG mice (about 30 g; 8–12weeks) bearing 43 (A), NR6M (B), and D270MG (C) tumors were randomized into four groups: Sham, 0.2% PBS-HSA, P588-IT, and D2C7-IT. The test mice were treated over a 3 (43 xenograft), 7 (NR6M), 11 (D270MG) -day period with a total of 1 μg of D2C7-IT diluted in 100 μL 0.2%HSA-PBS. Control mice were either left untreated (Sham) or treated with 0.2%HSA-PBS or 1 μg of P588-IT, diluted in 100 μL 0.2%HSA-PBS.

3.1.2.8 Assessment of D2C7-IT tumor distribution after CED

Sufficiently high concentrations of D2C7-IT in the tumor area are achieved by CED. However, the anti-tumor efficacy of D2C7-IT depends on its homogenous distribution within the tumor area. Tumor distribution of D2C7-IT administered by CED in D270MG intracranial model was examined by immunohistochemistry. Tumor sections from the D270MG-sham group and the D270MG-D2C7-IT group were used as the negative control (**Figure 15a**) and the test specimen (**Figure 15c**), respectively. The D270MG-D2C7-IT group, pre-stained with D2C7-IT, served as the positive control (**Figure 15b**). Figure 15b and 15c clearly show the identical staining pattern of both the positive control and the test specimen, thereby establishing the uniform distribution of D2C7-IT within the tumor area.

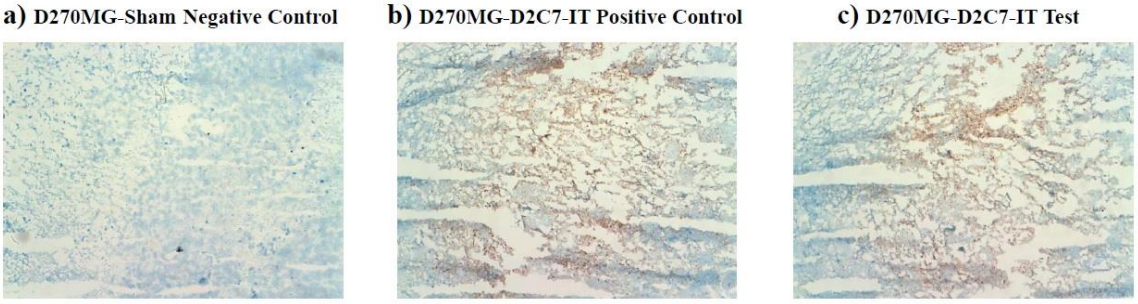

Figure 15: Immunohistochemical detection of D2C7-IT distribution in D270MG orthotopic model after immunotoxin treatment.

Acetone-fixed frozen D270MG-sham (negative control) (a) and D270MG-D2C7-IT group (test) (c) sections were stained with 1 μg of mouse-anti-PE38KDEL antibodies. Tumor sections from D270MG-D2C7-IT group, pre-stained with D2C7-IT was used as positive control (b).

3.1.2.9 Intracranial efficacy of NZ-1-IT on D425MED tumor model

To determine the time course of D425MED intracranial tumor growth in the xenograft model, 1×10^5 cells/5 μl was injected into male NSG mice (11 mice) and a survival curve was plotted (**Figure 16**). The D425MED survival curve demonstrated that 100% death occurred at day 14 post-tumor implantation; hence, post-tumor implantation day 4 was chosen as the optimal day to study the efficacy of NZ-1-IT. Further, to determine whether NZ-1-IT would be tolerated intracranially, NSG mice were given different concentrations of the NZ-1-IT (0.1–3.0 μg/100 μl) through an Alzet pump over a 3-day period (five mice per group). **Figure 17** depicts that both 0.1 and 0.3 μg of NZ-1-IT had no toxicity-associated mortality. Therefore, 0.3 μg of NZ-1-IT was selected to be the ideal concentration for intracranial therapy.

On the basis of the survival and toxicity studies, the efficacy study was performed on day 4 post-D425MED tumor implantation with 0.3 μg dose of the NZ-1-IT. The control groups were either left untreated (sham) or treated with 0.2% HSA-PBS or 0.3 μg of the nonspecific P588-IT. Treatment of the tumor-bearing mice with NZ-1-IT increased survival by 41% (**Figure 18**) and the Kaplan–Meier survival curve demonstrated a statistically significant (P = 0.001) increase in survival time in the 0.3 μg NZ-1-IT-treated mice when compared to the controls (**Figure 18**).

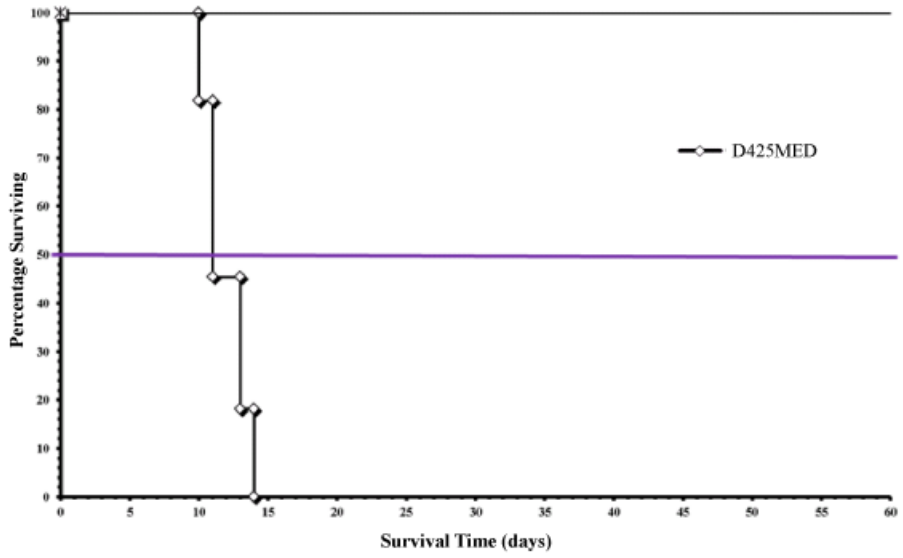

Figure 16: Survival of mice injected intracranially with D425MED xenograft cells.

From [52] with permission from publisher, see appendix for license.

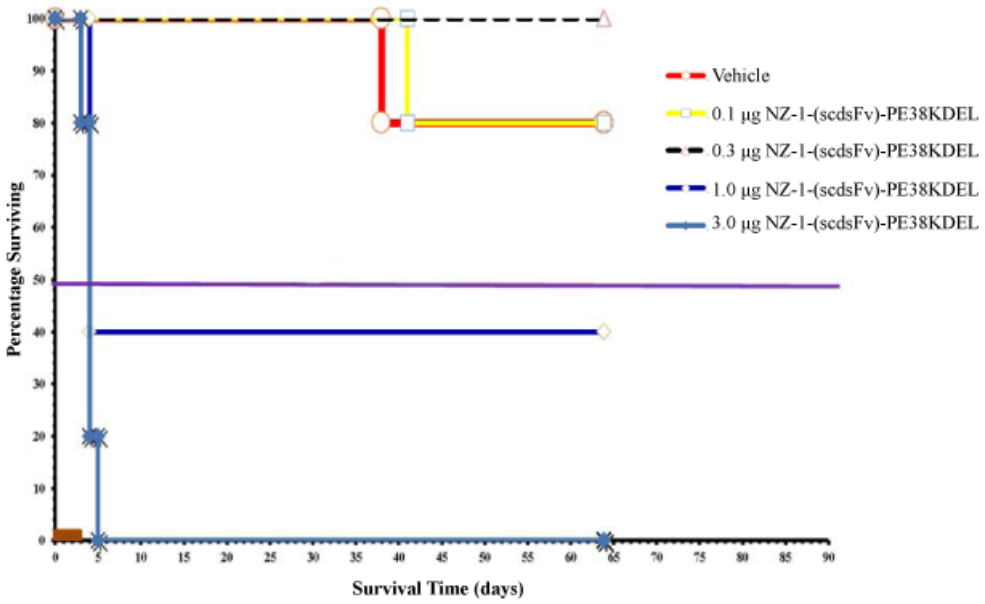

Figure 17: Toxicity of NZ-1-IT administered to NSG mice.

Different doses of D2C7-IT were delivered intracranially over a 3-day period to NSG mice (5 mice/group). Animals were monitored for toxicity related death. Data are expressed as percentage of mice surviving versus time. From [52] with permission from publisher, see appendix for license.

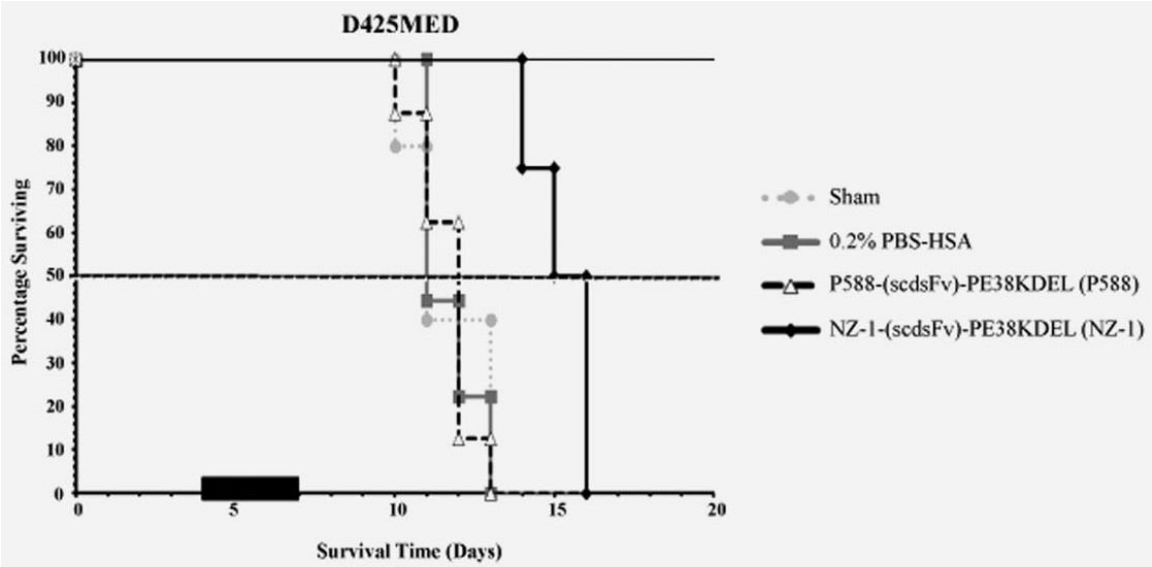

	0.2% PBS-HSA	P588	NZ1
% Increase in Survival:	0%	9%	41%
P Value:	≤0.499	≤0.472	≤0.001

Figure 18: Effect of NZ-1-IT on D425MED intracranial tumors in NSG mice.

Male NSG mice (about 20–30 g; 12 weeks) bearing D425MED tumors were randomized into four groups: sham (●), 0.2% HSA-PBS (■), P588-IT (Δ) and NZ-1-IT (♦). Four days post-tumor implantation, the mice were either left untreated (sham) or treated with 0.3 μg of P588-IT or NZ-1-IT diluted in 100 μl of 0.2% HSA-PBS or with 0.2% HSA-PBS alone, delivered intracranially through an Alzet pump over a 3-day period. From [52] with permission from publisher, see appendix for license.

3.1.3 Discussion and conclusions

3.1.3.1 EGFRwt/EGFRvIII and D2C7-IT preclinical study in glioblastomas

To achieve the clinical goal of successful immunotherapy for solid intracranial tumors, investigators have begun developing mAbs or recombinant scFvs against tumor

antigens. One such antibody, D2C7, recognizes both the EGFRwt and the mutant EGFRvIII, two proteins that are overexpressed in glioblastoma. The D2C7 mAb exhibited significant reactivity against both EGFRwt and EGFRvIII on tissue sections from glioblastoma patients. It also showed significant affinity by surface plasmon resonance and specificity by flow cytometry [47]. The high affinity, specificity, and reactivity of this mAb make it an ideal candidate for the construction of a recombinant immunotoxin that targets tumors overexpressing EGFRwt and EGFRvIII proteins. Due to the prevalence of different EGFR deletion mutants in glioblastoma, we deemed it necessary to identify the epitope for D2C7 on its target EGFRwt/EGFRvIII proteins. The 55 amino acid D2C7 epitope (EGFRwt 583–637 amino acids) is known to be present in EGFR deletion mutants C-958, Δ959–1030, Δ6–185, I, III–VII [10, 82], thereby increasing the number of antigenic targets for D2C7.

Subsequently, we cloned an EGFRwt/EGFRvIII-specific immunotoxin, D2C7-IT, from the D2C7 hybridoma and characterized its efficacy using *in vitro* and *in vivo* models. The *in vitro* cytotoxicity data showed that D2C7-IT effectively inhibits protein synthesis in a variety of EGFRwt- or EGFRwt–EGFRvIII-expressing glioblastoma xenograft cells and human tumor cell line. Notably, in the intracranial animal models of EGFRwt-expressing glioma xenograft 43, EGFRvIII-expressing NR6M, and EGFRwt- and EGFRvIII-expressing glioblastoma xenograft D270MG, D2C7-IT showed significant increase in survival, 310% ($P = 0.006$), 28%($P = 0.002$), and 166% ($P = 0.001$), respectively.

To the best of our knowledge, this is the first report showing that an immunotoxin can target both the EGFRwt and the mutant EGFRvIII in glioma models.

To show significant therapeutic efficacy when administered to patients with brain tumors, an immunotoxin has to be considerably stable over long periods of time. Therefore, in addition to the conventional 15-amino-acid peptide linker present between the V_H and V_L domain of D2C7 scFv, we introduced an inter-chain disulfide bond between the structurally conserved framework regions of the D2C7 V_H and V_L domains, to construct a new disulfide-stabilized immunotoxin termed D2C7-(scdsFv)-PE38KDEL. The disulfide-stabilized D2C7-IT was highly stable over a 7-day period.

In *in vitro* studies, D2C7-IT inhibited protein synthesis in EGFRvIII-expressing NR6M cells at a concentration 402 times lower than TP-38, an EGFRwt specific TGF-a–based immunotoxin. Furthermore, D2C7-IT inhibited protein synthesis at a concentration 160 times lower than MR1-1, an EGFRvIII-specific immunotoxin, in EGFRwt-expressing NR6W cells. Any therapy that fails to target the EGFRwt-expressing cells or constitutively autophosphorylated EGFRvIII-expressing cells will lead to enhanced proliferation and migration of these tumor cells. Furthermore, any surviving EGFRvIII only–expressing tumor cells in tumors that have both EGFRwt and EGFRvIII will promote resistance to EGFR antibody therapy [83]. In our *in vitro* studies with EGFRwt or both EGFRwt- and EGFRvIII-expressing human cancer cells, D2C7-IT showed significant inhibition of protein synthesis. Furthermore, the D2C7-IT prolonged

survival in *in vivo* tumor models with the 43 xenograft, NR6M, and D270MG xenograft. Examination of brain sections from the 8 euthanized mice from the D270MG-D2C7-IT treatment group by hematoxylin and eosin (HE) staining revealed no tumor cells in 8 of 8 mice. Macrophage or monocyte infiltration was observed in 4 of 8 mice. No expression of EGFRwt (EGFR1 mAb), EGFRvIII (L8A4 mAb), or EGFRwt and EGFRvIII (D2C7 mAb) was observed in 8 of 8 mice, indicating that all the 8 mice in the D270MG-D2C7-IT treatment group were cured. Therefore, we believe that D2C7-IT is likely to be more efficacious in treating patients of glioblastoma whose tumors express both EGFRwt and EGFRvIII or either EGFRwt or EGFRvIII alone. Furthermore, EGFR mutants form homo/heterodimers and currently available EGFR mAbs, cetuximab, matuzumab, and panitumumab are unable to block activation of these dimers [84]. As the D2C7 epitope is present on a wide variety of these EGFR deletion mutants, D2C7-IT treatment should prove efficacious for patients with glioblastoma harboring these mutations.

For effective *in vivo* therapy of glioblastoma, it is essential to achieve high local concentration and homogeneous distribution of the immunotoxin at the tumor site. In the 43, NR6M, and D270MG models, D2C7-IT was administered by continuous intracranial CED through osmotic mini-pumps. This delivery method will aid in achieving elevated concentrations and uniform distribution of D2C7-IT at the tumor site, which would be expected to optimize its anti-tumor activity. By this method, we were able to achieve significant increase in survival at a very low dose of 1 μg of D2C7-IT.

D2C7-IT might cause human skin and liver toxicity if the immunotoxin were administered by systemic injection. However, as we propose to administer the immunotoxin by CED directly into intracranial tumors, any systemic toxicity due to low and clinically insignificant amounts of immunotoxin gaining access to systemic organs and tissues would be minimized by this localized treatment. The regional drug delivery technique of CED has been used successfully to deliver recombinant toxins targeting EGFRwt [79] and EGFRvIII [70] in patients with malignant glioma, without any liver or other systemic organ toxicity.

The *in vitro* internalization studies showed rapid uptake of D2C7-IT by NR6W and NR6M cells within 1 to 2 hours of treatment (data not shown). We hypothesize a similar uptake of D2C7-IT by tumor cells upon infusion and fast clearance of the immunotoxin within the tumor area. Moreover, our immunohistochemical studies in the D270MG orthotopic model clearly show that homogenous distribution of the D2C7-IT is essential in generating a significant anti-tumor response. Consequently, tumor cells that failed to encounter D2C7-IT might regrow and repopulate the tumor area. Thus, tumor recurrence in our *in vivo* models might be due to both the swift depletion of the low levels of D2C7-IT (1 μg) and lack of uniform distribution, and not due to escape from immunotoxin efficacy.

Because of the recurrent nature of malignant gliomas, as well as the diversity of antigens populating the glioma cell surface, there is a need for innovative

immunotherapeutic approaches. In an earlier study, Schmidt and colleagues described a recombinant immunotoxin, scFv (14E1)-ETA, which bound both EGFRwt and EGFRvIII [85]. The activity of scFv (14E1)-ETA was shown both *in vitro* and *in vivo*, but only on the epidermoid carcinoma cell line A431 or the EGFRwt- or EGFRvIII-transfected murine renal carcinoma cells (Renca-lacZ/EGFR or Renca-lacZ/EGFRvIII) and not on EGFRwt- and EGFRvIII-expressing human glioma models. Moreover, the study by Schmidt and colleagues did not include immunohistochemical analyses that would show the binding of their construct to human glioma tissue or any other human cancer tissue. In this regard, D2C7-IT is a novel immunotoxin that can target both the EGFRwt and the EGFRvIII proteins that are frequently overexpressed in malignant gliomas.

Monoclonal antibodies 528 and 806, with dual specificity for wild-type and mutant EGFR proteins expressed on different cell lines, have been well described in previous studies [86, 87]. Combination therapy using mAbs 528 and 806 showed a significant decrease in tumor volume of xenografts expressing EGFRwt or EGFRvIII [88]. Such combination therapies targeting multiple tumor-associated molecules require high costs in the development, manufacturing, and treatment. These intrinsic issues associated with combination antibody therapies will be circumvented with our EGFRwt/EGFRvIII-specific D2C7-IT.

In conclusion, we have created a scFv molecule that is capable of mediating selective *in vitro* and *in vivo* tumor targeting. We believe this to be the first significant

evidence showing enhanced glioblastoma tumor targeting with high selectivity and specificity by an antibody specific for two glioma-associated antigens. Taken together, our results suggest that D2C7-IT should be clinically efficacious against brain tumors expressing EGFRwt or EGFRvIII alone or together. A GLP clinical preparation of D2C7-IT has been prepared, after which we will obtain a U.S. FDA IND. NCI funding (P01 CA154291-01) for phase I and II trials of D2C7-IT by CED in patients with glioblastoma has been obtained. We have recently shown successful imaging of an immunotoxin, MR1-1-PE38, similar in size to our D2C7-IT, in a clinical trial with CED. Successful imaging of the delivery of D2C7-IT will greatly improve treatment efficacy [70, 75]. As discussed earlier, the high levels of homogeneous expression of the D2C7-IT molecular targets, EGFRwt and EGFRvIII (both of which are major glioblastoma driver oncogenes), in more than 95% of newly diagnosed glioblastoma tumors will also improve D2C7-IT efficacy over other immunotoxins previously used in glioblastoma clinical trials.

3.1.3.2 PDPN and NZ-1-IT preclinical study in glioblastomas and medulloblastomas

The clinical success of mAbs and recombinant IT-based targeted therapies against solid intracranial tumors has led investigators to identify novel brain-tumor-specific antigen targets [89]. PDPN is one such antigen that is highly expressed on several CNS tumors [28, 29]. NZ-1 is a mAb exhibiting high reactivity to PDPN (K_D = 1.2 × 10^{-10} M) and when bound by glioblastoma cells expressing PDPN, NZ-1 mAb is efficiently internalized [51], thereby demonstrating its potential as an important

immunotherapeutic agent. In our study, we demonstrate the expression of PDPN on both glioblastoma and medulloblastoma xenografts by flow cytometry using NZ-1 mAb. Further, we constructed a recombinant IT, NZ-1-IT, by fusing the scFv segment of the NZ-1 mAb with the PE38KDEL molecule. Similar to the NZ-1 mAb, the NZ-1-IT exhibited considerable binding to both glioblastoma and medulloblastoma cells by flow cytometry. The affinity of NZ-1-IT was determined to be $K_D = 8.0 \times 10^{-8}$ M by Biacore. NZ-1-IT displayed considerable stability when incubated at 37°C for long time periods. NZ-1-IT demonstrated significant cytotoxicity against both glioblastoma and medulloblastoma cells. Further, in intracranial animal models, with PDPN-expressing medulloblastoma xenograft, NZ-1-IT demonstrated significant tumor growth delays ($P < 0.001$), which makes it a novel and efficacious immunotherapeutic agent against malignant brain tumors.

Consistent with earlier studies, we demonstrate PDPN to be present in both glioblastoma and medulloblastoma xenografts [28]. Flow cytometry analysis with cells isolated from glioblastoma (D2159MG, D08-0308MG and D08-0493MG) and medulloblastoma xenografts (D283MED and D425MED) and a medulloblastoma cell line (DAOY) demonstrates different levels of reactivity to NZ-1-IT. Further, the cytotoxic activity of NZ-1-IT was assessed on three PDPN-positive (D2159MG, D08-0308MG and D08-0493MG) and two PDPN-negative glioblastoma xenograft cells (D08-0695MG and D08-0537MG), and two medulloblastoma xenograft cells (D283MED and D425MED) and

a medulloblastoma cell line (DAOY). The NZ-1-IT was highly cytotoxic, with IC_{50} in the range of 1.6–3.3 and 9.7-29 ng/ml on the glioblastoma and medulloblastoma cells, respectively

Additionally, an IT has to be significantly stable over long periods of time to demonstrate therapeutic efficacy when administered to brain tumor patients. The V_H and V_L domains of NZ-1 scFv are held together by a 15-amino acid peptide linker, and it is well established that the noncovalent, interdomain interactions provided by the peptide linker are not strong enough to keep them together [90]. The linker is rather flexible, and this could promote the interaction between the V_H and V_L domains of NZ-1-(scFv)-PE38KDEL and a nearby IT molecule, which could thereby affect the stability of the IT. We hypothesized that this problem could be overcome by introducing an interchain disulfide bond between the structurally conserved framework regions of the NZ-1 V_H and V_L domains [81]. The new disulfide-stabilized IT is termed NZ-1-(scdsFv)-PE38KDEL (NZ-1-IT). As hypothesized, the incorporation of a disulfide bond, in addition to the peptide linker, offered higher stability to NZ-1-IT, which was evident from its lower IC_{50} values compared to NZ-1-(scFv)-PE38KDEL on both D2159MG xenograft cells and DOAY cells.

The *in vivo* results were compatible with the *in vitro* flow cytometry and cytotoxic activity data. In the treatment of malignant brain tumors, the NZ-1-IT will be administered directly into the tumor site and thus bypass the BBB by CED [70]. To

replicate an actual brain tumor model, the D425MED xenograft cells were implanted intracranially and were treated by NZ-1-IT via CED, which was extremely efficacious in the intracranial model and increased the survival of tumor-bearing mice by 41% ($P \leq 0.001$).

In conclusion, our results clearly demonstrate that the disulfide-stabilized recombinant NZ-1-IT is highly efficacious against CNS tumors expressing PDPN in a preclinical setting and hence is a suitable candidate for targeted therapy of malignant brain tumors.

3.2 Preclinical toxicity evaluation of D2C7-IT administered via intracerebral CED in rats

3.2.1 Introduction

Glioblastoma is the most aggressive malignant brain tumor among all primary brain and CNS tumors diagnosed in the United States. Glioblastomas represented 46.1 % of all malignant brain tumors from 2008 to 2012, according to a statistical report from the CBTRUS [2]. The median survival time for glioblastoma patients given the current standard treatment of surgery followed by radiation and chemotherapy is less than 15 months [2, 4]. Even with newly developed agents, such as temozolomide or bevacizumab, there is only a slight improvement in the survival time of glioblastoma patients [2, 4]. Thus, there is an urgent need for more advanced and efficient therapeutic approaches to improve the poor survival outlook of glioblastoma patients.

Recombinant ITs may provide a much needed breakthrough in glioblastoma therapy. In the past two decades, mAb-based studies have increasingly focused on ITs that are constructed by fusing genetically engineered scFv, which target antigens specifically expressed by brain tumor cells, to bacterial or plant toxins. Because the scFv-IT fusion protein is smaller than the original immunoglobulin (IgG), it has a superior capacity for tumor penetration, which can lead to enhanced anti-tumor therapeutic efficacy when it is delivered intrathecally or intratumorally [48, 52, 74, 91].

Previous studies have reported the amplification of *EGFR* in 40 % to 50 % of glioblastoma patients [48]. In contrast, the EGFR level in the normal brain is undetectable or extremely low [92]. In correlation with *EGFR* gene amplification, overexpression of EGFR protein is detected in approximately 60%to 90%of glioblastoma patients. Even without gene amplification, 12 % to 38 % of glioblastoma patients exhibit EGFR protein overexpression, which may be caused by other aberrant translational and posttranslational mechanisms [93]. Moreover, up to 67 % of all tumors with *EGFRwt* amplification express EGFRvIII, which lacks the extracellular ligand-binding domain (exons 2 through 7) [4, 10]. The development of mAb-based agents that can target both forms of the receptor for therapy would be advantageous because of the high prevalence of the EGFRvIII mutation in glioblastomas with *EGFRwt* amplification.

We have developed a novel targeted IT, D2C7-IT [48], which reacts with both the EGFRwt and EGFRvIII proteins by fusing the scFv of the D2C7 mAb with PE38KDEL. *In*

vitro cytotoxicity data shows that D2C7-IT effectively inhibited protein synthesis in a variety of EGFRwt-, EGFRvIII-, or both EGFRwt- and EGFRvIII- expressing glioblastoma xenograft cells and human tumor cell lines. Notably, in intracranial animal models of EGFRwt-expressing and EGFRwt-EGFRvIII-expressing glioblastoma xenografts, intracranial administration of D2C7-IT via CED has been shown to increase survival by more than 150% [48, 74]. Hence, D2C7-IT should be clinically efficacious against brain tumors expressing either EGFRwt or EGFRvIII, or expressing both EGFRwt and EGFRvIII. A preclinical study was performed under GLP regulations to evaluate the systemic toxicity of D2C7-IT administered via intracerebral CED using an osmotic pump in rats to support an initial US FDA IND application for a Phase I/II clinical trial in patients with glioblastoma [74, 75]. In patients, the distribution of IT by intracerebral CED can be monitored by co-infusion with a low-molecular-weight tracer, Gd-DTPA, and ^{124}I-HSA [70]. The IT was co-infused with Gd-DTPA and ^{124}I-HSA in this rat GLP study with the aim of replicating this formulation in the future D2C7-IT clinical trial.

3.2.2 Results

3.2.2.1 TOX-2013-001 preclinical toxicity trial

As shown in **Table 7**, the toxicity of D2C7-ITwas investigated in four dose groups (0, 0.30, 0.50, and 0.63 μg/rat) in the acute and chronic cohorts. The initial control formulation, which was recommended by the FDA to regulate the human clinical

formulation, consisted of 0.05 M PBS in saline, 0.2 % HSA, 2 μCi ^{124}I-HSA, and 1 mM Gd-DTPA. The dose formulations were delivered into the right caudate nucleus of each individual rat via a subcutaneously implanted osmotic pump (Alzet pump 2ML1) [75] at a nominal 10.1 μL/hour flow rate. Five rats per sex per treatment group were scheduled for necropsy on days 5 (the acute cohort) and 34 (the chronic cohort) of the study to examine the acute and chronic toxicities of the infused test article.

General adverse clinical signs, such as head-tilt, trembling, and loss of coordination, were observed among some animals in all of the groups of both cohorts (8/20 rats in the control group, 10/20 rats in the 0.3 μg dose group, 12/20 rats in the 0.5 μg dose group, and 14/20 rats in the 0.63 μg dose group). Unscheduled mortality was observed in 2/20 rats in the 0.3 μg dose group and 3/20 rats in the 0.63 μg dose group. Behavioral abnormalities, including the inability to walk or stand unassisted, abnormal posture, seizures, catalepsy, abnormal body temperature, and abnormal nasal or eye discharge were observed in all groups. At necropsy, no treatment-related gross lesions were observed. Histopathologic evaluation of the brains revealed regions of encephalomalacia (ECM) largely centered in the centrum semiovale area, which corresponded to the injection site, in all groups. The injection site was surrounded by haloes of gliosis and demyelination in all cases. The pump D2C7-IT test formulations under the same conditions showed an approximately 10-fold loss of biological activity compared to the bulk samples (reference standard control), as measured by the

inhibition of A431P (24–96 hours IC_{50}: Bulk 57–71 pg/mL vs Pump 750–850 pg/mL) and NR6M (24–96 hours IC_{50}: Bulk 490–600 pg/mL vs Pump 5900–7500 pg/mL) cell proliferation (**Table 8 and 9**), suggesting formulation issues with the test article. Thus, the trial was terminated after approximately one week of the in-life portion. In addition, the dose formulations (osmolality of approximately 370 mOsm/l H_2O) were proven to be hypertonic compared with the osmolality of the rat brain (290–300 mOsm/l H_2O).

Table 7: The summary of the TOX-2013-001 preclinical D2C7-IT toxicity trial

From [76] with permission from publisher, see appendix for license.

Group	Cohort[b]	D2C7-IT Total Dose (μg) in 3 days	No. of Animals	No. of rats showing abnormal clinical signs (Total No. from both cohorts)	No. of unscheduled mortality (Total No. from both cohorts)
Control[a]	Acute Chronic	0	10 (5 males, 5 females) 10 (5 males, 5 females)	8 (3 males, 5 females)	0
D2C7-IT Low Dose	Acute Chronic	0.3	10 (5 males, 5 females) 10 (5 males, 5 females)	10 (7 males, 3 females)	2 (1 male, 1 female)
D2C7-IT Median Dose	Acute Chronic	0.5	10 (5 males, 5 females) 10 (5 males, 5 females)	12 (7 males, 5 females)	0
D2C7-IT High Dose	Acute Chronic	0.63	10 (5 males, 5 females) 10 (5 males, 5 females)	14 (6 males, 8 females)	3 (2 male, 1 female)

[a] Control formulation: 0.05 M PBS in saline, 0.2 % HSA, 2 μCi ^{124}I-HSA, and 1 mM Gd-DTPA

[b] The TOX-2013-001 trial was terminated after 1 week of the in-life portion of the trial

Table 8: IC_{50} of the bulk and pump test articles (0.63 μg dose group) on A431P cells at different time points

From [76] with permission from publisher, see appendix for license.

Hours in Pump	A431P	
	Bulk IC_{50} (pg/ml)	Pump IC_{50} (pg/ml)
0	53	N/A
24	57	750
48	57	590
72	63	510
96	71	850

Table 9: IC_{50} of the bulk and pump test articles (0.63 μg dose group) on NR6M cells at different time points

From [76] with permission from publisher, see appendix for license.

Hours in Pump	NR6M	
	Bulk IC_{50} (pg/ml)	Pump IC_{50} (pg/ml)
0	600	N/A
24	490	5900
48	420	3900
72	550	4000
96	600	7500

3.2.2.2 TOX-2013-002 preclinical toxicity trial

TOX-2013-002 was initiated with a modified isotonic dose formulation using sodium phosphate buffer in saline with 3 % HSA, 2 μCi ^{124}I-HSA, 1 mM gadolinium, and D2C7-IT administered at four doses of 0, 0.075, 0.15, and 0.3 μg/rat over 72 hours using a

subcutaneously implanted osmotic pump (Alzet pump 2ML1) at a nominal 10.1 μL/hour flow rate. General adverse clinical signs, including weight loss, dehydration, and seizure-like activity, were observed among many animals from both cohorts in the control group (13/20 rats) and the test article groups (17/20 rats in the 0.075 μg dose group, 14/20 in the 0.15 μg dose group, and 14/20 in the 0.3 μg dose group). Unscheduled mortality was observed in 4/20 rats in the control group, 4/20 in the 0.075 μg dose group, 3/20 in the 0.15 μg dose group, and 3/20 in the 0.3 μg dose group (**Table 10**). Behavioral assessments revealed abnormalities in all groups of both cohorts, including the inability to stand or walk unassisted, abnormal posture, continuous rotation, stereotypies, seizures, catalepsy, abnormal body temperature, and eye/nasal discharge. At necropsy, no treatment-related gross lesions were present. Evaluation of brain histopathology revealed regions of ECM (destructive lesions) largely centered in the centrum semiovale corresponding to the injection site in all study groups, including the control group (no dose–response relationships were noted among the injection site injuries). The areas of ECM were surrounded by haloes of gliosis and demyelination that were not dose-related in all groups. Demyelination, gliosis, and hydrocephalus were noted in all four groups. Although there was not a clear dose–response relationship, a large area (5.0 × 2.5 mm or greater) of ECM occurred more frequently in the groups administered with the test article.

Kidney histopathology revealed a similar number of lesions in the control and test article dose groups, including acute tubular necrosis, foci of lymphocytes and inflammation, and areas of calcification. None of these lesions occurred in a dose-related manner. Due to these abnormal clinical observations of the rats in all dose groups, including the control group, the study was terminated after 10 days of the in-life portion.

Table 10: The summary of the TOX-2013-002 preclinical D2C7-IT toxicity trial

From [76] with permission from publisher, see appendix for license.

Group	Cohort[b]	D2C7-IT Total Dose (μg) in 3 days	No. of Animals	No. of rats showing abnormal clinical signs (Total No. from both cohorts)	No. of unscheduled mortality (Total No. from both cohorts)
Control[a]	Acute Chronic	0	10 (5 males, 5 females) 10 (5 males, 5 females)	13 (7 males, 6 females)	4 (3 males, 1 female)
D2C7-IT Low Dose	Acute Chronic	0.075	10 (5 males, 5 females) 10 (5 males, 5 females)	17 (10 males, 7 females)	4 (3 males, 1 female)
D2C7-IT Median Dose	Acute Chronic	0.15	10 (5 males, 5 females) 10 (5 males, 5 females)	14 (7 males, 7 females)	3 (2 males, 1 female)
D2C7-IT High Dose	Acute Chronic	0.3	10 (5 males, 5 females) 10 (5 males, 5 females)	14 (7 males, 7 females)	3 (1 male, 2 females)

[a] Control formulation: Sodium phosphates buffer in saline, 3 % HSA, 2 μCi ^{124}I-HSA, and 1 mM Gd-DTPA

[b] The TOX-2013-002 trial was terminated after 10 days of the in-life portion of the trial

3.2.2.3 Vehicle toxicity trial

A new control formulation (sodium phosphate buffer in saline with 2 % RSA) was tested to evaluate its toxicity. The dose formulation was administered intracerebrally into the rat brain over 72 hours using the smaller osmotic pump (Alzet pump 2001) at a slower nominal 1 μL/hour flow rate. The dose formulation was delivered into the right (Group 1) or left (Group 2) caudate nucleus of individual rats in

two groups consisting of five male rats and five female rats per group, and necropsy occurred on study day 7 for both groups. Clinical observations, body weight changes, and gross and microscopic pathologies were evaluated over a 7-day period in this trial. No apparent study-related adverse clinical signs were observed during the study. There were no obvious study-related differences in body weights between male or female rats in both groups. Microscopic histopathology showed normal brains in 13/20 rats, and the remaining 7 rats only displayed needle and catheter tracks and a slight degree of inflammation at the point of needle and catheter insertion. Because the rats in the vehicle toxicity trial showed better outcomes with this new control formulation, the HSA in the previous control formulation was replaced with RSA in the final D2C7-IT GLP toxicity trial.

3.2.2.4 TOX-2014-001 GLP preclinical toxicity trial

A final TOX-2014-001 GLP toxicity trial was performed to evaluate the acute and chronic toxicities of D2C7-IT administered via intracerebral CED to determine the MTD and the NOAEL in rats. D2C7-IT was formulated in an isotonic control formulation (potassium phosphate buffer in saline with 2 % RSA, 2 μCi ^{124}I-HSA and 1 mM gadolinium). Dose formulations were delivered into the right caudate nucleus of individual rats via subcutaneously implanted osmotic pumps (Alzet pump 2001) at a nominal 1.01 μL/hour flow rate. Each dose preparation passed the bacteria and endotoxin tests.

As summarized in **Table 11**, the test article was administered into five male rats and five female rats (total doses: 0, 0.05, 0.10, and 0.40 μg/rat) that underwent necropsy on study day 5 (the acute cohort) and five male rats and five female rats (total doses: 0, 0.05, 0.10, and 0.35 μg/rat) that underwent necropsy on study day 34 (the chronic cohort). Necropsy was completed in the acute cohort before the chronic cohort. Mortality occurred in 5/10 rats (3/5 males and 2/5 females) in the high-dose group (0.40 μg total dose) in the acute cohort. Consequently, the total dose was decreased from 0.40 to 0.35 μg for the high-dose group in the chronic cohort. Mortality was observed in 4/10 rats (2/5 males and 2/5 females) in the 0.35 μg total dose group in the chronic cohort.

There were no apparent study-related adverse clinical signs in either the acute and chronic cohort, except in the high-dose groups, in which weight loss, reluctance to ambulate, and difficulty in ambulating were observed in the rats that received either the 0.35 or 0.40 μg total dose. Seizure-like activities and moribund conditions were observed in the rats that received the 0.35 μg total dose in the chronic cohort. All study-related adverse clinical signs were noted on study days 4 to 6. There were no dose-related differences in body weight for male or female rats among the groups in the acute or the chronic cohort. Likewise, the effects of treatment over time on body weight did not differ among the groups of males or females in either cohort. There were no dose-related effects observed in terms of hematology, serum chemistry, or blood cell morphology in the males or females in either cohort.

Table 11: The summary of the final TOX-2014-001 GLP preclinical D2C7-IT toxicity trial

From [76] with permission from publisher, see appendix for license.

Group	Cohort	D2C7-IT Total Dose (μg) in 3 days	No. of Animals	No. of rats showing abnormal clinical signs	No. of unscheduled mortality	Histopathology Report			
						ECM	Edema	Demyelination	Others
Control[a]	Acute	0	10 (5 males, 5 females)	0	0	6	0	0	N/A
	Chronic		10 (5 males, 5 females)	0	0	4	0	0	1 gliosis
D2C7-IT low dose	Acute	0.05	10 (5 males, 5 females)	0	0	5	0	0	1 possible infarct, 1 mild hydrocephalus, 1 focal hemorrhage
	Chronic		10 (5 males, 5 females)	0	0	2	0	0	N/A
D2C7-IT median dose	Acute	0.1	10 (5 males, 5 females)	0	0	4	0	0	1 possible abscess
	Chronic		10 (5 males, 5 females)	0	0	3	0	0	1 mild hydrocephalus
D2C7-IT high dose 1	Chronic	0.35	10 (5 males, 5 females)	4	4 (2 males, 2 females)	7	2	4	2 abscess, 1 mild hydrocephalus, 1 gliosis
D2C7-IT high dose 2	Acute	0.4	10 (5 males, 5 females)	5	5 (3 males, 2 females)	9	8	2	3 mild hydrocephalus, 1 hemorrhage

[a] Control formulation: Potassium phosphates in saline, 2 % RSA, 2 μCi ^{124}I-HSA, 1 mM Gd-DTPA

The FOB was analyzed by Drs. William Wetsel and Ramona Rodriguiz with their research team. The FOB was conducted on the acute cohort on study day 4 for the 5-day study revealed that the male rats treated with the high dose of D2C7-IT displayed abnormal behaviors, including impaired exploration of the open field (**Figure 19**), which was secondary to gait and posture problems (**Figure 20**).

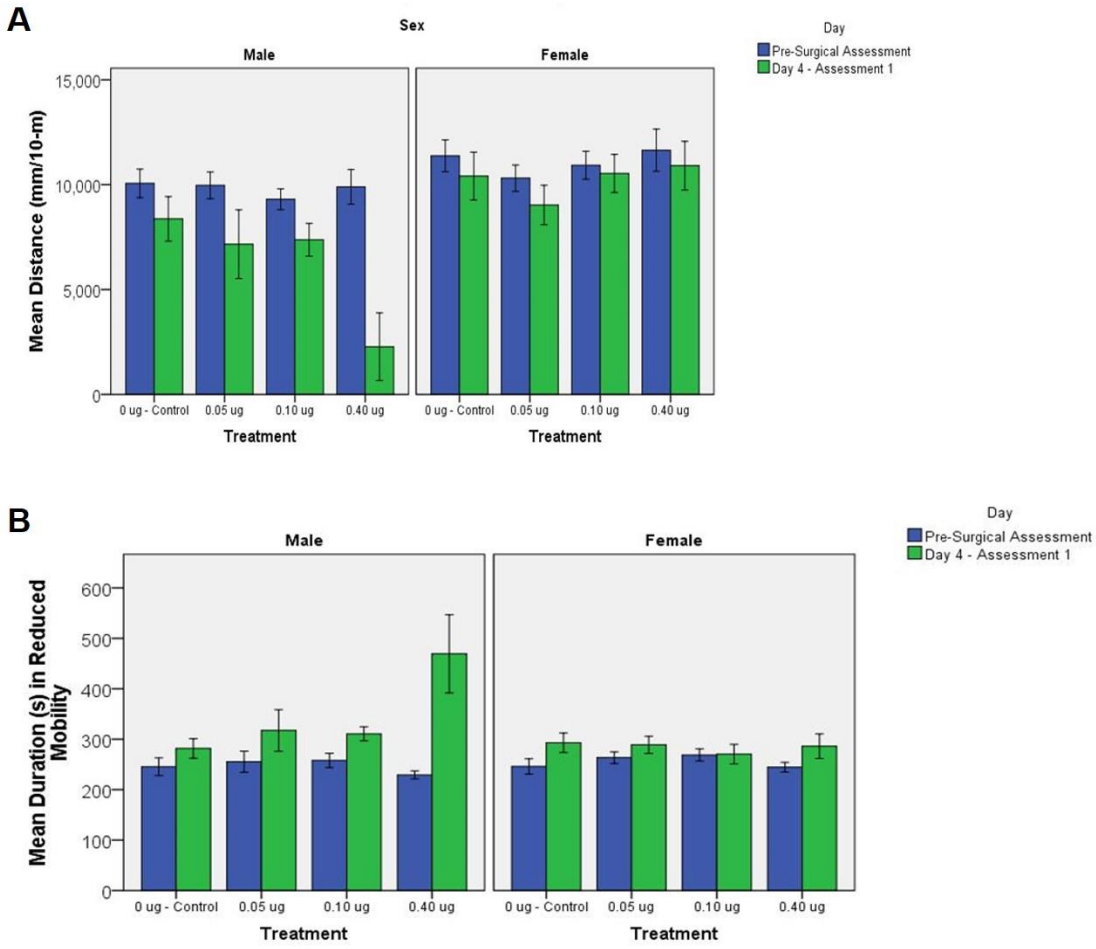

Figure 19: Open field test conducted on the acute cohort on study day 4 for the 5-day study.

(A) Mean distance in different treatment groups among genders; (B) Mean duration(s) in reduced mobility in different treatment groups among genders. From [76] with permission from publisher, see appendix for license.

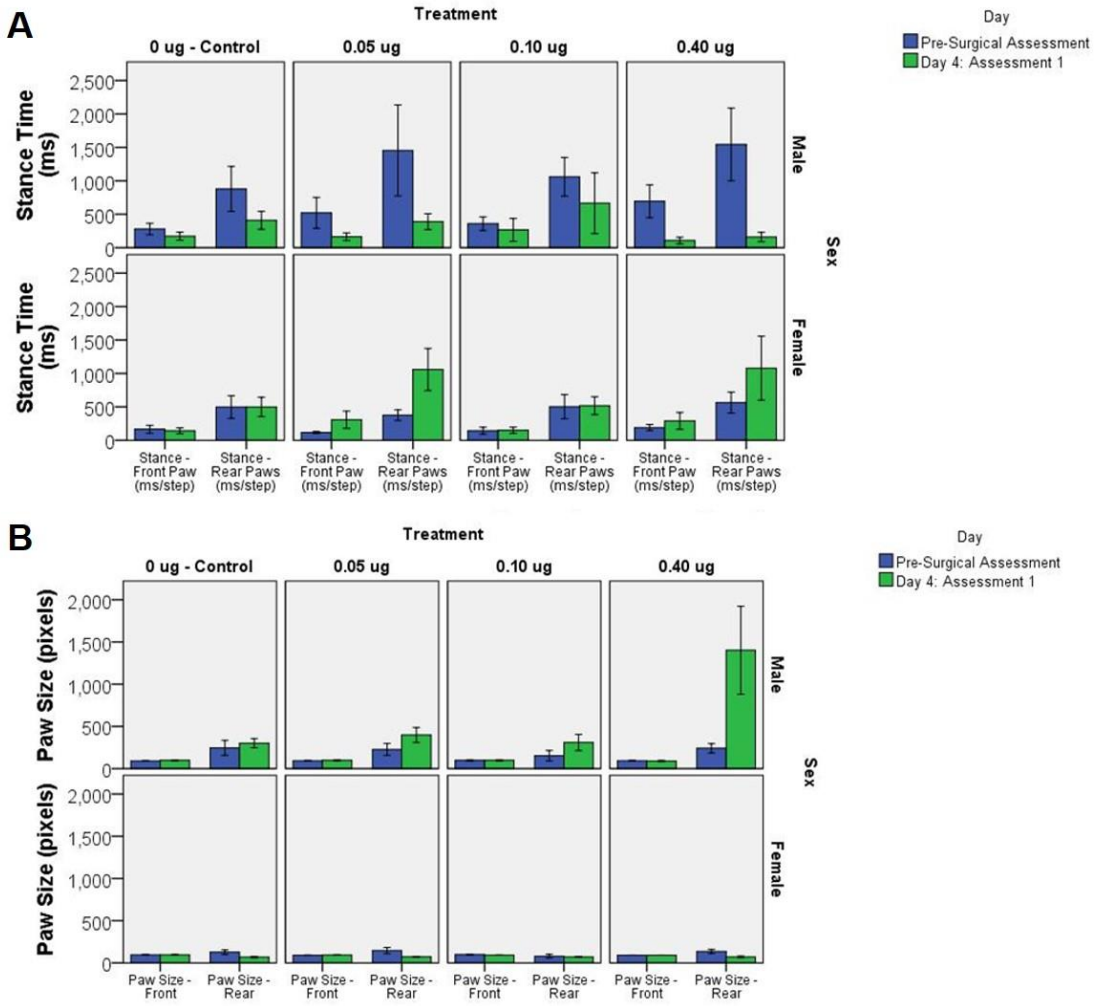

Figure 20: (A) Gait and (B) Posture measurement on the acute cohort on study day 4 for the 5-day study

From [76] with permission from publisher, see appendix for license.

Rats that were treated with 0.05 or 0.10 μg total doses of D2C7-IT, however, exhibited few changes. In addition to activity and gait, rats were assessed for general appearance, reactivity to handling, reaction to a single auditory "click" and core body temperature on day 4 of the 5-day assessment. No statistically significant overall effects were found for general appearance and reactivity to handling of the rats. Following surgery, 33.3 % of rats in the 0.40 μg treatment group failed to exhibit a startle response. For core body temperature, no effects of treatment were detected for females (**Figure 21**).

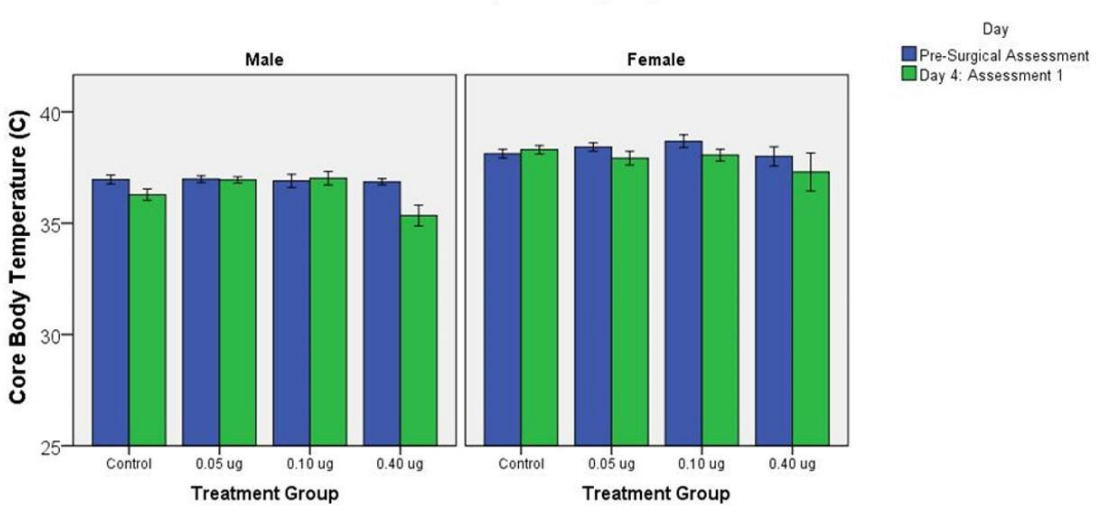

Figure 21: Core body temperature in different treatment groups among genders on the acute cohort on study day 4 for the 5-day study

From [76] with permission from publisher, see appendix for license.

By comparison, males given 0.40 μg D2C7-IT had a significant reduction in post-surgical relative to pre-surgical body temperatures. Together, these data show that by day 4 of the 5-day study, male rats given the highest dose of D2C7-IT were more likely to have

reductions in activity secondary to abnormalities in gait, reduced startle reactivity, and decreased core body temperatures. By comparison, female rats remained relatively unaffected with this treatment.

The rats in the D2C7-IT high-dose groups during both the 5- and 34-day studies showed similar behavioral changes during the FOB. However, in the 34-day study, many of the behavioral abnormalities observed on day 4 in the chronic cohort were not evident on study days 15 and 31, or they had declined in prevalence or severity. In the open field, female rats showed no marked effects of treatment on activity, whereas males administered 0.35 µg D2C7-IT failed to exhibit habituation to the open field across repeated exposures (**Figure 22**).

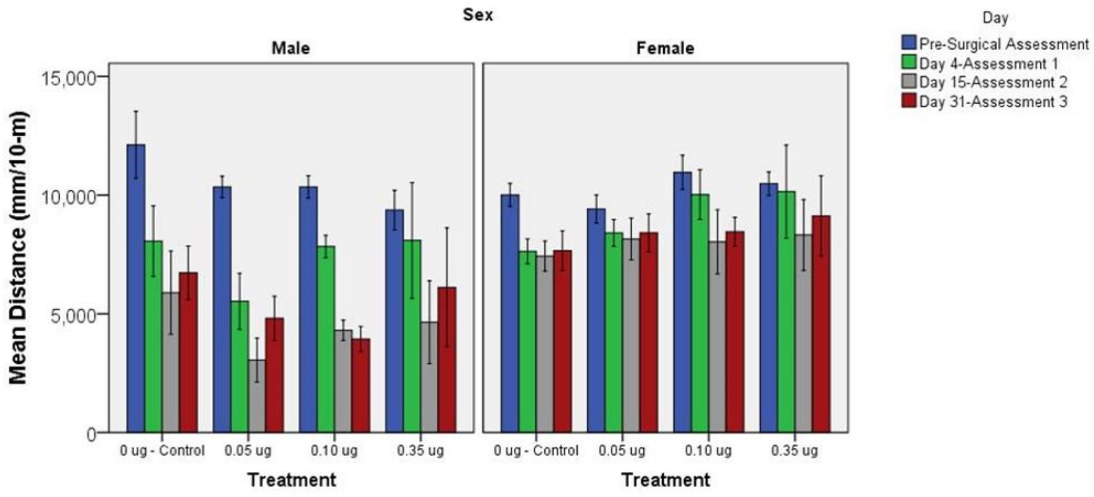

Figure 22: Open field test (distance) conducted on the chronic cohort on study days 4, 15, and 31 for the 34-day study

From [76] with permission from publisher, see appendix for license.

Furthermore, males that received 0.10 or 0.35 μg compound spent more time in low mobility on days 15 and 31 relative to females undergoing the same treatments (**Figure 23**). An investigation of gait during open field testing found the treatment effects were similar to those observed in the 5-day study (**Figure 24**).

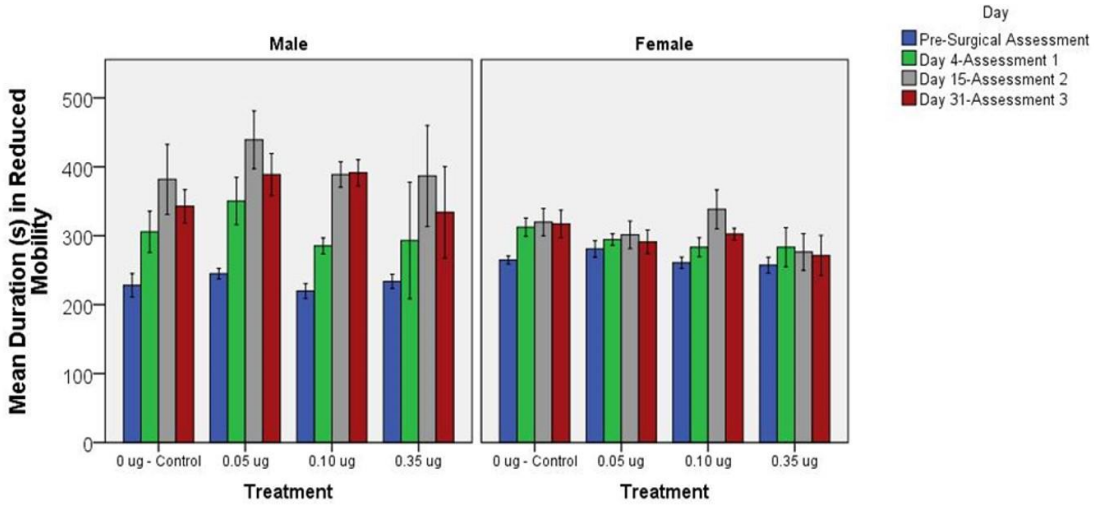

Figure 23: Open field test (duration in reduced mobility) conducted on the chronic cohort on study days 4, 15, and 31 for the 34-day study

From [76] with permission from publisher, see appendix for license.

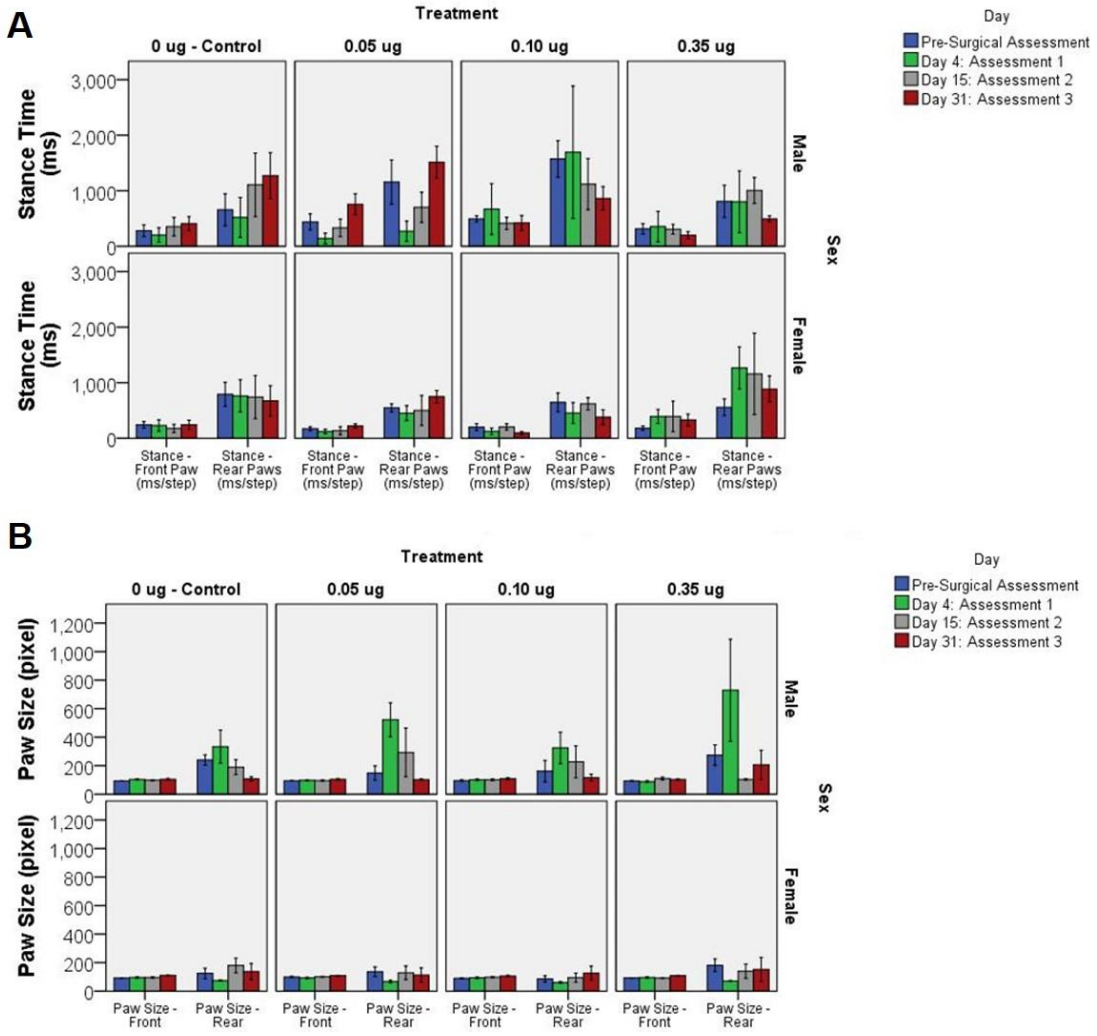

Figure 24: (A) Gait and (B) Posture measurement on the chronic cohort on study days 4, 15, and 31 for the 34-day study

From [76] with permission from publisher, see appendix for license.

The male rats treated with D2C7-IT exhibited changes in open field activity, which may be related to gait alterations. During the 34-day study, a few other observations were notable, including salivation/drooling, changes in the coloration of the oral tissues and gums, coordination of the animal during handling, and startle reactivity to an auditory

"click" stimulus. In each case, the effects of D2C7-IT were mild and only temporary, being fully resolved over the 34 days. Finally, no marked effects of D2C7-IT were found on core body temperature in the 34-day study. Taken together, the observations in the 34-day study support the findings of the short-term study. Behavioral abnormalities with D2C7-IT were observed in the animals treated with the highest doses of D2C7-IT and they were most pronounced in males. Despite these results, the behavioral effects of D2C7-IT were transient, and were not observed by the end of the 34-day study.

With regard to brain histopathology, the animals in the acute cohort exhibited features consistent with dose-related injuries, which were confined to those in the high-dose group. Edema (8/10 rats), ECM (9/10), and demyelination (2/10 rats) were more widely distributed and more frequently found in the high-dose group than in the other groups of the acute cohort (**Table 11 and Figure 25**).

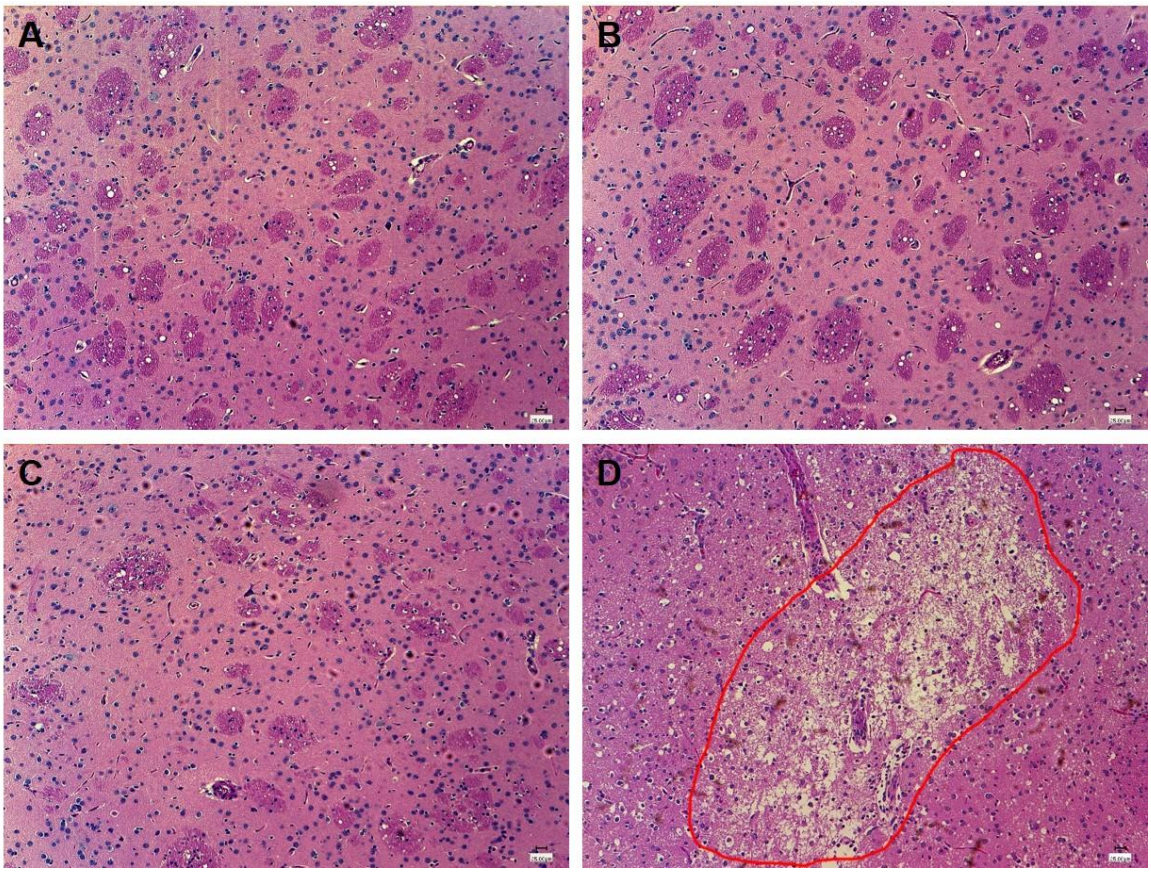

Figure 25: Brain histopathologic examination for different dose groups.

The pictures show that the ECM (within the red circle, 10X) more frequently occurred in the ipsilateral brain hemisphere of rats from the (D) high dose group than the (A) control, (B) low dose, or (C) median dose groups.

Among the animals in the high-dose group of the chronic cohort, a less obvious dose-related response was noted, with ECM, edema, and demyelination present in 7/10, 2/10, and 4/10 rats, respectively (**Table 11**). ECM was present at the injection site in the control group (10/20), low-dose group (7/20), and medium-dose group (7/10) of both cohorts (**Table 11**). However, edema and demyelination were not observed in the control, low-,

and medium-dose groups of either cohort (**Table 11**). Pathologic examination of the systemic tissues from the animals in both cohorts revealed no dose-related or drug-related findings.

The MTD of D2C7-IT administered by intracerebral CED over a 72-hour period was between 0.10 and 0.35 μg total dose (**Figure 26**). Considering the histopathologic and clinical findings, we conclude that the 0.05 μg total dose is the appropriate NOAEL for D2C7-IT in rats.

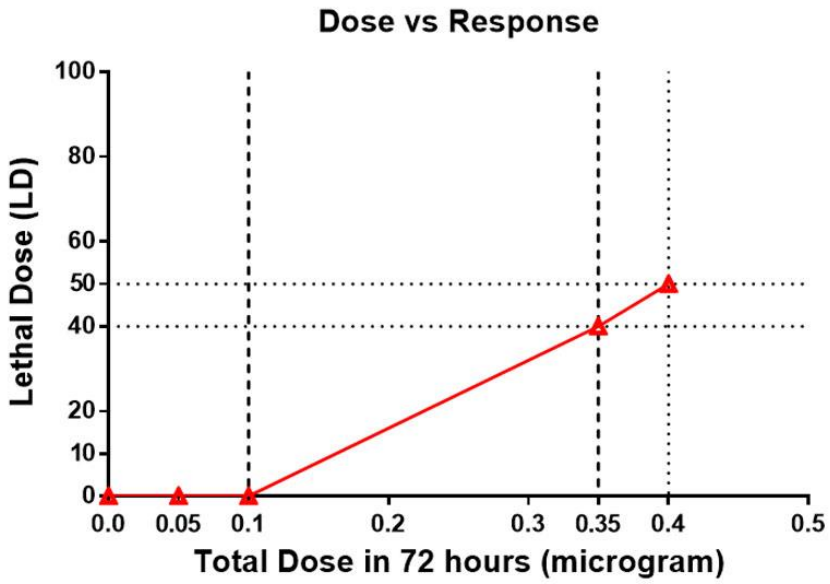

Figure 26: The D2C7-IT dose–response curve in the SD rat intracerebral CED model.

The curve demonstrates that the LD_{40} dose of the D2C7-ITwas 0.35 μg over 72 hours, while the anticipated LD_{10} dose lay between 0.1 and 0.35 μg over a 72-hour CED. From [76] with permission from publisher, see appendix for license.

3.2.3 Discussion and conclusions

Glioblastoma, the most malignant brain tumor, has the poorest prognosis, with a median survival time of less than 2 years. There is an urgent need for the development of advanced novel therapies to treat this fatal disease. D2C7-IT is a novel targeted IT developed in our laboratory. D2C7-IT has high affinity and specificity for both the EGFRwt and EGFRvIII proteins, it exhibits robust cytotoxic activities against glioblastoma cells expressing EGFRwt, EGFRvIII, or both (*in vitro*), and it significantly improves (>150 %) the survival of orthotopic mouse glioma models [48, 76]. Because the intravenous or oral delivery of macromolecules into the CNS is impeded by the BBB, especially with large soluble molecules such as antibodies or ITs [66], intratumoral administration of D2C7-IT was performed in our animal model by a CED method, in which we used an osmotic pump to deliver the protein directly into the brain [48, 76]. Intracerebral CED for IT delivery has been well established and has shown promise [71-73]. Co-infusion of Gd-DTPA (a small-molecule contrast agent) and ^{124}I-HSA has enabled the uses of MRI and PET scanning to accurately display imaging of the intracerebral distribution of an infused IT administered by CED. Co-infusion of Gd-DTPA and ^{124}I-HSA has been demonstrated to be a safe and minimally invasive technique for patients [70].

A preclinical rat GLP study was performed to evaluate the systemic toxicity of intracerebral CED of D2C7-IT in a formulation containing Gd-DTPA and ^{124}I-HSA,

because co-infusion of these tracers will be used to monitor D2C7-IT intracerebral delivery and distribution in patients. Several preclinical toxicity trials were performed to determine the MTD and NOAEL as references for the initial dosing in our Phase I clinical trial. Nevertheless, numerous unexpected obstacles emerged during these trials, including the osmolality of the dose formulation, the potential absorption of the IT into the interior reservoir of the osmotic pump, non-optimal pump flow rate for the rat brain, and potential immunogenicity and adverse effects of HSA in the formulation.

3.2.3.1 Osmolality of the dose formulation

As summarized in **Table 7**, abnormal clinical signs were observed in animals in all dose groups in the TOX-2013-001 trial. Histopathologic lesions (including ECM, gliosis, and demyelination) were detected in the brains of animals in all dose groups, including the control group. Because all animal groups were equally affected, the control formulation, which was a common parameter across all groups, was assessed for potential flaws. Osmolality is a critical factor for agents delivered into the CNS [94, 95]. The osmolality of a normal rat's CNS is 290–300 mOsm/l H_2O. In the TOX-2013-001 trial, 0.05 M PBS-0.9 % saline was used in the control formulation to dilute D2C7-IT, Gd-DTPA, and ^{124}I-HSA, because it is widely used clinically as a diluent. However, the osmolality of the 0.05 M PBS-0.9 % saline solution was approximately 370 mOsm/l H_2O, which was more hypertonic than a normal rat's CNS. The hypertonicity of the formulation could have been one of the major factors causing the adverse events

observed in all groups. Therefore, in subsequent trials, the osmolality of the dose formulation was adjusted to 290–300 mOsm/l H_2O with an appropriate concentration of phosphate buffer (**Tables 10 and 11**).

3.2.3.2 Potential adsorption of the IT into the interior reservoir of the osmotic pump

In the TOX-2-13-001 trial, the pumped-out D2C7-IT test formulation showed an approximately 10-fold loss of biological activity compared with the bulk D2C7-IT under the same conditions based on the inhibition of A431P and NR6M cell viability measured after 48 hours of incubation (**Tables 8 and 9**,respectively). This finding suggested that the concentration of D2C7-IT in the pumped-out solution was much lower than that in the bulk solution. Because a 1–5 % concentration of the carrier protein was recommended by the pump manufacturer to be included in the formulation to minimize test article (D2C7-IT) adsorption in the osmotic pump, the HSA concentration was increased from 0.2 to 3 % to prevent D2C7-IT adsorption into the interior reservoir of the pump. The increased HSA concentration in the formulation restored the *in vitro* cytotoxic activity of the pumped-out D2C7-IT (in 3 % HSA solution) (data not shown). As a result, a 3 % HSA concentration was used in the dose formulation in the TOX-2013-002 trial.

3.2.3.3 Optimal pump flow rate for the rat brain

Adverse events, body weight loss, and unscheduled mortality were again observed after intracerebral delivery of the new control formulation in all treatment

groups during the TOX-2013-002 trial. Brain histopathology revealed regions of ECM largely centered in the centrum semiovale that corresponded to the injection site in all study groups. The observed abnormalities could have developed because the volume of the pumped out formulation was too high for the rat brain. Based on the results of a previous IT preclinical toxicity study, an Alzet pump 2ML1 (size: 2 ml; duration: 7 days) was used in the TOX-2013-001 and TOX-2013-002 trials to continuously deliver the formulations into the rat brain at a flow rate of 10 μL/hour for 72 hours [75, 96]. However, upon consultation with the pump manufacturer and senior investigators from the Department of Psychiatry and Behavioral Sciences at Duke University, who have extensive experience with the use of osmotic pumps in preclinical animal models, a lower flow rate (e.g., less than 5 μL/hour) was suggested to be preferential for administering compounds into the rat brain parenchyma. Therefore, in subsequent trials, we switched to a smaller Alzet pump 2001 (size: 200 μL; duration: 7 days) with a slower flow rate of 1 μL/hour for intracerebral infusion.

3.2.3.4 Potential HSA immunogenicity and adverse effects in rats

A second unexpected finding of the TOX-2013-002 trial was the occurrence of kidney lesions after infusion. Kidney histopathology revealed a similar number of lesions in the control and test article dose groups, including acute tubular necrosis, foci of lymphocytes and inflammation, and areas of calcification. None of these lesions occurred in a dose-related manner, implying that a common component of the control

and test articles was responsible for the abnormal findings in the kidney. Because its concentration was increased from 0.2 to 3 %, the total amount of HSA infused into the CNS was nearly 22 mg per rat over the 72-hour period. Harling-Berg and colleagues [97] have previously reported efficient immunization of rats with only 90 μg HSA microinfused into the rat's lateral ventricle. Moreover, HSA has been demonstrated to be more immunogenic when microinfused into cerebrospinal fluid (CSF) than when injected intravenously, intramuscularly, or intraperitoneally. HSA antigenicity leads to the formation of soluble circulating immune complexes, which can result in glomerular injury [98]. Possible HSA immunogenicity may explain the kidney lesions found in all treatment groups, including the control group. The HSA formulation was actually used to accurately replicate the intended human clinical formulation; however, after demonstrating the potential toxicity of HSA in SD rats, the FDA agreed to substitute RSA for HSA.

A satisfactory outcome was observed with the uses of the modified control formulation containing 2 % RSA and a smaller osmotic pump with a slower flow rate, which was used in the vehicle-only trial. Unfortunately, right after the vehicle test trial, the sodium phosphate injection (Hospira, Lake Forest, IL) used in the dose formulation was nationally back ordered. Upon consultation with the Duke Medical Center pharmacist, potassium phosphate injection was utilized as an alternative to sodium phosphate buffer for the official GLP trial (TOX-2014-001). After successful completion

of the TOX-2014-001 trial, the MTD of the D2C7-IT administered via intracerebral CED over a 72-hour period was determined to be between a total dose of 0.1 and 0.35 μg and the NOAEL was a total dose of 0.05 μg in SD rats. Based on this successful GLP toxicity study, an FDA IND (#116855) is now in effect for a Phase I/II D2C7-IT clinical trial (NCT02303678, D2C7 for Adult Patients with Recurrent Malignant Glioma, clinicaltrials.gov), and patients with recurrent glioblastomas have been treated without obvious toxicity at the doses of 40, 80, and 120 ng of D2C7-IT administered by CED intratumorally for 72 hours.

In this preclinical GLP study, the systemic toxicity of a novel IT, D2C7-(scdsFv)-PE38KDEL, was examined in a rat intracerebral CED model over a 72-hour period. Several critical issues emerged during the first two trials, including the osmolality of the dose formulation, the pump flow rate, the adsorption of the IT into the pump interior reservoir, and the HSA immunogenicity and adverse effects in rats. These issues were addressed by correcting the osmolality of the dose formulation, selecting a smaller osmotic pump with a slower flow rate, and substituting 2 % RSA for 3 % HSA. Ultimately, the MTD of D2C7-IT was determined to be between a total dose of 0.10 and 0.35 μg, and the NOAEL of D2C7-IT was a total dose of 0.05 μg in SD rats. Both the MTD and NOAEL were utilized as references for the D2C7-IT clinical trial design.

3.3 The secondary anti-tumor immunity induced by D2C7-IT therapy in immunocompetent mouse glioma models

3.3.1 Introduction

It is known that immunotoxins can induce direct killing of cancer cells that express high levels of the targeted tumor antigen. When tumor cells are dying from the immunotoxin therapy, they may release tumor antigens and/or other neoantigens. These antigens can be presented by the APCs to host T cells, which will activate specific CTLs to eliminate remaining or recurrent tumor cells [56]. This phenomenon was reported in the subcutaneous (SC) melanoma mouse model treated with an immunotoxin targeting IL-13, in which CTLs played a major role in mediating an immunotoxin-induced anti-tumor response [99]. In the previous clinical trial that involved the use of TP-38 immunotoxin to treat malignant brain tumors [79, 100], the postponed regressions of tumors and adverse effects were observed in one patient (**Figure 27**), which was incompatible with the direct and rapid cell killing caused by the localized immunotoxin therapy, indicating a secondary anti-tumor immunologic mechanism that promoted the primary killing of immunotoxins.

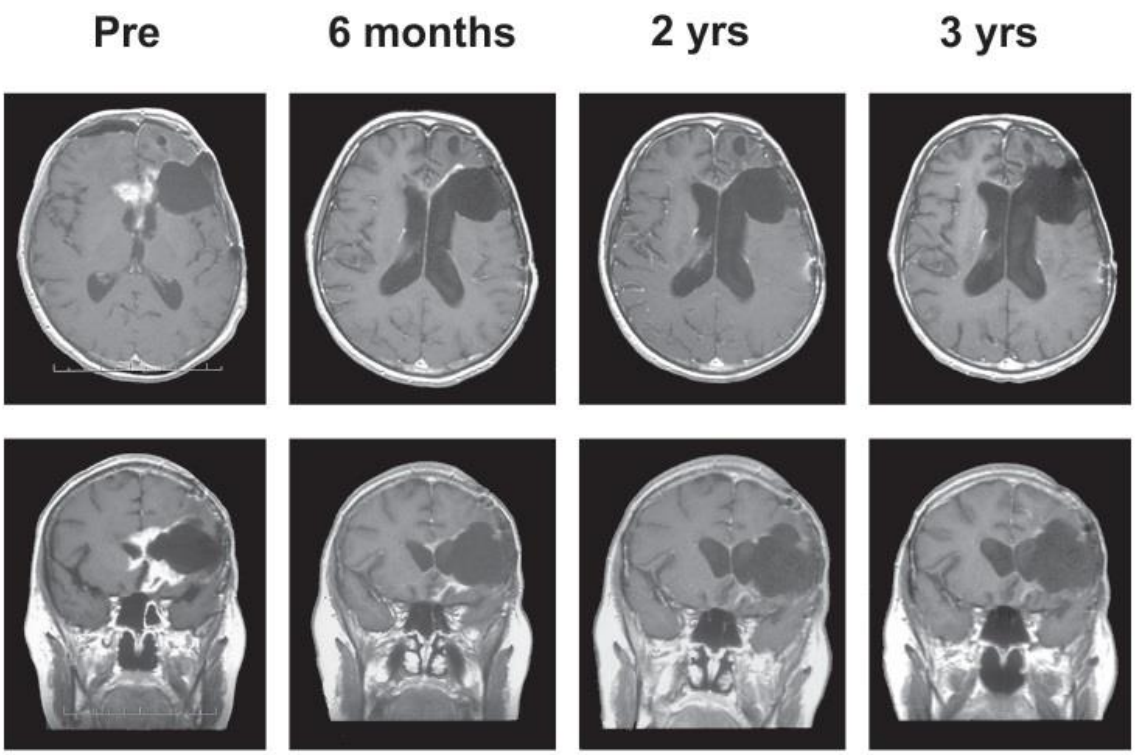

Figure 27: Contrast-enhanced axial (top panels) and coronal (bottom panels) MRI images showing extent of tumor prior to treatment and at six months, two years, and three years after TP-38 treatment.

TP-38 was an immunotoxin targeting EGFRwt, which was overexpressed on glioblastoma cells. After the TP-38 treatment, the pre-treatment enhanced tumor region disappeared in the long term. From [100] with permission from publisher, see appendix for license.

One of our collaborators revealed that an EGFRvIII-targeted immunotoxin can induce anti-tumor immunity in a SC mouse glioma model, which can be inhibited in the absence of $CD4^+$ and $CD8^+$ T cells [101]. However, in the previous IL-13 immunotoxin study, researchers investigated the secondary immune response against melanoma, which is a dramatically different type of tumor compared to malignant gliomas in the

CNS. Because the EGRFvIII-targeted immunotoxin study used a SC glioma model, in which the intratumoral (i.t.) immunotoxin treatment was performed immediately after the SC inoculation of the tumor cell suspension, it was hardly able to represent the i.t. treatment against the natural SC grown tumor mass. Therefore, it is necessary to establish appropriate animal experiments to investigate the secondary immune response, induced by immunotoxins, against glioblastomas.

The interaction between tumor cells and the host immune system is a critical determinant of tumorigenesis. It is hypothesized that the immune system will try to eliminate tumor cells through a multiple-step response cycle after the primary immunotoxin therapy. The antigens from tumor cells destroyed by localized immunotoxin therapy are released at the tumor site, then presented by APCs to prime and activate T cells against those tumor-specific antigens in the local drainage lymph nodes, such as cervical lymph nodes for malignant brain tumors [102]. These activated CTLs can then migrate back to the tumor site at which they can infiltrate the tumor tissue and specifically detect and kill the tumor cells expressing those specific antigens. This CTL-mediated cell killing then results in the release of increasing tumor-associated antigens to continue this cascade [102]. During the immune response cycle, diverse immune checkpoint pathways between T cells and APCs and/or between T cells and tumor cells trigger co-stimulatory or co-inhibitory signals to enhance or suppress the activation of T cells, respectively. The balance among various immune checkpoint

pathways can regulate the continuation and intensity of the T-cell-mediated anti-tumor immunity [102]. Many previous studies have demonstrated that immune checkpoint inhibitors, such as anti-CTLA4 and anti-PD1 mAbs, can block those co-inhibitory mechanisms and therefore enhance the tumor cell killing by lymphocytes (**Figure 28**).

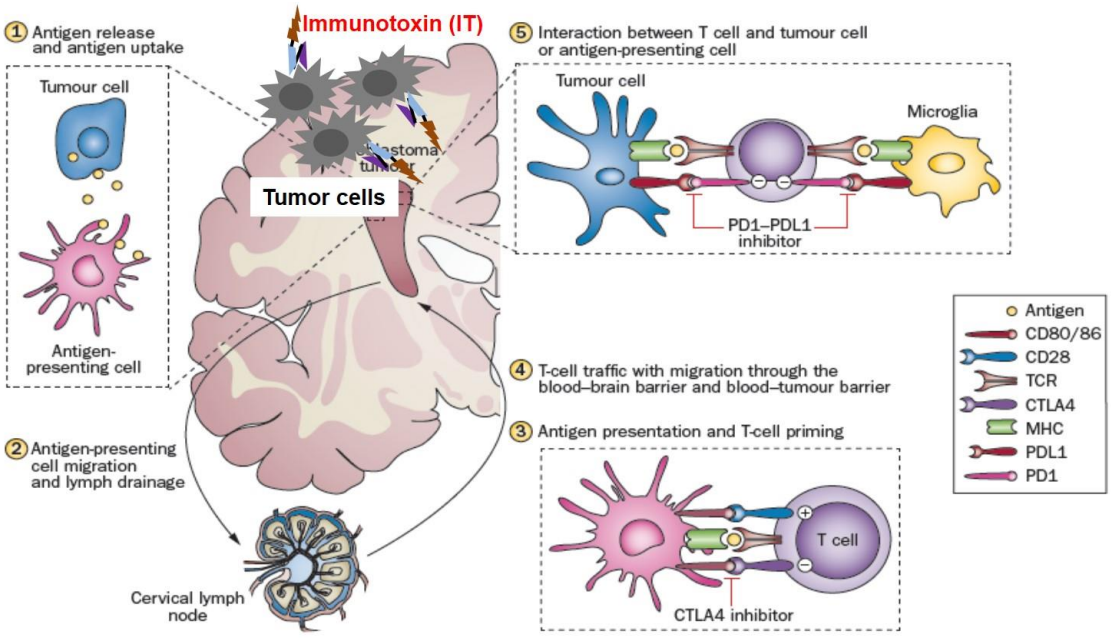

Figure 28: Overview of the immune response and major immune checkpoint molecules in the immune cycle of glioblastoma.

Antigens released from tumour cells killed by immunotoxins are taken up by APCs, microglia and macrophages (1) Antigens are trafficked to lymph nodes via migration of APCs, and via drainage through lymphatic vessels in the meningeal sinuses (2) In the lymphatic tissues, antigen presentation and T cell priming takes place. This interaction is tightly regulated by a multitude of co-inhibitory (CTLA4) and co-stimulatory (CD28, CD80, CD86) immune checkpoint molecules, and could be modulated by specific therapeutic antibodies, such as the CTLA4 inhibitor (3) Activated T cells reach the tumour via the blood stream and migration through the blood–brain or blood–tumour barrier (4) Tumour-associated immunosuppressive factors, including immune checkpoint molecules, inhibit tumour cell destruction by T cells. PDL1 is expressed on tumour cells and microglia and inhibits T cells via binding to PD1. PD1–PDL1 inhibitors block this immunosuppressive mechanism and thereby increase tumour cell lysis by

lymphocytes (5) Adapted from [56] with permission from publisher, see appendix for license.

3.3.2 Results

3.3.2.1 Antigen-binding specificity of D2C7 mAb to epitope-expressing mouse glioma cell lines

Assessment of D2C7-IT immunotherapy in syngeneic murine immunocompetent models requires special consideration because D2C7-IT does not target and bind mouse EGFR (mEGFRwt/mEGFRvIII) proteins. The D2C7 epitope is composed of a conformational determinant of 55 amino acids. There is a mismatch of 7 amino acids between the human (h) and mouse (m) EGFR sequence in the D2C7 epitope region. To facilitate D2C7 binding to mEGFRwt/mEGFRvIII, our laboratory developed two mouse glioma cell lines by mutating the DNA sequence corresponding to the seven amino acids in the mEGFR protein using site-directed mutagenesis to create the human D2C7 epitope. This chimeric construct was designated mD2C7 and was used to generate mouse brain tumor cell lines for D2C7-IT targeted therapy in syngeneic immunocompetent mouse models. The mouse glioma cell lines CT2A and SMA560 [103] were transduced with the mD2C7 construct to establish CT2A-mD2C7and SMA560-mD2C7 cell lines. The D2C7 mAb exhibited binding to these two cell lines in the flow cytometry analysis (**Figure 29**).

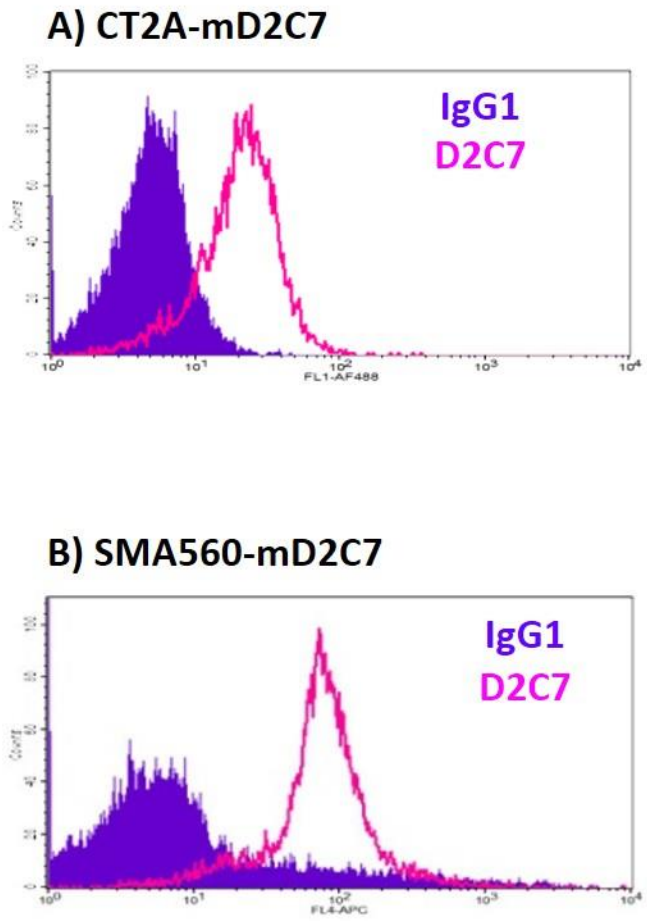

Figure 29: Binding of D2C7 mAb to mouse mD2C7 glioma cell lines, (A) CT2A-mD2C7, and (B) SMA560-mD2C7 cells.

3.3.2.2 *In vitro* cytotoxicity of D2C7-IT against epitope-expressing mouse glioma cell lines

After the D2C7 mAb exhibited binding to the two cell lines, we then examined the effects of D2C7-IT on the two epitope-expressing mouse glioma cell lines, CT2A-mD2C7 and SMA560-mD2C7. The cytotoxicity of D2C7-IT was determined by WST-1 cell proliferation assay. The cytotoxicity of D2C7-IT on the CT2A-mD2C7 and SMA560-

mD2C7 cells were 0.47 ng/mL and 1.05 ng/mL, respectively (**Figure 30**). The control immunotoxin, P588-IT, exhibited no (>1000 ng/mL) or non-specific (510 ng/mL) cytotoxic activity against both CT2A-mD2C7 and SMA560-mD2C7 cells, respectively.

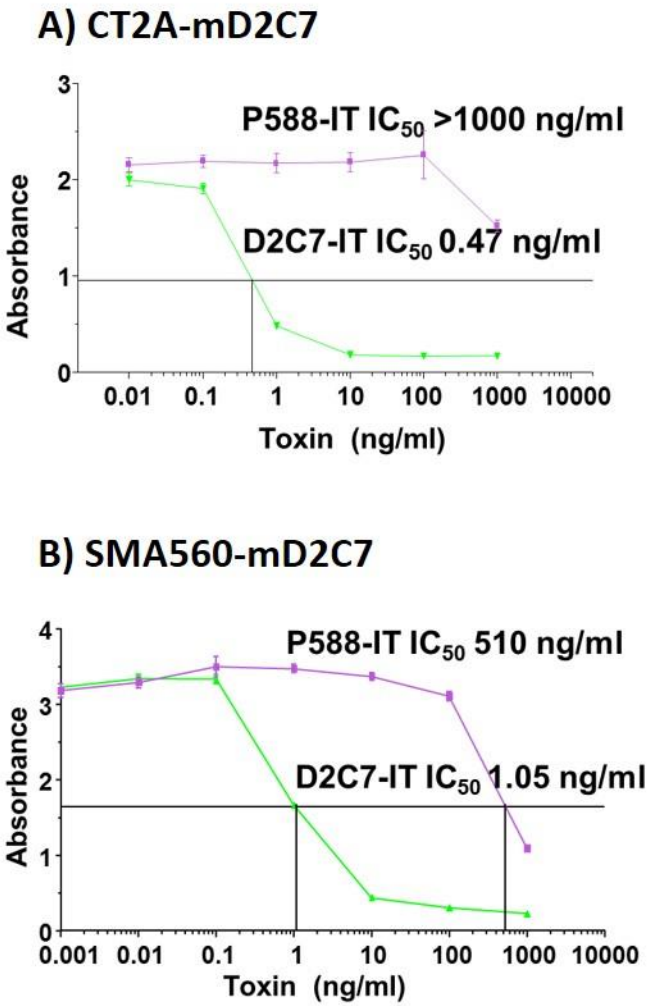

Figure 30: ***In vitro*** **cytotoxicity of D2C7-IT against mD2C7 glioma cell lines, (A) CT2A-mD2C7, and (B) SMA560-mD2C7 cells.**

3.3.2.3 Mouse major histocompatibility complex (MHC) class I expression on mD2C7 mouse glioma cell lines

The mouse MHC, which is also called the H2 complex, is located on chromosome 17 [104]. As shown in **Figure 8**, the MHC complex is essential to the functioning of the immune system. The proteins made by these genes show a dramatic amount of polymorphism. The main function of MHC molecules is to bind and present small peptides to the cell surface [104]. These presented peptides, along with specific areas of the MHC class I molecule, are the structures that interact with the TCR of $CD8^+$ CTLs leading to the activation of a CTL response, which plays an important role in the anti-tumor immunity (**Figure 28**). One of the most common means by which tumors escape from the host immune response is to down-regulate the MHC class I molecule expression, leading to the ineffectiveness of endogenous or therapeutic anti-tumor T cell responses [105]. Therefore, it is important to examine the MHC class I molecule expression on the mouse glioma cells before conducting the experiments to investigate the secondary immune response induced by the immunotoxin therapy. Although the CT2A-mD2C7 and SMA560-mD2C7 cell lines originate from two different mouse strains C57BL/6 and VM/Dk, respectively, the MHC class I molecules for both mouse strains are the same H-$2K^b$ and H-$2D^b$ molecules [104, 106]. Direct FACS analysis shows that both CT2A-mD2C7 and SMA560-mD2C7 cell lines have a robust expression of the MHC class I molecules (**Figure 31**).

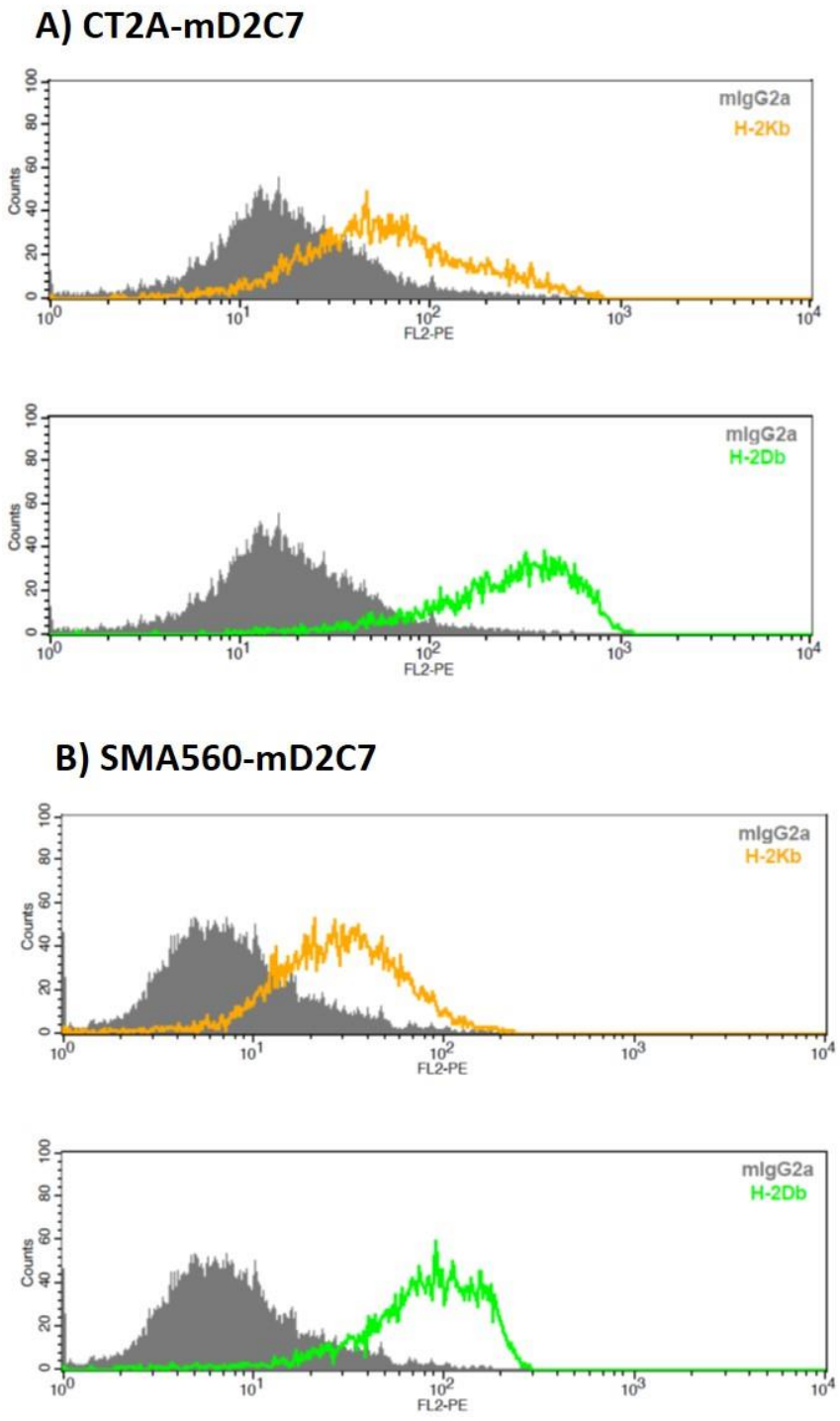

Figure 31: Expression of mouse H-2K^b (yellow) and H-2D^b (green) on (A) CT2A-mD2C7 and (B) SMA560-D2C7 cells

3.3.2.4 Mouse PDL1 expression on mD2C7 mouse glioma cell lines

Considering the heterogeneity of PD1 ligands level and their potential to be indicators for anti-PD1 immunotherapy, it is critical to know what mechanisms regulate their expression on tumor cells. Two common mechanisms to regulate PDL1 expression by tumor cells are the innate and adaptive resistance. In glioblastomas, it was revealed that PDL1 expression is constitutive as the innate immune resistance [53]. Thus, the direct FACS analysis was used to detect the PDL1 expression on those two mouse glioma cell lines, which shows that both cell lines have a high constitutive expression of PDL1 on the cell surface (**Figure 32**).

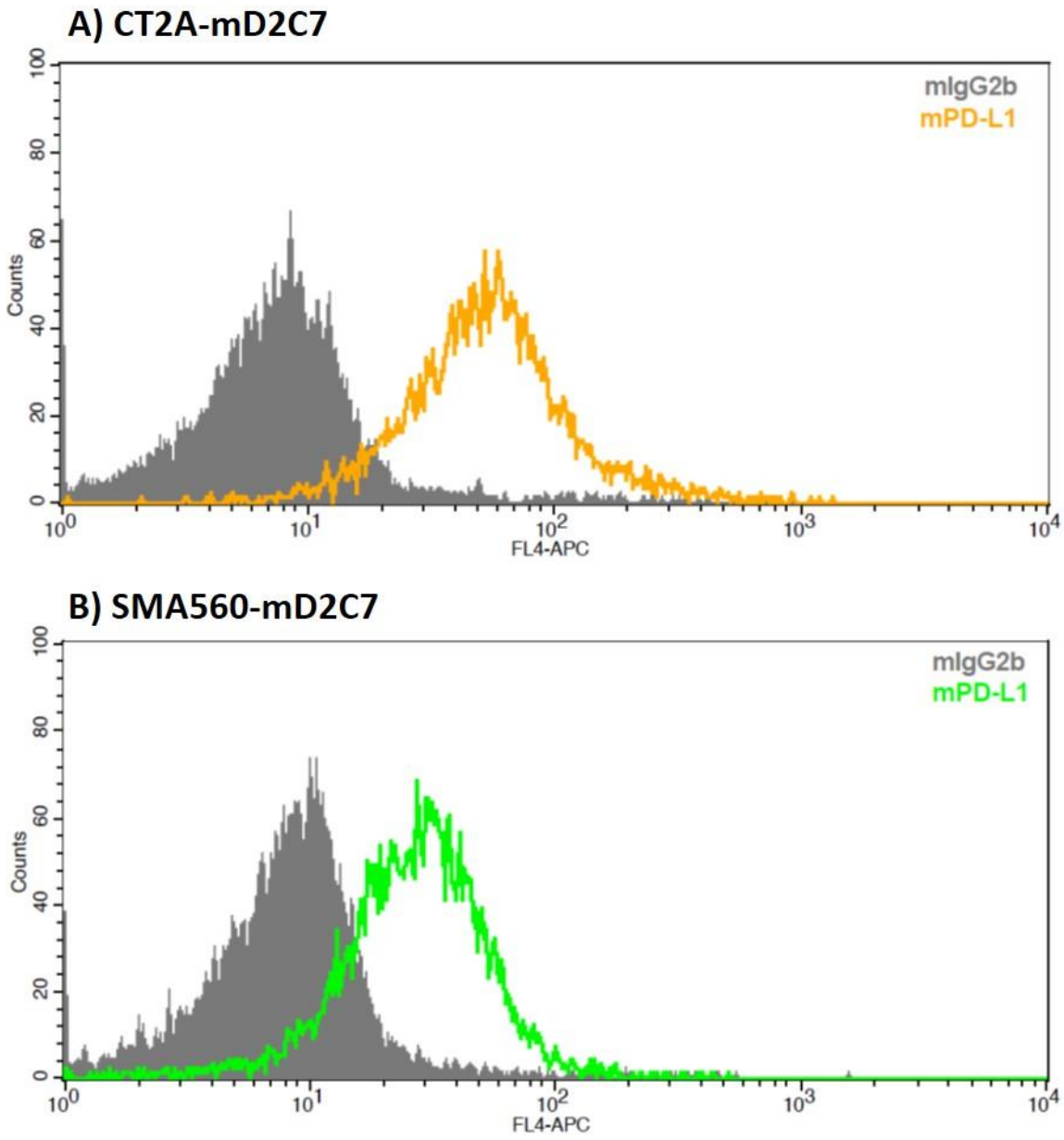

Figure 32: Expression of mouse PD-L1 on (A) CT2A-mD2C7 and (B) SMA560-D2C7 cells

3.3.2.5 *In vivo* efficacy of D2C7-IT+anti-CTLA4/anti-PD1 inhibitors combinatorial therapy in a SC CT2A-mD2C7 glioma model.

In my previous pilot studies, it was observed that the SC rechallenged mouse glioma allografts were rejected in those immunocompetent mice bearing SC mouse glioma allografts cured by the i.t. immunotoxin therapy (**Figure 33**), suggesting that there can be a memory anti-tumor immune response following the SC immunotoxin therapy. This phenomenon was also reported in the SC melanoma mouse model treated by an immunotoxin targeted IL-13, in which CTLs played a major role in mediating this immunotoxin-induced anti-tumor response [99], although melanoma is a dramatically different type of tumor compared to malignant gliomas in the CNS. Therefore, it is necessary to establish appropriate mouse glioma models to investigate the secondary immune response, induced by immunotoxins, against glioblastomas, and to determine how to enhance this response by the combinatorial therapy of immune checkpoint inhibitors, such as anti-CTLA4/PD1 antibodies (αCTLA4/PD1), in order to achieve a long-lasting remission.

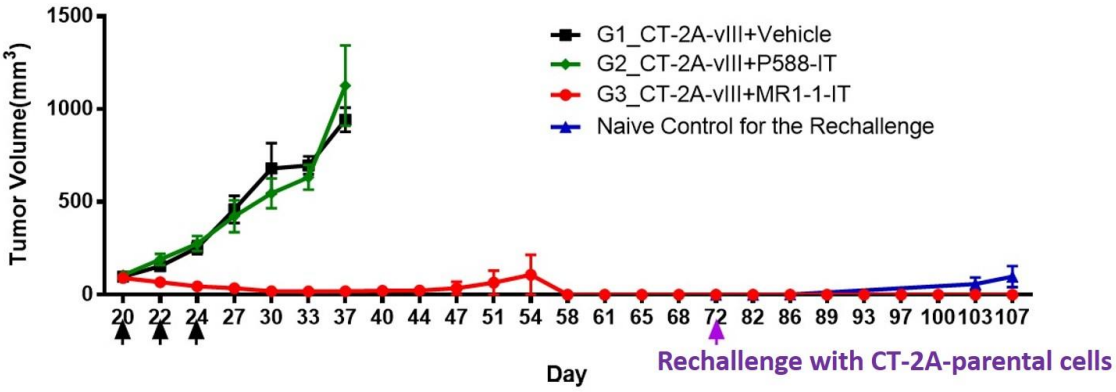

Figure 33: Preliminary *in vivo* experiment to show the secondary anti-tumor immunity induced by the immunotoxin monotherapy.

Three high doses of MR1-1-IT (an immunotoxin targeting EGFRvIII) were i.t. administered to treat the SC (right flank) CT2A-vIII glioma-bearing C57BL/6 immunocompetent mice. All cured mice by MR1-1-IT therapy rejected the rechallenged CT2A parental cells (left flank), whereas the CT2A parental cell grew in all the naïve control mice.

I established a SC mouse CT2A-mD2C7 glioma model in C57BL/6 immunocompetent mice with six groups, in which the mice were treated by the control immunotoxin P588-IT or D2C7-IT, combined with αCTLA4 or αPD1 inhibitors. In this *in vivo* SC CT2A-mD2C7 glioma model, four doses (every 3 days) of the D2C7-IT (low dose, 1.5 μg per mouse per dose, i.t.) but not αCTLA4 (100 μg per mouse per dose, i.p.) or αPD1 (250 μg per mouse per dose, i.p.) monotherapy and D2C7-IT+αCTLA-4/αPD-1 combinatorial therapy (immune checkpoint inhibitors administered on the next day after IT therapy) generated a significant delay in tumor growth compared to the control immunotoxin P588-IT treatment groups ($P < 0.01$, **Figure 34A**). Importantly, complete cures were only observed in D2C7-IT+αCTLA4 (n = 4/10) and D2C7-IT+αPD-1 (n = 5/10)

combinatorial therapy groups (**Figure 34B**), although D2C7-IT monotherapy could also significantly delay the tumor growth.

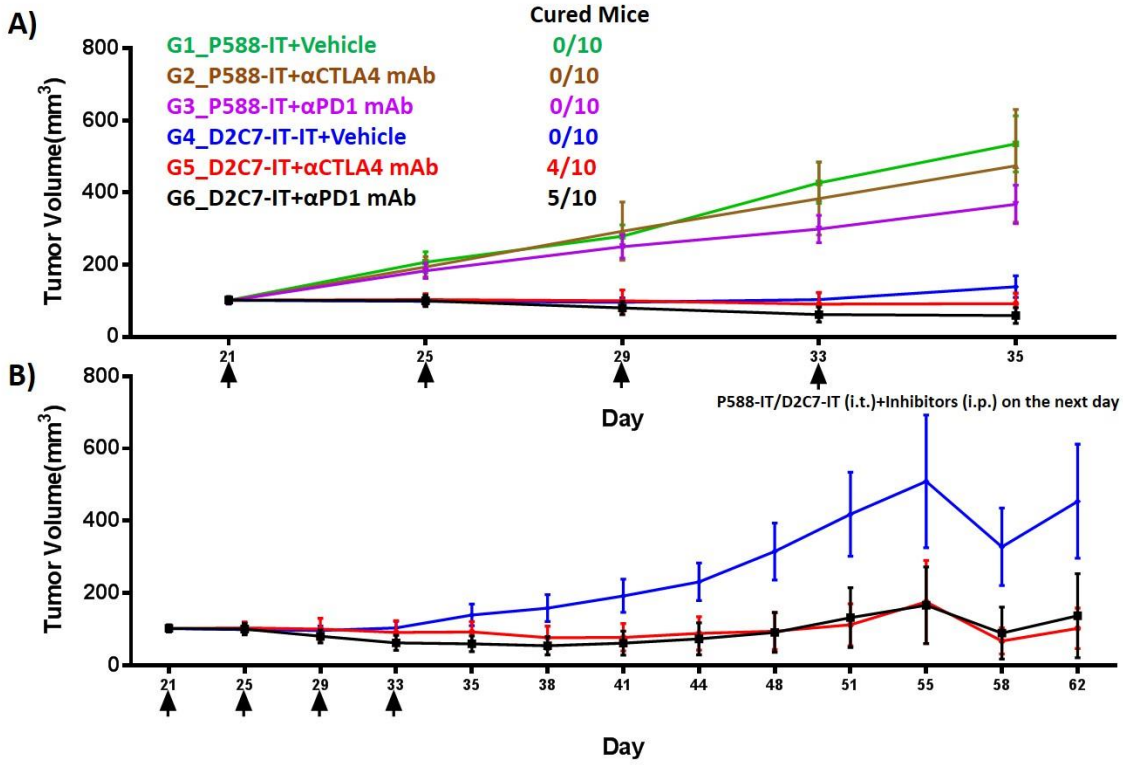

Figure 34: *In vivo* efficacy of D2C7-IT and αCTLA-4/αPD-1 mAb combinatorial therapy in SC CT2A-mD2C7 glioma-bearing C57BL/6 immunocompetent mice.

(A) All the treatment groups followed up to Day 35 after the initial tumor inoculation. Group 4-6 showed significant tumor growth delay compared to other groups ($P < 0.01$); (B) Group 4-6 followed up to Day 62 after initial tumor inoculation. 4 out of 10 and 5 out of 10 mice were cured only in Group 5 and Group 6, respectively. Data were plotted in Mean ± Standard Error (SE), and n = 10 for each group.

3.3.2.6 Tumor rechallenging studies in the cured mice from the D2C7-IT and immune checkpoint inhibitors combinatorial treatment groups described in Chapter 3.3.2.5

To determine whether those cured mice from D2C7-IT and immune checkpoint inhibitors combinatorial treatment groups can recall a protective anti-tumor memory immune response, on Day 72 after the initial tumor challenge, all nine cured mice were then first SC rechallenged (1° SCR) with another dose of 10^6 CT2A parental cells in the left flank. All these mice rejected the mD2C7-negative tumors, whereas tumors grew in all untreated naïve mice, suggesting that the combinatorial treatment provided long lasting anti-tumor immunity that extended to mD2C7-negative parental cells as well (**Figure 35A**).

To determine whether this protective anti-tumor immunity can protect the mice from the tumor rechallenging in a remote immune-privileged region, for example, the brain, all nine cured mice were then intracranially (IC) rechallenged (2° ICR) for a second time on Day 126 (after the initial tumor challenge) with a dose of 3×10^5 CT2A-mD2C7 cells in the brain. At the end of this study, all survived mice were euthanized for brain histopathologic examination, which did not show tumors in the brains (data not shown). All these mice rejected the CT2A-mD2C7 2° ICR, whereas tumors grew in all untreated naïve mice, suggesting that the combinatorial treatment also provided long lasting anti-tumor immunity that extended to the remote immune-privileged CNS as well (**Figure 35B**).

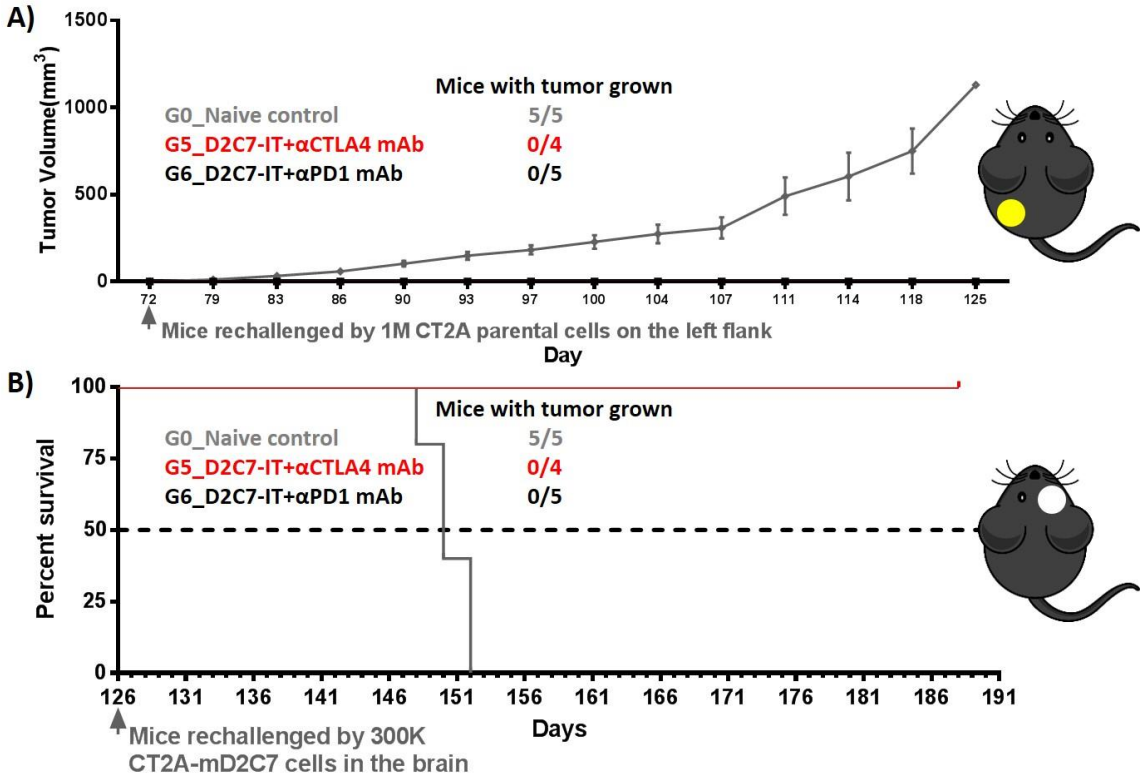

Figure 35: Tumor rechallenging studies on the cured mice in the combinatorial treatment groups.

Nine cured mice were first rechallenged by (A) 10^6 CT2A parental cells in the left flank on Day 72 after the initial tumor challenge, and then (B) by 3×10^5 CT2A-mD2C7 cells in the brain on Day 126 after the initial tumor challenge. Tumors grew in all untreated naïve mice, whereas no tumor grew in those cured mice. Data were plotted in Mean ± SE.

3.3.2.7 *In vivo* efficacy of D2C7-IT+anti-CTLA4/anti-PD1 inhibitors combinatorial therapy in a bilateral SC CT2A-mD2C7 glioma model.

In this *in vivo* bilateral SC CT2A-mD2C7 glioma model, tumor cells were inoculated in both sides of the flank simultaneously in C57BL/6 mice, with a high density (3×10^6 cells) on the right side and a low density (10^6 cells) on the left side. The

larger tumors (on the right) were treated with four doses (every two days) of D2C7-IT/αCTLA4/αPD1 monotherapy or D2C7-IT+αCTLA4/αPD1 combination therapy (immune checkpoint inhibitors administered on the same day of IT therapy), while the left tumors were untreated. The D2C7-IT monotherapy (high dose, 4.5 μg per mouse per dose, i.t.), D2C7-IT+αCTLA4 (100 μg per mouse per dose, i.p.), and D2C7-IT+αPD1 (250 μg per mouse per dose, i.p.) combinatorial therapies led to significant growth delays of the right tumor ($P < 0.01$), which cured 4/10, 6/10, and 5/10 right tumors, respectively (**Figure 36A**).

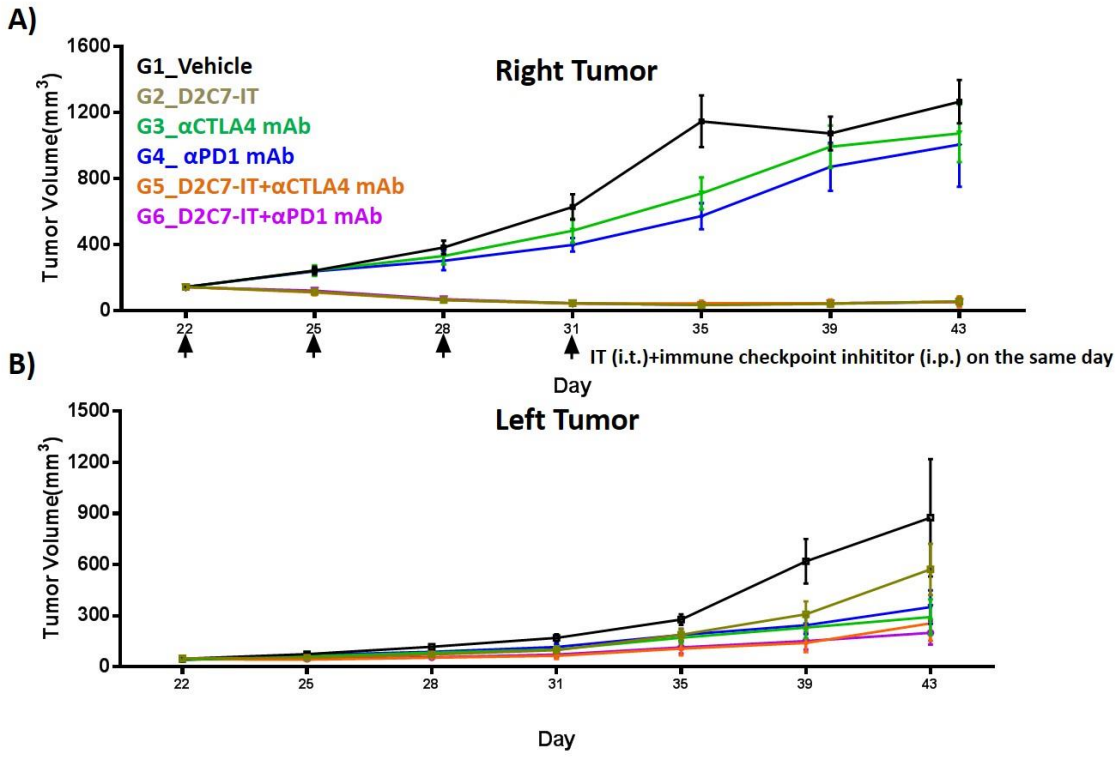

Figure 36: *In vivo* efficacy of D2C7-IT+αCTLA4/αPD1 combinatorial therapy in bilateral SC CT2A-mD2C7 glioma-bearing C57BL/6 immunocompetent mice.

(A) The tumor growth curve for the right treated tumors, in which G2, G5, and G6 showed the most significant tumor growth delay. (B) The tumor growth curve for the left untreated tumors, which indicated the combinatorial therapy on the right side could also exert a better anti-tumor effect on the contralateral distal tumors. Data were plotted in Mean ± SE.

Interestingly, in the groups where the right tumors were treated with D2C7-IT/αCTLA-4/αPD-1 monotherapy or D2C7-IT+αCTLA-4/αPD-1 combinatorial therapy, the left untreated tumors also grew much slower compared to the control group (**Figure 36B and 37A**), which indicates that a high dose of localized D2C7-IT monotherapy can achieve a similar anti-tumor immunity in the left untreated tumors compared to the systemic immune checkpoint inhibitor monotherapy. Furthermore, the D2C7-IT+αCTLA-4/αPD-1 combinatorial therapy in the right tumors led to the most significantly delayed growth of the left untreated tumors in the mice (**Figure 36B and 37B**), which suggests that immune checkpoint inhibitors can enhance the anti-tumor immunity induced by the immunotoxin to restrict the tumor growth in the remote area.

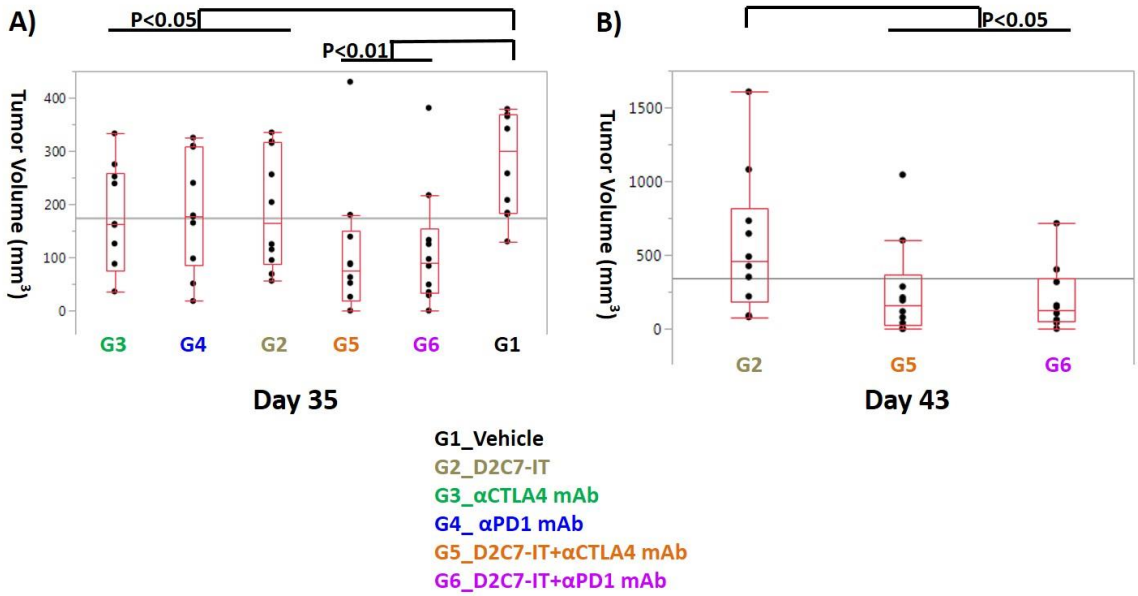

Figure 37: Left tumor volume among groups on Day 35 and Day 43 after the initial tumor inoculation.

(A) On Day 35, compared to the vehicle group (G1), the left tumor growth was significantly delayed in all other treatment groups ($P < 0.05$ for G2, 3, and 4, $P < 0.01$ for G5 and 6). Since several mice in G1 had to be euthanized due to the volume of the right tumor after Day 35, Day 35 was chosen as the cut-off date to run the statistical analysis. (B) On Day 43, the left tumor growth was significantly delayed by the combinatorial therapy compared to the D2C7-IT monotherapy on the right tumor ($P < 0.05$).

3.3.2.8. Intracranial tumorigenesis of CT2A-mD2C7 and SMA560-mD2C7 in C57BL/6 mice and VM/Dk mice

Before replicating the similar combinatorial treatment experiments in orthotopic mouse glioma models, the intracranial tumorigenesis of those two mouse glioma cell lines must first be examined in their host strains. CT2A-mD2C7 and SMA560-mD2C7 cells were inoculated into the brain of 10 C57BL/6 and VM/Dk mice, respectively. Kaplan-Meier survival curves were used to monitor the tumorigenesis in these two

models (**Figure 38**), which demonstrated that the median survival time for CT2A-mD2C7-bearing C57BL/6 mice was 25 days, whereas that for SMA560-mD2C7-bearing VM/Dk mice was 20 days. Both curves will be used as a reference to choose the treatment window in the future intracranial treatment studies.

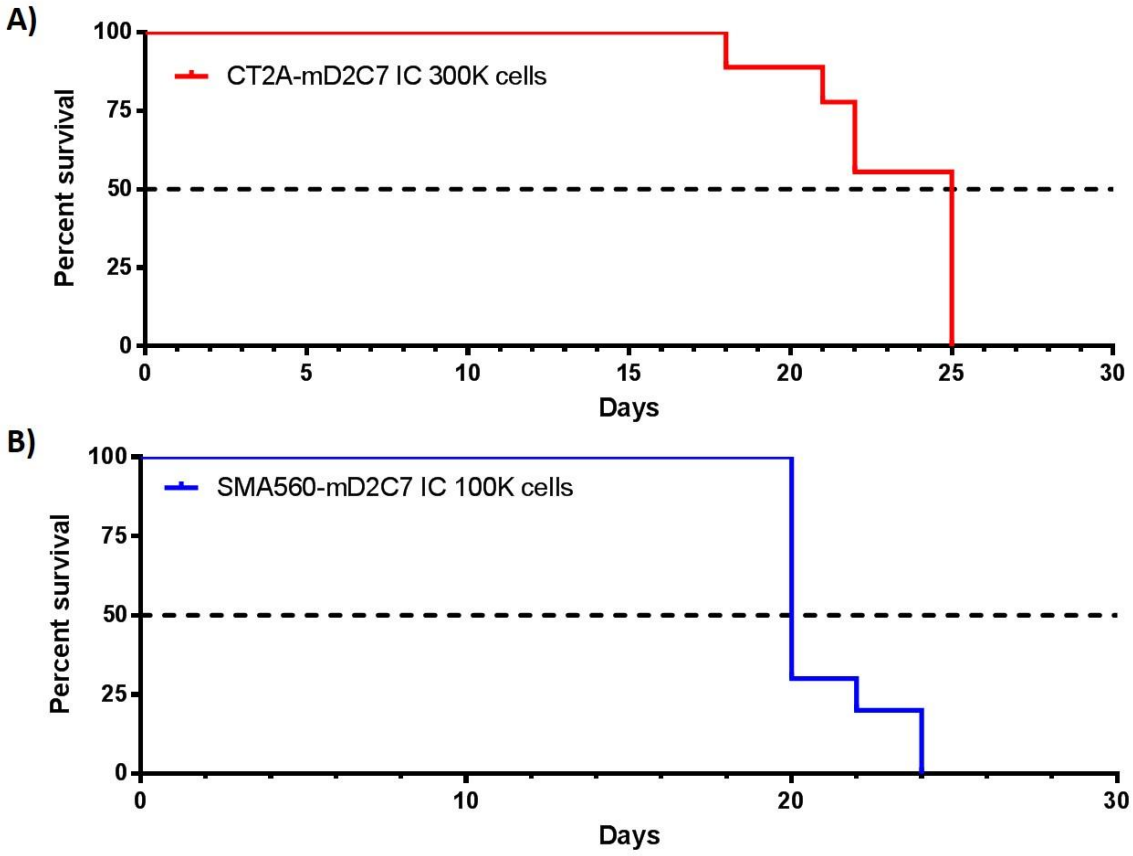

Figure 38: Kaplan-Meier survival curves for orthotopic (A) CT2A-mD2C7 and (B) SMA560-mD2C7 mouse glioma models

3.3.3 Discussion and conclusions

It is reported that immunotoxins can directly kill cancer cells that express high levels of the targeted tumor antigen. It has been shown that immunotoxin monotherapy can efficiently and directly destroy tumor cells expressing targeted epitopes, such as PDPN, EGFRwt and/or its truncated variant, EGFRvIII, in xenograft malignant brain tumor models in immunocompromised mice [48, 52]. However, since I used the NSG mice, which are a strain among the most immunodeficient mice that lack natural killer (NK) cells, mature T cells, B cells, and numerous cytokine pathways [107-109], the prolonged survival from the D2C7-IT monotherapy should be attributed to its direct tumor cell killing mechanism driven by *Pseudomonas* Exotoxin without examining how the immune system incorporates in the therapy [37]. A previous study indicated that the immunotoxin therapy can induce a secondary anti-tumor immune response in a mouse melanoma model, which is different from the direct killing mechanism and needs the incorporation of the immune system [99]. Since malignant brain tumors are always a heterogeneous mass [110], it is possible that some tumor cells can escape from the direct targeted attack of the immunotoxin therapy due to the lack of epitopes. For this reason, the secondary anti-tumor immune response stimulated by the immunotoxin may play an important role in eliminating those tumor cells not directly targeted. Therefore, it is necessary to establish appropriate animal experiments to investigate the secondary immune response induced by immunotoxins against glioblastomas. It is critical to

investigate this anti-tumor immunity in immunocompetent mice at the preclinical level to prove the concept. Fortunately, several syngeneic immunocompetent murine glioma models have been established for the preclinical animal experiments, including CT2A-C57BL/6 and SMA560-VM/Dk model systems.

The CT2A cell line was chemically induced with 20-methylcholanthrene by Seyfried and colleagues in 1992. After serially transplanting tumor fragments into C57BL/6 mice, this syngeneic mouse brain tumor model was developed to represent mouse anaplastic astrocytomas with high malignancy and poor differentiation [111]. The CT2A mouse glioma model accurately displays several features of glioblastoma, such as intratumoral heterogeneity, *in vivo* migratory patterns, and the resistance to radiation and chemotherapy [103]. In 1980, Serano et al. successfully developed the P560 cell line (SMA560 cell line) based on a spontaneous mouse glioma model within the VM mouse strain first reported by H. Fraser in 1971 [112]. The SMA560 cell line maintained tumorigenicity throughout all passages [113]. SMA560 tumor cells excellently represents anaplastic astrocytomas, lack MHC class II molecules, but do express MHC class I molecules, which outstands their potential to be recognized by $CD8^+$ T effector cells [103]. Based on the CT2A and SMA560 models, our laboratory has established a CT2A-mD2C7 line and SMA560-mD2C7 line. Both cell lines react with the D2C7 mAb in the flow cytometry analysis (**Figure 29**). An *in vitro* cytotoxicity assay showed that the cytotoxicity of D2C7-IT on the CT2A-mD2C7 and SMA560-mD2C7 cells were 0.47

ng/mL and 1.05 ng/mL, respectively (**Figure 30**), while the control immunotoxin, P588-IT, exhibited no (>1000 ng/mL) or non-specific (510 ng/mL) cytotoxic activity against both CT2A-mD2C7 and SMA560-mD2C7 cells, respectively. The specific binding affinity and robust *in vitro* cytotoxicity ensure the further *in vivo* D2C7-IT treatment in these two murine glioma models in C57BL/6 and VM/Dk mice.

In addition, the flow cytometry analysis also shows that both CT2A-mD2C7 and SMA560-mD2C7 lines have a high expression of MHC class I molecules (**Figure 31**), which form the structures that interact with the TCR of $CD8^+$ CTLs, leading to the activation of a CTL response that plays an important role in the anti-tumor immunity. Furthermore, both cell lines show a high expression of PDL1 on the cell surface in the flow cytometry analysis (**Figure 32**), which perfectly mimics the constitutively high PDL1 expression in human glioblastomas. Expression of immune checkpoint molecule PDL1 has been reported as a useful immunosuppressive factor in glioblastomas [114, 115]. In a previous study of 135 glioblastoma cases, 88% of newly diagnosed and 72% of recurrent patient samples displayed the diffuse/fibrillary PDL1 expression, although there was no association between the PDL1 expression level and patient survival [115]. In addition, the PDL1 molecule expression level may also be used as a biomarker to indicate the therapeutic response to immune checkpoint inhibitors targeting the PD1–PDL1 axis, although the true predictive role of this indicator still needs extensive preclinical and clinical investigation in the future [116, 117].

Recently, several studies successfully demonstrated that tumor regression and significantly improved survival were achieved in murine glioma models by suppressing co-inhibitory molecules, such as CTLA4 and PD1 [118, 119]. Based on the promising preclinical data, several clinical trials have started to investigate the utilization of immune checkpoint inhibitors to treat malignant brain tumors, either as monotherapy or combinatorial therapy with other anti-tumor agents (**Table 12**).

Table 12: Representative clinical trials of immune checkpoint inhibitors in glioblastomas and brain metastases.

From [56] with permission from publisher, see appendix for license.

National Clinical Trial registration number	Mechanism of tested agent	Therapy and/or treatment groups	Tumour type	No. of patients	Phase
NCT02017717	Anti-PD1, anti-CTLA4	Nivolumab (anti-PD1) Nivolumab + ipilimumab (anti-CTLA4) Bevacizumab (control group)	Recurrent glioblastoma	*n*=372	III
NCT01952769	Anti-PD1	Pidilizumab (two cohorts)	Relapsed glioblastoma, diffuse intrinsic pontine glioma	*n*=30	I/II
NCT02311920	Anti-PD1, anti-CTLA4	TMZ + nivolumab TMZ + ipilimumab TMZ + nivolumab + ipilimumab	Newly-diagnosed glioblastoma or gliosarcoma	*n*=42	I
NCT02336165	Anti-PDL1	MEDI4736 MEDI4736 + radiotherapy MEDI4736 + bevacizumab	Newly-diagnosed or recurrent glioblastoma	*n*=84	II
NCT02115139	Anti-CTLA4	Ipilimumab + whole-brain radiotherapy	Melanoma BM	*n*=66	II
NCT02097732	Anti-CTLA4	Ipilimumab followed by stereotactic radiosurgery, followed by ipilimumab Stereotactic surgery followed by ipilimumab	Melanoma BM	*n*=40	II
NCT02107755	Anti-CTLA4	Ipilimumab followed by stereotactic radiosurgery	Oligometastatic melanoma	*n*=32	II
NCT01703507	Anti-CTLA4	Ipilimumab + whole-brain radiotherapy Ipilimumab + stereotactic radiosurgery	Melanoma BM	*n*=24	I
NCT01950195	Anti-CTLA4	Ipilimumab + stereotactic radiosurgery	Melanoma BM	*n*=30	I
NCT02337491	Anti-PD1	Pembrolizumab monotherapy Pembrolizumab + bevacizumab	Recurrent glioblastoma	*n*=79	II
NCT02085070	Anti-PD1	Pembrolizumab	Non-small cell lung cancer BM or melanoma BM	*n*=64	II

Abbreviations: BM, brain metastases; CTLA4, cytotoxic T-lymphocyte antigen-4; PD1, programmed cell death protein 1; PDL1, programmed cell death 1 ligand 1; TMZ, temozolomide.

However, malignant gliomas, including glioblastomas, have relatively low mutation rates [120], which may generate fewer and subtle tumor antigens, leading to relatively poor basal immunogenicity compared to other tumor types that well respond to immunotherapies, for example, melanoma and NSCLC. Therefore, a combination of targeted cytotoxic immunotherapy and immune checkpoint inhibitors may provide synergistic anti-tumor effect to achieve a "1 + 1 > 2" effect (**Figure 39**).

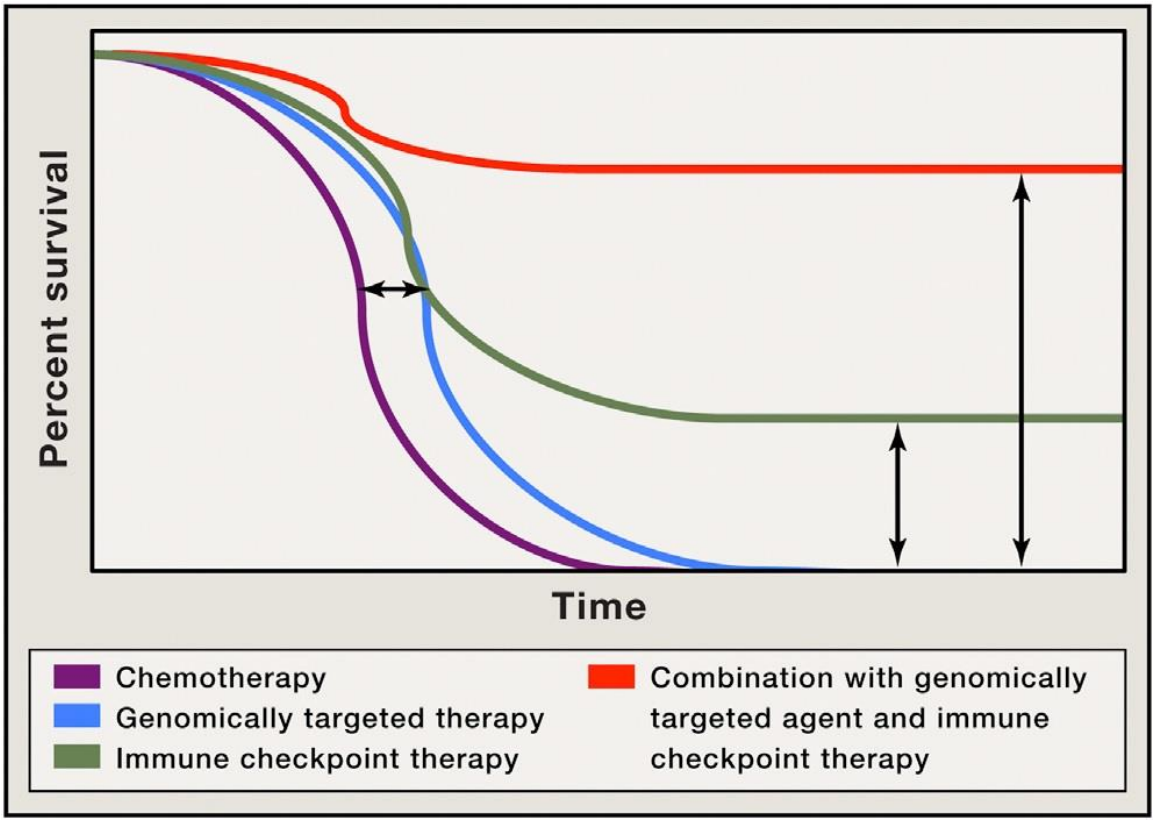

Figure 39: Improved overall survival as a result of combination therapy.

Depiction of Kaplan-Meier survival curve with genomically targeted agents (blue line) as compared to standard therapies (purple line), indicating an improvement in median overall survival but lack of durable responses; improved median overall

survival and durable responses in a fraction of patients treated with immune checkpoint therapy (green line); possibility for improved median overall survival with durable responses for the majority of patients in the setting of combination treatment with genomically targeted agents and immune checkpoint therapy (red line). From [121] with permission from publisher, see appendix for license.

The ideal combinatorial therapy may have a lower dose of targeted cytotoxic immunotherapy to limit its side effects to the minimum, and achieve a long-term anti-tumor immunity with the help of checkpoint inhibitors. Immunotoxin therapy can efficiently and directly kill cancer cells that express high levels of the targeted antigen through its unique cytotoxic mechanism. It is probable that cancer cells destroyed by localized immunotoxin therapy can release tumor antigens and/or other neoantigens. These antigens can then be presented by the APCs to host T cells in the local drainage lymph nodes, which will activate CTLs to migrate and eliminate the remaining or recurrent tumor cells expressing specific tumor antigens at the tumor site. Throughout this process, various co-inhibitory checkpoint pathways between T cells and APCs and/or between T cells and tumor cells can trigger different mechanisms to de-activate T cells, and to adjust the continuation and intensity of the anti-tumor immunity [102]. Immune checkpoint inhibitors, such as anti-CTLA4 and anti-PD1 mAbs, can block these immunosuppressive pathways and therefore augment the tumor cell death caused by lymphocytes activated by the targeted immunotoxin therapy.

One of our collaborators revealed that an EGFRvIII-targeted immunotoxin can induce anti-tumor immunity in their SC mouse glioma model, which can be inhibited in

the absence of $CD4^+$ and $CD8^+$ T cells [101]. However, in their SC glioma model, the i.t. immunotoxin treatment was performed immediately after the SC inoculation of the tumor cell suspension, and thus barely represents the i.t. treatment against the natural grown SC tumor with the infiltration of other types of cells, including immune cells. Therefore, we established a SC mouse CT2A-mD2C7 glioma model in C57BL/6 immunocompetent mice with six groups, in which the mice were treated by the control immunotoxin P588-IT or D2C7-IT, combined with αCTLA4 or αPD1 inhibitors after the tumor grew to a certain size. In this *in vivo* SC CT2A-mD2C7 glioma model, four doses of the low-dose D2C7-IT but not αCTLA4 or αPD1 monotherapy, and D2C7-IT+αCTLA-4/αPD-1 combinatorial therapy generated a significant delay in tumor growth compared to the control immunotoxin P588-IT treatment groups (**Figure 34A**). Importantly, complete cures were only observed in D2C7-IT+αCTLA4 (n = 4/10) and D2C7-IT+αPD-1 (n = 5/10) combinatorial therapy groups (**Figure 34B**), although D2C7-IT monotherapy could also significantly delay the tumor growth. These results demonstrated that low doses of cytotoxic immunotoxin therapy can significantly delay the tumor growth but fail to cure the tumor-bearing mice. Combined with immune checkpoint inhibitors, cytotoxic immunotoxin therapy can increase the initial cure rate of low-dose immunotoxin therapy from zero to over 40%. Furthermore, all cured mice rejected the mD2C7-negative tumors 1° SCR, whereas tumors grew in untreated naïve mice, suggesting that the combinatorial treatment provided long lasting anti-tumor immunity

that even extended to mD2C7-negative parental cells, as well (**Figure 35A**). All nine cured mice then rejected the CT2A-mD2C7 2° ICR in the brain, whereas tumors grew in untreated naïve mice, indicating that the combinatorial treatment also provided long lasting anti-tumor immunity that extended to the remote immune-privileged CNS as well (**Figure 35B**), in which the central memory T cells (T_{CM}) might play an important role [122].

Subsequently, we established a bilateral SC mouse glioma model to investigate whether a localized high-dose immunotoxin treatment can provide a systemic anti-tumor effect on the tumors in the distal region, and whether the combination of immune checkpoint inhibitors can enhance this systemic anti-tumor immunity induced by the localized immunotoxin therapy. The D2C7-IT monotherapy, D2C7-IT+αCTLA4, and D2C7-IT+αPD1 combinatorial therapy led to significant growth delay of the right tumors ($P < 0.01$), and cured 4/10, 6/10, and 5/10 right tumors, respectively (**Figure 36A**). Interestingly, in the groups where the right tumors were treated by D2C7-IT/αCTLA-4/αPD-1 monotherapy or D2C7-IT+αCTLA-4/αPD-1 combinatorial therapy, the left untreated tumors also grew much slower compared to the control group (**Figure 36B and 36A**), which indicates that a high dose of localized D2C7-IT monotherapy can achieve a similar anti-tumor immunity on the left untreated tumors compared to the systemic immune checkpoint inhibitor monotherapy. Furthermore, the combinatorial therapy in the right tumors led to the most significantly delayed growth of the left

untreated tumors in the mice (**Figure 36B and 37B**), which suggests that immune checkpoint inhibitors can enhance the anti-tumor immunity induced by the localized immunotoxin therapy to restrict the tumor growth in the remote area.

Although my data showed a promising potential of the immunotoxin and immune checkpoint inhibitors combinatorial therapy to treat malignant brain tumors, more extensive investigation needs to be performed in an orthotopic mouse glioma model in the future in order to replicate the similar combinatorial treatment experiments. Therefore, intracranial tumorigenesis of the two mouse glioma cell lines was first examined in their host strains. Survival curves will be used as a reference to choose the treatment window in the future intracranial treatment studies. For the future orthotopic mouse glioma model, more details will be investigated to characterize the immunotoxin and immune checkpoint inhibitor combinatorial therapy, including the function of the infiltrated immune cells, tumor-tissue microenvironment interaction, tumor antigen spreading and T cell diversity, and inflammatory response to immunotoxin therapy in the CNS.

To summarize, I have demonstrated that the intratumoral delivery of D2C7-IT induces secondary anti-tumor immunity, which destroys not only mD2C7-expressing tumor cells, but also tumor cells not expressing mD2C7 at the systemic level. A combination of immune checkpoint inhibitors can enhance this immunotoxin-induced anti-tumor immunity to achieve a synergistic long-term anti-tumor effect.

4. Significance and future directions

4.1 Significance

D2C7-IT is a novel scFv immunotoxin developed in our lab, and reacts with both the EGFRwt and EGFRvIII proteins by fusing the scFv of the D2C7 mAb with domains II and III of *Pseudomonas* exotoxin A (PE38KDEL). Although immunotoxins reacting with EGFRwt or EGFRvIII were being used to treat brain tumors, D2C7-IT is a unique immunotoxin that reacts with both overexpressed proteins on glioblastoma cells, which results in a significant improvement in the anti-tumor efficacy for the majority of glioblastomas expressing either or both epitopes. D2C7-IT has several promising traits that make it an ideal candidate to treat glioblastomas, including (1) high binding affinity to EGFRwt/vIII proteins expressed on glioblastoma cells, (2) high stability at 37°C for a period of seven days, and (3) promising *in vitro* cytotoxicity and *in vivo* anti-tumor efficacy against glioblastoma cells expressing EGFRwt and/or EGFRvIII proteins. My thesis work examined the preclinical efficacy and toxicity of D2C7-IT in order to realize its clinical translation as a monotherapy and/or a combination therapy with other agents. Thanks to my thesis work, D2C7-IT is now being investigated in a Phase I/II clinical trial for recurrent malignant glioma patients (NCT02303678, D2C7 for Adult Patients With Recurrent Malignant Glioma) led by my advisor, Dr. Darell Bigner. In addition, NZ-1-IT is another unique immunotoxin developed in our laboratory showing

robust anti-tumor potential, which will be thoroughly investigated in the same pattern in the future.

Furthermore, my thesis work using the SC mouse glioma models also shows that D2C7-IT therapy not only directly kills tumor cells, but also induces a secondary anti-tumor immune response in immunocompetent mice that rejects the formation/growth of the tumor when rechallenged with the parental mouse glioma cells in a distal region, and rechallenged with the same epitope-expressing mouse glioma cells in the immune-privileged CNS. In such cases, T cells play an important role. Many previous studies show that immune checkpoint inhibitors, such as anti-CTLA4 and anti-PD1 mAbs, can block the inhibitory signals that shut down the activated T cells in orthotopic murine glioma models, which suggests that these inhibitors have a robust potential to synergize with the T cell-mediated secondary anti-tumor immune response of D2C7-IT. In my thesis work, I investigated the secondary immune response induced by D2C7-IT therapy in the mouse glioma models, and investigated how to utilize immune checkpoint inhibitors to enhance this anti-tumor effect. To the best of my knowledge, this is the first study to investigate the combinatorial therapy of an immunotoxin and checkpoint inhibitors in preclinical glioma models. The outcome of my thesis work may establish paradigm shifts in future glioblastoma treatments.

4.2 Future directions

Although my thesis work shows promising potential for the immunotoxin and immune checkpoint inhibitors combinatorial therapy to treat malignant brain tumors in SC mouse glioma models, more extensive investigation needs to be performed in an orthotopic mouse glioma model in order to establish a foundation for future translation to the clinic.

4.2.1 Establish and characterize orthotopic mouse glioma models in immunocompetent mice

As described, two orthotopic mouse glioma models were established in C57BL/6 and VM/Dk mice. A collaboration with Dr. M. Dee Gunn's laboratory at Duke University Medical Center has been established to compare the infiltrated immune cells in the tumor-bearing brain to the normal brain using the flow cytometry analysis, which showed a huge increase of T cells in the tumor-bearing brain (**Figure 40**). I will further utilize flow cytometry and multiplex immunofluorescent analyses (PerkinElmer) (**Figure 41**) to investigate the tumor-infiltrated immune cells at different time points (pre-treatment, during treatment, and post-treatment) to better characterize the secondary anti-tumor immunity induced by immunotoxin therapy.

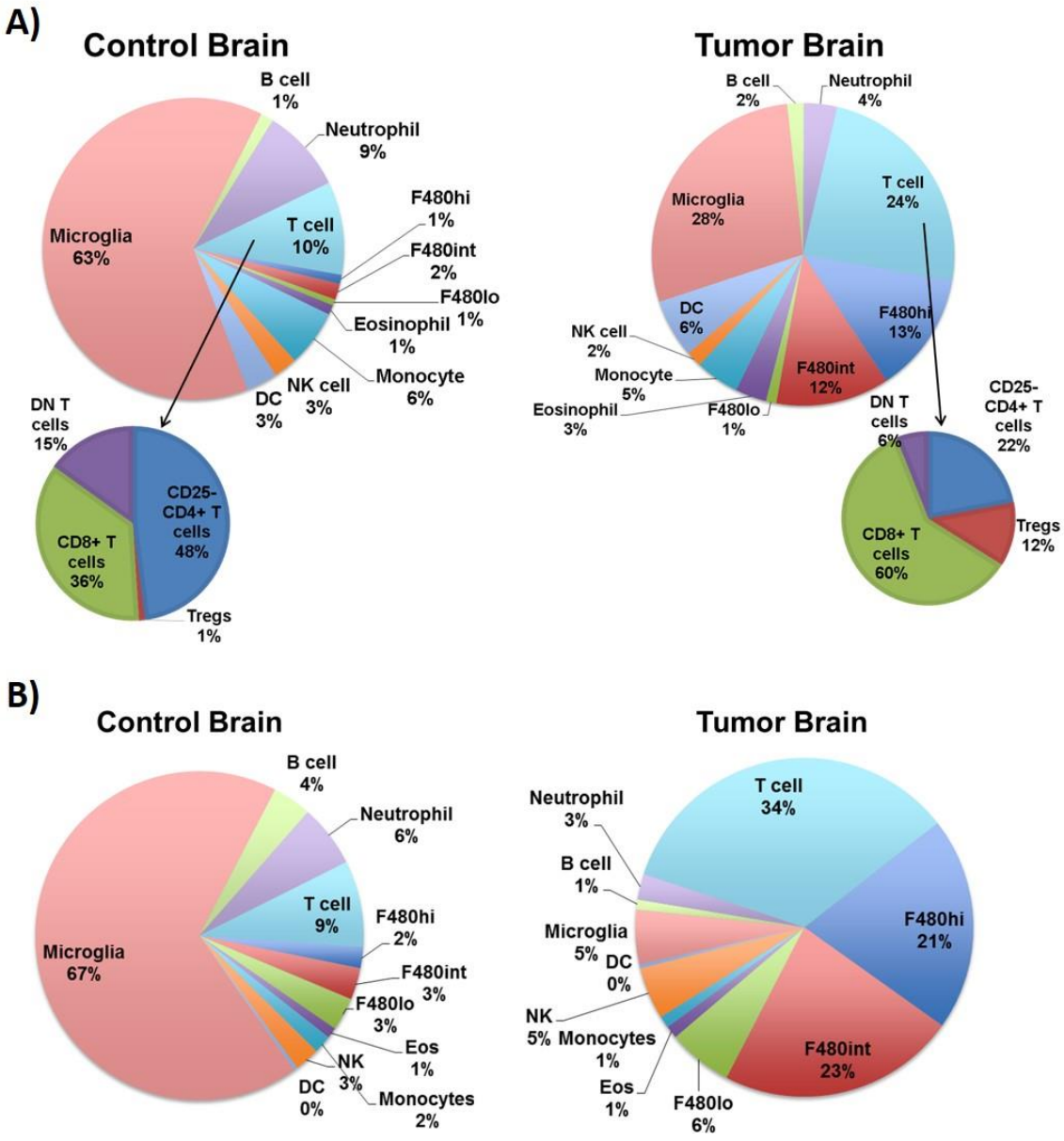

Figure 40: Characterization of immune cells infiltrating (A) CT2A-mD2C7 and (B) SMA560-mD2C7 intracranial tumors in the CNS.

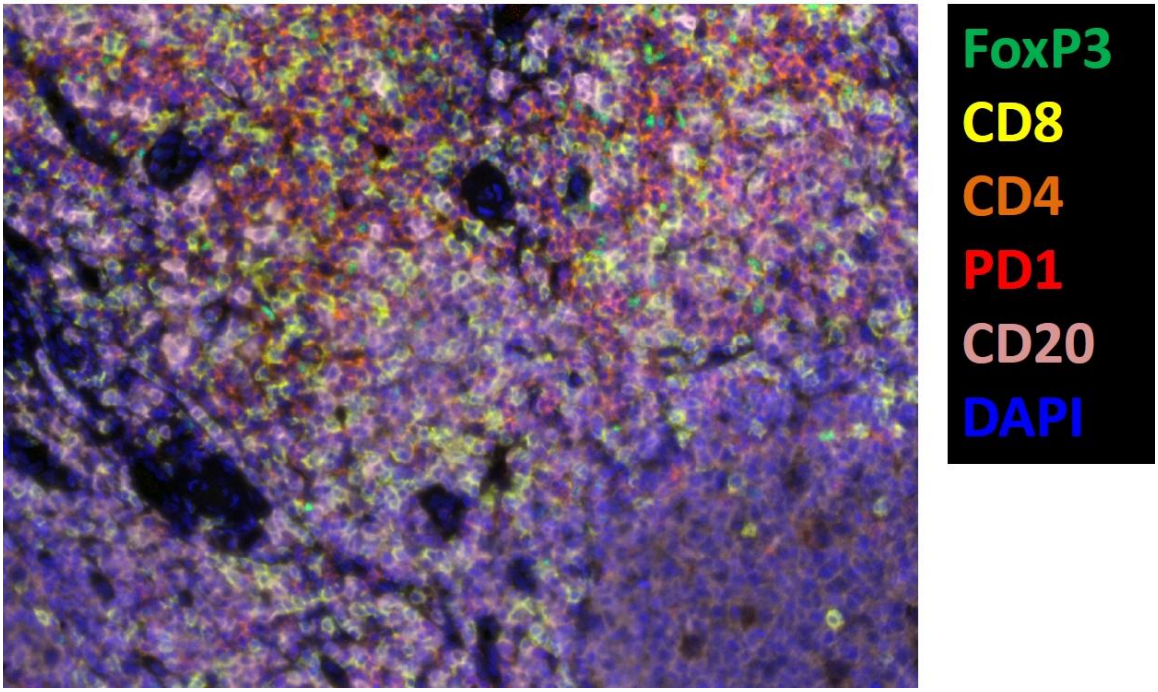

Figure 41: The multiplexed biomarker imaging of a section of human tonsil.

In this multiplexed biomarker imaging of a human tonsil section, FoxP3, CD8, CD4, PD1, CD20, and nuclear were labeled by Opal 520 (green), Opal 540 (yellow), Opal 570 (orange), Opal 620 (red), Opal 690 (pink), and 4',6-diamidino-2-phenylindole (DAPI) (blue), respectively. (Courtesy of Dr. Hailan Piao from Dr. Darell Bigner's laboratory)

I will also collaborate with Dr. Qi-Jing Li's laboratory to design experiments to investigate the dynamics of TCR repertoire at different time points (pre-treatment, during treatment, and post-treatment) by deep sequencing. By investigating the TCR repertoire, we hope to demonstrate: (1) the expansion and diversity of the repertoire of tumor infiltrating T cells; (2) the origin and destination of different clonetypes of those expanded T cells in CNS glioma tissue; and, (3) the association between therapeutic outcomes and the diversity of T-cell repertoire [123].

4.2.2 Optimization of immunotoxin and immune checkpoint inhibitor combinatorial therapy in orthotopic mouse glioma models

By replicating the SC experimental design, I will treat the intracranial CT2A-mD2C7 and SMA560-mD2C7 gliomas using the intracerebral CED of D2C7-IT monotherapy or the D2C7-IT+αCTLA-4/αPD-1 combinatorial therapy. I will first perform the dose selection experiments to find the optimal dose of D2C7-IT for both CT2A-mD2C7 and SMA560-mD2C7 models in immunocompetent mice. The Kaplan-Meier survival curve will be utilized to compare the benefits of different treatment groups. Immunohistochemistry, flow cytometry, and TCR sequencing analyses will be used to examine the subtypes of tumor-infiltrating lymphocytes in the CNS tumor at different time points in different treatment groups. Subsequently, depletion antibodies will be utilized to confirm the function of different infiltrative lymphocytes that mediate the immunotoxin-induced secondary anti-tumor immune response in the brain. Immune function assays will be used to identify the tumor-specific CTL response induced by D2C7-IT monotherapy and combinatorial therapy. All surviving mice will be rechallenged by the CT2A and SMA560 parental cells subcutaneously or intracranially (contralateral) to determine the systemic anti-tumor immune response induced by immunotoxin monotherapy or combinatorial therapy with immune checkpoint inhibitors.

The orthotopic mouse glioma models will be critical in allowing us to not only investigate the therapeutic benefits of the immunotoxin and immune checkpoint

inhibitors combinatorial therapy, but also to develop and optimize important diagnostic assays to monitor the dynamics of immune responses throughout the treatment, which will all be utilized as references in future clinical trials investigating the combinatorial therapy.

Appendix: Licenses for figures and tables used in the dissertation (when required)

License #: 3917810002531
Order Date: 07/28/2016
Journal: Neuro-Oncology
Title: CBTRUS Statistical Report: Primary Brain and Central Nervous System Tumors Diagnosed in the United States in 2008-2012
Type of use: reuse in a dissertation / thesis
Fee: 0.00 USD

License #: 3917810285920
Order Date: 07/28/2016
Journal: Journal of Clinical Neuroscience
Title: The EGFRvIII variant in glioblastoma multiforme
Type of use: reuse in a dissertation / thesis
Fee: 0.00 USD

License #: https://creativecommons.org/licenses/by/3.0/
Order Date: 07/28/2016
Journal: Toxins
Title: Toxin-based therapeutic approaches
Type of use: reuse in a dissertation / thesis
Fee: 0.00 USD

License #: https://creativecommons.org/licenses/by/3.0/
Order Date: 07/28/2016
Journal: Frotiers in immunology
Title: Podoplanin: emerging functions in development, the immune system, and cancer
Type of use: reuse in a dissertation / thesis
Fee: 0.00 USD

License #: 3917811445532
Order Date: 07/28/2016
Journal: Neurosurgery
Title: Colocalization of Gadolinium Diethylene Triamine Pentaacetic Acid With High Molecular Weight Molecules After Intracerebral Convection-Enhanced Delivery in Humans

Type of use: reuse in a dissertation / thesis
Fee: 0.00 USD

License #: 3917820098784
Order Date: 07/28/2016
Journal: Neuro-Oncology
Title: Sustained radiographic and clinical response in patient with bifrontal recurrent glioblastoma multiforme with intracerebral infusion of the recombinant targeted toxin TP38: Case study
Type of use: reuse in a dissertation / thesis
Fee: 0.00 USD

License #: 3917820367115
Order Date: 07/28/2016
Journal: Nature Reviews Cancer
Title: The blockade of immune checkpoints in cancer immunotherapy
Type of use: reuse in a dissertation / thesis
Fee: 0.00 USD

License #: 3921700456465
Order Date: 08/03/2016
Journal: Nature Reviews Neurology
Title: Prospects of immune checkpoint modulators in the treatment of glioblastoma
Type of use: reuse in a dissertation / thesis
Fee: 0.00 USD

License #: 3927100702827
Order Date: 08/13/2016
Journal: Investigational New Drugs
Title: Preclinical toxicity evaluation of a novel immunotoxin, D2C7-(scdsFv)-PE38KDEL, administered via intracerebral convection-enhanced delivery in rats
Type of use: reuse in a dissertation / thesis
Fee: 0.00 USD

License #: 3927100992371
Order Date: 08/13/2016
Journal: International Journal of Cancer
Title: Recombinant anti-podoplanin (NZ-1) immunotoxin for the treatment of malignant brain tumors
Type of use: reuse in a dissertation / thesis

Fee: 0.00 USD

License #: 3946780515250
Order Date: 09/12/2016
Journal: Cell
Title: Immune Checkpoint Targeting in Cancer Therapy: Toward Combination Strategies with Curative Potential
Type of use: reuse in a dissertation / thesis
Fee: 0.00 USD

Bibliography

1. Louis, D.N., A. Perry, G. Reifenberger, A. von Deimling, D. Figarella-Branger, W.K. Cavenee, H. Ohgaki, O.D. Wiestler, P. Kleihues, and D.W. Ellison, *The 2016 World Health Organization Classification of Tumors of the Central Nervous System: a summary.* Acta Neuropathol, 2016. **131**(6): p. 803-20.

2. Ostrom, Q.T., H. Gittleman, J. Fulop, M. Liu, R. Blanda, C. Kromer, Y. Wolinsky, C. Kruchko, and J.S. Barnholtz-Sloan, *CBTRUS Statistical Report: Primary Brain and Central Nervous System Tumors Diagnosed in the United States in 2008-2012.* Neuro Oncol, 2015. **17 Suppl 4**: p. iv1-iv62.

3. Omuro, A. and L.M. DeAngelis, *Glioblastoma and other malignant gliomas: a clinical review.* JAMA, 2013. **310**(17): p. 1842-50.

4. Wen, P.Y. and S. Kesari, *Malignant gliomas in adults.* The New England journal of medicine, 2008. **359**(5): p. 492-507.

5. Salomon, D.S., R. Brandt, F. Ciardiello, and N. Normanno, *Epidermal growth factor-related peptides and their receptors in human malignancies.* Critical reviews in oncology/hematology, 1995. **19**(3): p. 183-232.

6. Libermann, T.A., H.R. Nusbaum, N. Razon, R. Kris, I. Lax, H. Soreq, N. Whittle, M.D. Waterfield, A. Ullrich, and J. Schlessinger, *Amplification, enhanced expression and possible rearrangement of EGF receptor gene in primary human brain tumours of glial origin.* Nature, 1985. **313**(5998): p. 144-7.

7. Wikstrand, C.J., C.J. Reist, G.E. Archer, M.R. Zalutsky, and D.D. Bigner, *The class III variant of the epidermal growth factor receptor (EGFRvIII): characterization and utilization as an immunotherapeutic target.* J Neurovirol, 1998. **4**(2): p. 148-58.

8. Chaffanet, M., C. Chauvin, M. Laine, F. Berger, M. Chedin, N. Rost, M.F. Nissou, and A.L. Benabid, *EGF receptor amplification and expression in human brain tumours.* European journal of cancer, 1992. **28**(1): p. 11-7.

9. Pedersen, M.W., M. Meltorn, L. Damstrup, and H.S. Poulsen, *The type III epidermal growth factor receptor mutation. Biological significance and potential target for anti-cancer therapy.* Ann Oncol, 2001. **12**(6): p. 745-60.

10. Frederick, L., X.Y. Wang, G. Eley, and C.D. James, *Diversity and frequency of epidermal growth factor receptor mutations in human glioblastomas.* Cancer Res, 2000. **60**(5): p. 1383-7.

11. Schwechheimer, K., S. Huang, and W.K. Cavenee, *EGFR gene amplification--rearrangement in human glioblastomas.* Int J Cancer, 1995. **62**(2): p. 145-8.

12. Schlegel, J., A. Merdes, G. Stumm, F.K. Albert, M. Forsting, N. Hynes, and M. Kiessling, *Amplification of the epidermal-growth-factor-receptor gene correlates with different growth behaviour in human glioblastoma.* Int J Cancer, 1994. **56**(1): p. 72-7.

13. Ekstrand, A.J., N. Sugawa, C.D. James, and V.P. Collins, *Amplified and rearranged epidermal growth factor receptor genes in human glioblastomas reveal deletions of sequences encoding portions of the N- and/or C-terminal tails.* Proc Natl Acad Sci U S A, 1992. **89**(10): p. 4309-13.

14. Ekstrand, A.J., C.D. James, W.K. Cavenee, B. Seliger, R.F. Pettersson, and V.P. Collins, *Genes for epidermal growth factor receptor, transforming growth factor alpha, and epidermal growth factor and their expression in human gliomas in vivo.* Cancer Res, 1991. **51**(8): p. 2164-72.

15. Yamazaki, H., Y. Ohba, N. Tamaoki, and M. Shibuya, *A deletion mutation within the ligand binding domain is responsible for activation of epidermal growth factor receptor gene in human brain tumors.* Jpn J Cancer Res, 1990. **81**(8): p. 773-9.

16. Humphrey, P.A., A.J. Wong, B. Vogelstein, M.R. Zalutsky, G.N. Fuller, G.E. Archer, H.S. Friedman, M.M. Kwatra, S.H. Bigner, and D.D. Bigner, *Anti-synthetic peptide antibody reacting at the fusion junction of deletion-mutant epidermal growth factor receptors in human glioblastoma.* Proc Natl Acad Sci U S A, 1990. **87**(11): p. 4207-11.

17. Bigner, S.H., P.A. Humphrey, A.J. Wong, B. Vogelstein, J. Mark, H.S. Friedman, and D.D. Bigner, *Characterization of the epidermal growth factor receptor in human glioma cell lines and xenografts.* Cancer Res, 1990. **50**(24): p. 8017-22.

18. Gan, H.K., A.H. Kaye, and R.B. Luwor, *The EGFRvIII variant in glioblastoma multiforme.* J Clin Neurosci, 2009. **16**(6): p. 748-54.

19. Moscatello, D.K., M. Holgado-Madruga, A.K. Godwin, G. Ramirez, G. Gunn, P.W. Zoltick, J.A. Biegel, R.L. Hayes, and A.J. Wong, *Frequent expression of a mutant epidermal growth factor receptor in multiple human tumors.* Cancer Res, 1995. **55**(23): p. 5536-9.

20. Wong, A.J., J.M. Ruppert, S.H. Bigner, C.H. Grzeschik, P.A. Humphrey, D.S. Bigner, and B. Vogelstein, *Structural alterations of the epidermal growth factor receptor gene in human gliomas.* Proc Natl Acad Sci U S A, 1992. **89**(7): p. 2965-9.

21. Batra, S.K., S. Castelino-Prabhu, C.J. Wikstrand, X. Zhu, P.A. Humphrey, H.S. Friedman, and D.D. Bigner, *Epidermal growth factor ligand-independent, unregulated, cell-transforming potential of a naturally occurring human mutant EGFRvIII gene.* Cell Growth Differ, 1995. **6**(10): p. 1251-9.

22. Choi, B.D., G.E. Archer, D.A. Mitchell, A.B. Heimberger, R.E. McLendon, D.D. Bigner, and J.H. Sampson, *EGFRvIII-targeted vaccination therapy of malignant glioma.* Brain Pathol, 2009. **19**(4): p. 713-23.

23. Gerber, N.U., M. Mynarek, K. von Hoff, C. Friedrich, A. Resch, and S. Rutkowski, *Recent developments and current concepts in medulloblastoma.* Cancer Treat Rev, 2014. **40**(3): p. 356-65.

24. Roussel, M.F. and G. Robinson, *Medulloblastoma: advances and challenges.* F1000 Biol Rep, 2011. **3**: p. 5.

25. Raica, M., A.M. Cimpean, and D. Ribatti, *The role of podoplanin in tumor progression and metastasis.* Anticancer Res, 2008. **28**(5B): p. 2997-3006.

26. Astarita, J.L., S.E. Acton, and S.J. Turley, *Podoplanin: emerging functions in development, the immune system, and cancer.* Front Immunol, 2012. **3**: p. 283.

27. Schacht, V., M.I. Ramirez, Y.K. Hong, S. Hirakawa, D. Feng, N. Harvey, M. Williams, A.M. Dvorak, H.F. Dvorak, G. Oliver, and M. Detmar, *T1alpha/podoplanin deficiency disrupts normal lymphatic vasculature formation and causes lymphedema.* EMBO J, 2003. **22**(14): p. 3546-56.

28. Shibahara, J., T. Kashima, Y. Kikuchi, A. Kunita, and M. Fukayama, *Podoplanin is expressed in subsets of tumors of the central nervous system.* Virchows Arch, 2006. **448**(4): p. 493-9.

29. Mishima, K., Y. Kato, M.K. Kaneko, R. Nishikawa, T. Hirose, and M. Matsutani, *Increased expression of podoplanin in malignant astrocytic tumors as a novel molecular marker of malignant progression.* Acta Neuropathol, 2006. **111**(5): p. 483-8.

30. Kato, Y., M.K. Kaneko, A. Kunita, H. Ito, A. Kameyama, S. Ogasawara, N. Matsuura, Y. Hasegawa, K. Suzuki-Inoue, O. Inoue, Y. Ozaki, and H. Narimatsu, *Molecular analysis of the pathophysiological binding of the platelet aggregation-inducing factor podoplanin to the C-type lectin-like receptor CLEC-2.* Cancer Sci, 2008. **99**(1): p. 54-61.

31. Kunita, A., T.G. Kashima, Y. Morishita, M. Fukayama, Y. Kato, T. Tsuruo, and N. Fujita, *The platelet aggregation-inducing factor aggrus/podoplanin promotes pulmonary metastasis.* Am J Pathol, 2007. **170**(4): p. 1337-47.

32. Wicki, A., F. Lehembre, N. Wick, B. Hantusch, D. Kerjaschki, and G. Christofori, *Tumor invasion in the absence of epithelial-mesenchymal transition: podoplanin-mediated remodeling of the actin cytoskeleton.* Cancer Cell, 2006. **9**(4): p. 261-72.

33. Martin-Villar, E., D. Megias, S. Castel, M.M. Yurrita, S. Vilaro, and M. Quintanilla, *Podoplanin binds ERM proteins to activate RhoA and promote epithelial-mesenchymal transition.* J Cell Sci, 2006. **119**(Pt 21): p. 4541-53.

34. Furnari, F.B., T. Fenton, R.M. Bachoo, A. Mukasa, J.M. Stommel, A. Stegh, W.C. Hahn, K.L. Ligon, D.N. Louis, C. Brennan, L. Chin, R.A. DePinho, and W.K. Cavenee, *Malignant astrocytic glioma: genetics, biology, and paths to treatment.* Genes Dev, 2007. **21**(21): p. 2683-710.

35. Thaker, N.G. and I.F. Pollack, *Molecularly targeted therapies for malignant glioma: rationale for combinatorial strategies.* Expert Rev Neurother, 2009. **9**(12): p. 1815-36.

36. Bullard, D.E. and D.D. Bigner, *Applications of monoclonal antibodies in the diagnosis and treatment of primary brain tumors.* J Neurosurg, 1985. **63**(1): p. 2-16.

37. Shapira, A. and I. Benhar, *Toxin-based therapeutic approaches.* Toxins (Basel), 2010. **2**(11): p. 2519-83.

38. Chandramohan, V., J.H. Sampson, I. Pastan, and D.D. Bigner, *Toxin-based targeted therapy for malignant brain tumors.* Clin Dev Immunol, 2012. **2012**: p. 480429.

39. Weldon, J.E. and I. Pastan, *A guide to taming a toxin--recombinant immunotoxins constructed from Pseudomonas exotoxin A for the treatment of cancer.* FEBS J, 2011. **278**(23): p. 4683-700.

40. Eiklid, K., S. Olsnes, and A. Pihl, *Entry of lethal doses of abrin, ricin and modeccin into the cytosol of HeLa cells.* Exp Cell Res, 1980. **126**(2): p. 321-6.

41. Yamaizumi, M., E. Mekada, T. Uchida, and Y. Okada, *One molecule of diphtheria toxin fragment A introduced into a cell can kill the cell.* Cell, 1978. **15**(1): p. 245-50.

42. Carrasco, L., C. Fernandez-Puentes, and D. Vazquez, *Effects of ricin on the ribosomal sites involved in the interaction of the elongation factors.* Eur J Biochem, 1975. **54**(2): p. 499-503.

43. Moolten, F., S. Zajdel, and S. Cooperband, *Immunotherapy of experimental animal tumors with antitumor antibodies conjugated to diphtheria toxin or ricin.* Ann N Y Acad Sci, 1976. **277**(00): p. 690-9.

44. Moolten, F.L. and S.R. Cooperband, *Selective destruction of target cells by diphtheria toxin conjugated to antibody directed against antigens on the cells.* Science, 1970. **169**(3940): p. 68-70.

45. Ahmad, Z.A., S.K. Yeap, A.M. Ali, W.Y. Ho, N.B. Alitheen, and M. Hamid, *scFv antibody: principles and clinical application.* Clin Dev Immunol, 2012. **2012**: p. 980250.

46. Pastan, I., R. Hassan, D.J. Fitzgerald, and R.J. Kreitman, *Immunotoxin therapy of cancer.* Nat Rev Cancer, 2006. **6**(7): p. 559-65.

47. Zalutsky, M.R., A. Boskovitz, C.T. Kuan, C.N. Pegram, J. Ayriss, C.J. Wikstrand, A.F. Buckley, E.S. Lipp, J.E. Herndon, 2nd, R.E. McLendon, and D.D. Bigner, *Radioimmunotargeting of malignant glioma by monoclonal antibody D2C7 reactive against both wild-type and variant III mutant epidermal growth factor receptors.* Nucl Med Biol, 2012. **39**(1): p. 23-34.

48. Chandramohan, V., X. Bao, S.T. Keir, C.N. Pegram, S.E. Szafranski, H. Piao, C.J. Wikstrand, R.E. McLendon, C.T. Kuan, I.H. Pastan, and D.D. Bigner, *Construction of an immunotoxin, D2C7-(scdsFv)-PE38KDEL, targeting EGFRwt and EGFRvIII for brain tumor therapy.* Clin Cancer Res, 2013. **19**(17): p. 4717-27.

49. Ogasawara, S., M.K. Kaneko, J.E. Price, and Y. Kato, *Characterization of anti-podoplanin monoclonal antibodies: critical epitopes for neutralizing the interaction between podoplanin and CLEC-2.* Hybridoma (Larchmt), 2008. **27**(4): p. 259-67.

50. Kato, Y., M.K. Kaneko, A. Kuno, N. Uchiyama, K. Amano, Y. Chiba, Y. Hasegawa, J. Hirabayashi, H. Narimatsu, K. Mishima, and M. Osawa, *Inhibition of tumor cell-induced platelet aggregation using a novel anti-podoplanin antibody reacting with its platelet-aggregation-stimulating domain.* Biochem Biophys Res Commun, 2006. **349**(4): p. 1301-7.

51. Kato, Y., G. Vaidyanathan, M.K. Kaneko, K. Mishima, N. Srivastava, V. Chandramohan, C. Pegram, S.T. Keir, C.T. Kuan, D.D. Bigner, and M.R. Zalutsky, *Evaluation of anti-podoplanin rat monoclonal antibody NZ-1 for targeting malignant gliomas.* Nucl Med Biol, 2010. **37**(7): p. 785-94.

52. Chandramohan, V., X. Bao, M. Kato Kaneko, Y. Kato, S.T. Keir, S.E. Szafranski, C.T. Kuan, I.H. Pastan, and D.D. Bigner, *Recombinant anti-podoplanin (NZ-1) immunotoxin for the treatment of malignant brain tumors.* Int J Cancer, 2013. **132**(10): p. 2339-48.

53. Pardoll, D.M., *The blockade of immune checkpoints in cancer immunotherapy.* Nat Rev Cancer, 2012. **12**(4): p. 252-64.

54. Zou, W. and L. Chen, *Inhibitory B7-family molecules in the tumour microenvironment.* Nat Rev Immunol, 2008. **8**(6): p. 467-77.

55. Greenwald, R.J., G.J. Freeman, and A.H. Sharpe, *The B7 family revisited.* Annu Rev Immunol, 2005. **23**: p. 515-48.

56. Preusser, M., M. Lim, D.A. Hafler, D.A. Reardon, and J.H. Sampson, *Prospects of immune checkpoint modulators in the treatment of glioblastoma.* Nat Rev Neurol, 2015. **11**(9): p. 504-14.

57. Escors, D., *Tumour immunogenicity, antigen presentation and immunological barriers in cancer immunotherapy.* New J Sci, 2014. **2014**.

58. Postow, M.A., M.K. Callahan, and J.D. Wolchok, *Immune Checkpoint Blockade in Cancer Therapy.* J Clin Oncol, 2015. **33**(17): p. 1974-1982.

59. Ott, P.A., F.S. Hodi, and C. Robert, *CTLA-4 and PD-1/PD-L1 blockade: new immunotherapeutic modalities with durable clinical benefit in melanoma patients.* Clin Cancer Res, 2013. **19**(19): p. 5300-9.

60. Tarhini, A.A. and F. Iqbal, *CTLA-4 blockade: therapeutic potential in cancer treatments.* Onco Targets Ther, 2010. **3**: p. 15-25.

61. Hodi, F.S., S.J. O'Day, D.F. McDermott, R.W. Weber, J.A. Sosman, J.B. Haanen, R. Gonzalez, C. Robert, D. Schadendorf, J.C. Hassel, W. Akerley, A.J. van den Eertwegh, J. Lutzky, P. Lorigan, J.M. Vaubel, G.P. Linette, D. Hogg, C.H. Ottensmeier, C. Lebbe, C. Peschel, I. Quirt, J.I. Clark, J.D. Wolchok, J.S. Weber, J. Tian, M.J. Yellin, G.M. Nichol, A. Hoos, and W.J. Urba, *Improved survival with ipilimumab in patients with metastatic melanoma.* N Engl J Med, 2010. **363**(8): p. 711-23.

62. O'Day, S.J., M. Maio, V. Chiarion-Sileni, T.F. Gajewski, H. Pehamberger, I.N. Bondarenko, P. Queirolo, L. Lundgren, S. Mikhailov, L. Roman, C. Verschraegen, R. Humphrey, R. Ibrahim, V. de Pril, A. Hoos, and J.D. Wolchok, *Efficacy and*

safety of ipilimumab monotherapy in patients with pretreated advanced melanoma: a multicenter single-arm phase II study. Ann Oncol, 2010. **21**(8): p. 1712-7.

63. Margolin, K., M.S. Ernstoff, O. Hamid, D. Lawrence, D. McDermott, I. Puzanov, J.D. Wolchok, J.I. Clark, M. Sznol, T.F. Logan, J. Richards, T. Michener, A. Balogh, K.N. Heller, and F.S. Hodi, *Ipilimumab in patients with melanoma and brain metastases: an open-label, phase 2 trial.* Lancet Oncol, 2012. **13**(5): p. 459-65.

64. Queirolo, P., F. Spagnolo, P.A. Ascierto, E. Simeone, P. Marchetti, A. Scoppola, M. Del Vecchio, L. Di Guardo, M. Maio, A.M. Di Giacomo, A. Antonuzzo, F. Cognetti, V. Ferraresi, L. Ridolfi, M. Guidoboni, M. Guida, J. Pigozzo, and V. Chiarion Sileni, *Efficacy and safety of ipilimumab in patients with advanced melanoma and brain metastases.* J Neurooncol, 2014. **118**(1): p. 109-16.

65. Luke, J.J. and P.A. Ott, *PD-1 pathway inhibitors: the next generation of immunotherapy for advanced melanoma.* Oncotarget, 2015. **6**(6): p. 3479-92.

66. Blanchette, M. and D. Fortin, *Blood-brain barrier disruption in the treatment of brain tumors.* Methods Mol Biol, 2011. **686**: p. 447-63.

67. Bobo, R.H., D.W. Laske, A. Akbasak, P.F. Morrison, R.L. Dedrick, and E.H. Oldfield, *Convection-enhanced delivery of macromolecules in the brain.* Proc Natl Acad Sci U S A, 1994. **91**(6): p. 2076-80.

68. Grossi, P.M., H. Ochiai, G.E. Archer, R.E. McLendon, M.R. Zalutsky, A.H. Friedman, H.S. Friedman, D.D. Bigner, and J.H. Sampson, *Efficacy of intracerebral microinfusion of trastuzumab in an athymic rat model of intracerebral metastatic breast cancer.* Clin Cancer Res, 2003. **9**(15): p. 5514-20.

69. Heimberger, A.B., G.E. Archer, R.E. McLendon, C. Hulette, A.H. Friedman, H.S. Friedman, D.D. Bigner, and J.H. Sampson, *Temozolomide delivered by intracerebral microinfusion is safe and efficacious against malignant gliomas in rats.* Clin Cancer Res, 2000. **6**(10): p. 4148-53.

70. Sampson, J.H., M. Brady, R. Raghavan, A.I. Mehta, A.H. Friedman, D.A. Reardon, N.A. Petry, D.P. Barboriak, T.Z. Wong, M.R. Zalutsky, D. Lally-Goss, and D.D. Bigner, *Colocalization of gadolinium-diethylene triamine pentaacetic acid with high-molecular-weight molecules after intracerebral convection-enhanced delivery in humans.* Neurosurgery, 2011. **69**(3): p. 668-76.

71. Mehta, A.I., B.D. Choi, D. Ajay, R. Raghavan, M. Brady, A.H. Friedman, I. Pastan, D.D. Bigner, and J.H. Sampson, *Convection enhanced delivery of macromolecules for brain tumors.* Curr Drug Discov Technol, 2012. **9**(4): p. 305-10.

72. Sampson, J.H., R. Raghavan, M. Brady, A.H. Friedman, and D. Bigner, *Convection-enhanced delivery.* J Neurosurg, 2011. **115**(3): p. 463-4; discussion 465-6.

73. Sampson, J.H., G. Akabani, G.E. Archer, M.S. Berger, R.E. Coleman, A.H. Friedman, H.S. Friedman, K. Greer, J.E. Herndon, 2nd, S. Kunwar, R.E. McLendon, A. Paolino, N.A. Petry, J.M. Provenzale, D.A. Reardon, T.Z. Wong, M.R. Zalutsky, I. Pastan, and D.D. Bigner, *Intracerebral infusion of an EGFR-targeted toxin in recurrent malignant brain tumors.* Neuro Oncol, 2008. **10**(3): p. 320-9.

74. Bao, X., V. Chandramohan, S.T. Keir, C.N. Pegram, R.E. McLendon, C.-T. Kuan, I.H. Pastan, and D.D. Bigner, *Antitumor efficacy of D2C7-(scdsFv)-PE38KDEL, a novel immunotoxin targeting EGFRwt and EGFRvIII, by convection-enhanced delivery in orthotopic brain tumor mouse models.* Journal for ImmunoTherapy of Cancer, 2013. **1**(Suppl 1): p. P126.

75. Ding, D., C.W. Kanaly, D.D. Bigner, T.J. Cummings, J.E. Herndon, 2nd, I. Pastan, R. Raghavan, and J.H. Sampson, *Convection-enhanced delivery of free gadolinium with the recombinant immunotoxin MR1-1.* J Neurooncol, 2010. **98**(1): p. 1-7.

76. Bao, X., V. Chandramohan, R.P. Reynolds, J.N. Norton, W.C. Wetsel, R.M. Rodriguiz, D.K. Aryal, R.E. McLendon, E.D. Levin, N.A. Petry, M.R. Zalutsky, B.K. Burnett, C.T. Kuan, I.H. Pastan, and D.D. Bigner, *Preclinical toxicity evaluation of a novel immunotoxin, D2C7-(scdsFv)-PE38KDEL, administered via intracerebral convection-enhanced delivery in rats.* Invest New Drugs, 2016. **34**(2): p. 149-58.

77. Moser, V.C., *Applications of a Neurobehavioral Screening Battery.* International Journal of Toxicology, 1991. **10**(6): p. 661-669.

78. Neyns, B., J. Sadones, E. Joosens, F. Bouttens, L. Verbeke, J.F. Baurain, L. D'Hondt, T. Strauven, C. Chaskis, P. In't Veld, A. Michotte, and J. De Greve, *Stratified phase II trial of cetuximab in patients with recurrent high-grade glioma.* Ann Oncol, 2009. **20**(9): p. 1596-603.

79. Sampson, J.H., G. Akabani, G.E. Archer, D.D. Bigner, M.S. Berger, A.H. Friedman, H.S. Friedman, J.E. Herndon, 2nd, S. Kunwar, S. Marcus, R.E. McLendon, A. Paolino, K. Penne, J. Provenzale, J. Quinn, D.A. Reardon, J. Rich,

T. Stenzel, S. Tourt-Uhlig, C. Wikstrand, T. Wong, R. Williams, F. Yuan, M.R. Zalutsky, and I. Pastan, *Progress report of a Phase I study of the intracerebral microinfusion of a recombinant chimeric protein composed of transforming growth factor (TGF)-alpha and a mutated form of the Pseudomonas exotoxin termed PE-38 (TP-38) for the treatment of malignant brain tumors.* J Neurooncol, 2003. **65**(1): p. 27-35.

80. Beers, R., P. Chowdhury, D. Bigner, and I. Pastan, *Immunotoxins with increased activity against epidermal growth factor receptor vIII-expressing cells produced by antibody phage display.* Clin Cancer Res, 2000. **6**(7): p. 2835-43.

81. Reiter, Y., U. Brinkmann, B. Lee, and I. Pastan, *Engineering antibody Fv fragments for cancer detection and therapy: disulfide-stabilized Fv fragments.* Nat Biotechnol, 1996. **14**(10): p. 1239-45.

82. Rasheed, B.K., R.N. Wiltshire, S.H. Bigner, and D.D. Bigner, *Molecular pathogenesis of malignant gliomas.* Curr Opin Oncol, 1999. **11**(3): p. 162-7.

83. Sok, J.C., F.M. Coppelli, S.M. Thomas, M.N. Lango, S. Xi, J.L. Hunt, M.L. Freilino, M.W. Graner, C.J. Wikstrand, D.D. Bigner, W.E. Gooding, F.B. Furnari, and J.R. Grandis, *Mutant epidermal growth factor receptor (EGFRvIII) contributes to head and neck cancer growth and resistance to EGFR targeting.* Clin Cancer Res, 2006. **12**(17): p. 5064-73.

84. Gajadhar, A.S., E. Bogdanovic, D.M. Munoz, and A. Guha, *In situ analysis of mutant EGFRs prevalent in glioblastoma multiforme reveals aberrant dimerization, activation, and differential response to anti-EGFR targeted therapy.* Mol Cancer Res, 2012. **10**(3): p. 428-40.

85. Schmidt, M., M. Maurer-Gebhard, B. Groner, G. Kohler, G. Brochmann-Santos, and W. Wels, *Suppression of metastasis formation by a recombinant single chain antibody-toxin targeted to full-length and oncogenic variant EGF receptors.* Oncogene, 1999. **18**(9): p. 1711-21.

86. Johns, T.G., E. Stockert, G. Ritter, A.A. Jungbluth, H.J. Huang, W.K. Cavenee, F.E. Smyth, C.M. Hall, N. Watson, E.C. Nice, W.J. Gullick, L.J. Old, A.W. Burgess, and A.M. Scott, *Novel monoclonal antibody specific for the de2-7 epidermal growth factor receptor (EGFR) that also recognizes the EGFR expressed in cells containing amplification of the EGFR gene.* Int J Cancer, 2002. **98**(3): p. 398-408.

87. Masui, H., T. Kawamoto, J.D. Sato, B. Wolf, G. Sato, and J. Mendelsohn, *Growth inhibition of human tumor cells in athymic mice by anti-epidermal growth factor receptor monoclonal antibodies.* Cancer Res, 1984. **44**(3): p. 1002-7.

88. Perera, R.M., Y. Narita, F.B. Furnari, H.K. Gan, C. Murone, M. Ahlkvist, R.B. Luwor, A.W. Burgess, E. Stockert, A.A. Jungbluth, L.J. Old, W.K. Cavenee, A.M. Scott, and T.G. Johns, *Treatment of human tumor xenografts with monoclonal antibody 806 in combination with a prototypical epidermal growth factor receptor-specific antibody generates enhanced antitumor activity.* Clin Cancer Res, 2005. **11**(17): p. 6390-9.

89. Li, Y.M. and W.A. Hall, *Targeted toxins in brain tumor therapy.* Toxins (Basel), 2010. **2**(11): p. 2645-62.

90. Reiter, Y. and I. Pastan, *Antibody engineering of recombinant Fv immunotoxins for improved targeting of cancer: disulfide-stabilized Fv immunotoxins.* Clin Cancer Res, 1996. **2**(2): p. 245-52.

91. Piao, H., C.T. Kuan, V. Chandramohan, S.T. Keir, C.N. Pegram, X. Bao, J.E. Mansson, I.H. Pastan, and D.D. Bigner, *Affinity-matured recombinant immunotoxin targeting gangliosides 3'-isoLM1 and 3',6'-isoLD1 on malignant gliomas.* MAbs, 2013. **5**(5): p. 748-62.

92. Salomon, D.S., R. Brandt, F. Ciardiello, and N. Normanno, *Epidermal growth factor-related peptides and their receptors in human malignancies.* Crit Rev Oncol Hematol, 1995. **19**(3): p. 183-232.

93. Chaffanet, M., C. Chauvin, M. Laine, F. Berger, M. Chedin, N. Rost, M.F. Nissou, and A.L. Benabid, *EGF receptor amplification and expression in human brain tumours.* Eur J Cancer, 1992. **28**(1): p. 11-7.

94. Kawamata, T., T. Mori, S. Sato, and Y. Katayama, *Tissue hyperosmolality and brain edema in cerebral contusion.* Neurosurg Focus, 2007. **22**(5): p. E5.

95. Bandaranayake, N.M., E.M. Nemoto, and S.W. Stezoski, *Rat brain osmolality during barbiturate anesthesia and global brain ischemia.* Stroke, 1978. **9**(3): p. 249-254.

96. Noker, P.E., R. Fulton, A.C. Pickett, and J.F. Mann, *Multiple dose toxicity study of MR1-1-(MR1-1dsFvPE38KDEL, NSC-718877) in Sprague Dawley Rats.*, in *Conducted at Southern Research Institute, Birmingham,Alabama and sponsored by National Cancer Institute, Bethesda, Maryland.* 2007.

97. Harling-Berg, C., P.M. Knopf, J. Merriam, and H.F. Cserr, *Role of cervical lymph nodes in the systemic humoral immune response to human serum albumin microinfused into rat cerebrospinal fluid.* J Neuroimmunol, 1989. **25**(2-3): p. 185-93.

98. Palestro, G., G. Mazzucco, R. Navone, M.G. Canese, R. Coda, D. Novero, F.B. Micca, and E. Leonardo, *Role of the T-cell system in glomerulonephritis induced in rats by human serum albumin (HSA). An immunological and morphological study.* Virchows Arch B Cell Pathol Incl Mol Pathol, 1980. **35**(1): p. 19-32.

99. Kawakami, K., M. Terabe, M. Kioi, J.A. Berzofsky, and R.K. Puri, *Intratumoral therapy with IL13-PE38 results in effective CTL-mediated suppression of IL-13Ralpha2-expressing contralateral tumors.* Clin Cancer Res, 2006. **12**(15): p. 4678-86.

100. Sampson, J.H., D.A. Reardon, A.H. Friedman, H.S. Friedman, R.E. Coleman, R.E. McLendon, I. Pastan, and D.D. Bigner, *Sustained radiographic and clinical response in patient with bifrontal recurrent glioblastoma multiforme with intracerebral infusion of the recombinant targeted toxin TP-38: case study.* Neuro Oncol, 2005. **7**(1): p. 90-6.

101. Ochiai, H., G.E. Archer, J.E. Herndon, 2nd, C.T. Kuan, D.A. Mitchell, D.D. Bigner, I.H. Pastan, and J.H. Sampson, *EGFRvIII-targeted immunotoxin induces antitumor immunity that is inhibited in the absence of CD4+ and CD8+ T cells.* Cancer Immunol Immunother, 2008. **57**(1): p. 115-21.

102. Chen, D.S. and I. Mellman, *Oncology meets immunology: the cancer-immunity cycle.* Immunity, 2013. **39**(1): p. 1-10.

103. Oh, T., S. Fakurnejad, E.T. Sayegh, A.J. Clark, M.E. Ivan, M.Z. Sun, M. Safaee, O. Bloch, C.D. James, and A.T. Parsa, *Immunocompetent murine models for the study of glioblastoma immunotherapy.* J Transl Med, 2014. **12**: p. 107.

104. Stuart, P.M., *Major Histocompatibility Complex (MHC): Mouse.* 2015: p. 1-7.

105. Haworth, K.B., J.L. Leddon, C.Y. Chen, E.M. Horwitz, C.L. Mackall, and T.P. Cripe, *Going back to class I: MHC and immunotherapies for childhood cancer.* Pediatr Blood Cancer, 2015. **62**(4): p. 571-6.

106. Friese, M.A., M. Platten, S.Z. Lutz, U. Naumann, S. Aulwurm, F. Bischof, H.J. Buhring, J. Dichgans, H.G. Rammensee, A. Steinle, and M. Weller, *MICA/NKG2D-mediated immunogene therapy of experimental gliomas.* Cancer Res, 2003. **63**(24): p. 8996-9006.

107. Fuller, G.N. and B.W. Scheithauer, *The 2007 Revised World Health Organization (WHO) Classification of Tumours of the Central Nervous System: newly codified entities.* Brain Pathol, 2007. **17**(3): p. 304-7.

108. Shultz, L.D., B.L. Lyons, L.M. Burzenski, B. Gott, X. Chen, S. Chaleff, M. Kotb, S.D. Gillies, M. King, J. Mangada, D.L. Greiner, and R. Handgretinger, *Human lymphoid and myeloid cell development in NOD/LtSz-scid IL2R gamma null mice engrafted with mobilized human hemopoietic stem cells.* J Immunol, 2005. **174**(10): p. 6477-89.

109. Shultz, L.D., P.A. Schweitzer, S.W. Christianson, B. Gott, I.B. Schweitzer, B. Tennent, S. McKenna, L. Mobraaten, T.V. Rajan, D.L. Greiner, and et al., *Multiple defects in innate and adaptive immunologic function in NOD/LtSz-scid mice.* J Immunol, 1995. **154**(1): p. 180-91.

110. Inda, M.M., R. Bonavia, and J. Seoane, *Glioblastoma multiforme: a look inside its heterogeneous nature.* Cancers (Basel), 2014. **6**(1): p. 226-39.

111. Seyfried, T.N., M. el-Abbadi, and M.L. Roy, *Ganglioside distribution in murine neural tumors.* Mol Chem Neuropathol, 1992. **17**(2): p. 147-67.

112. Fraser, H., *Astrocytomas in an inbred mouse strain.* J Pathol, 1971. **103**(4): p. 266-70.

113. Serano, R.D., C.N. Pegram, and D.D. Bigner, *Tumorigenic cell culture lines from a spontaneous VM/Dk murine astrocytoma (SMA).* Acta Neuropathol, 1980. **51**(1): p. 53-64.

114. Vlahovic, G., P.E. Fecci, D. Reardon, and J.H. Sampson, *Programmed death ligand 1 (PD-L1) as an immunotherapy target in patients with glioblastoma.* Neuro Oncol, 2015. **17**(8): p. 1043-5.

115. Berghoff, A.S., B. Kiesel, G. Widhalm, O. Rajky, G. Ricken, A. Wohrer, K. Dieckmann, M. Filipits, A. Brandstetter, M. Weller, S. Kurscheid, M.E. Hegi, C.C. Zielinski, C. Marosi, J.A. Hainfellner, M. Preusser, and W. Wick, *Programmed death ligand 1 expression and tumor-infiltrating lymphocytes in glioblastoma.* Neuro Oncol, 2015. **17**(8): p. 1064-75.

116. Taube, J.M., A. Klein, J.R. Brahmer, H. Xu, X. Pan, J.H. Kim, L. Chen, D.M. Pardoll, S.L. Topalian, and R.A. Anders, *Association of PD-1, PD-1 ligands, and other features of the tumor immune microenvironment with response to anti-PD-1 therapy.* Clin Cancer Res, 2014. **20**(19): p. 5064-74.

117. Topalian, S.L., F.S. Hodi, J.R. Brahmer, S.N. Gettinger, D.C. Smith, D.F. McDermott, J.D. Powderly, R.D. Carvajal, J.A. Sosman, M.B. Atkins, P.D. Leming, D.R. Spigel, S.J. Antonia, L. Horn, C.G. Drake, D.M. Pardoll, L. Chen, W.H. Sharfman, R.A. Anders, J.M. Taube, T.L. McMiller, H. Xu, A.J. Korman, M.

Jure-Kunkel, S. Agrawal, D. McDonald, G.D. Kollia, A. Gupta, J.M. Wigginton, and M. Sznol, *Safety, activity, and immune correlates of anti-PD-1 antibody in cancer.* N Engl J Med, 2012. **366**(26): p. 2443-54.

118. Reardon, D.A., P.C. Gokhale, S.R. Klein, K.L. Ligon, S.J. Rodig, S.H. Ramkissoon, K.L. Jones, A.S. Conway, X. Liao, J. Zhou, P.Y. Wen, A.D. Van Den Abbeele, F.S. Hodi, L. Qin, N.E. Kohl, A.H. Sharpe, G. Dranoff, and G.J. Freeman, *Glioblastoma Eradication Following Immune Checkpoint Blockade in an Orthotopic, Immunocompetent Model.* Cancer Immunol Res, 2016. **4**(2): p. 124-35.

119. Wainwright, D.A., A.L. Chang, M. Dey, I.V. Balyasnikova, C. Kim, A.L. Tobias, Y. Cheng, J. Kim, L. Zhang, J. Qiao, Y. Han, and M.S. Lesniak, *Durable therapeutic efficacy utilizing combinatorial blockade against IDO, CTLA-4 and PD-L1 in mice with brain tumors.* Clin Cancer Res, 2014.

120. Lawrence, M.S., P. Stojanov, P. Polak, G.V. Kryukov, K. Cibulskis, A. Sivachenko, S.L. Carter, C. Stewart, C.H. Mermel, S.A. Roberts, A. Kiezun, P.S. Hammerman, A. McKenna, Y. Drier, L. Zou, A.H. Ramos, T.J. Pugh, N. Stransky, E. Helman, J. Kim, C. Sougnez, L. Ambrogio, E. Nickerson, E. Shefler, M.L. Cortes, D. Auclair, G. Saksena, D. Voet, M. Noble, D. DiCara, P. Lin, L. Lichtenstein, D.I. Heiman, T. Fennell, M. Imielinski, B. Hernandez, E. Hodis, S. Baca, A.M. Dulak, J. Lohr, D.A. Landau, C.J. Wu, J. Melendez-Zajgla, A. Hidalgo-Miranda, A. Koren, S.A. McCarroll, J. Mora, R.S. Lee, B. Crompton, R. Onofrio, M. Parkin, W. Winckler, K. Ardlie, S.B. Gabriel, C.W. Roberts, J.A. Biegel, K. Stegmaier, A.J. Bass, L.A. Garraway, M. Meyerson, T.R. Golub, D.A. Gordenin, S. Sunyaev, E.S. Lander, and G. Getz, *Mutational heterogeneity in cancer and the search for new cancer-associated genes.* Nature, 2013. **499**(7457): p. 214-8.

121. Sharma, P. and J.P. Allison, *Immune checkpoint targeting in cancer therapy: toward combination strategies with curative potential.* Cell, 2015. **161**(2): p. 205-14.

122. Klebanoff, C.A., L. Gattinoni, and N.P. Restifo, *CD8+ T-cell memory in tumor immunology and immunotherapy.* Immunol Rev, 2006. **211**: p. 214-24.

123. Jia, Q., J. Zhou, G. Chen, Y. Shi, H. Yu, P. Guan, R. Lin, N. Jiang, P. Yu, Q.J. Li, and Y. Wan, *Diversity index of mucosal resident T lymphocyte repertoire predicts clinical prognosis in gastric cancer.* Oncoimmunology, 2015. **4**(4): p. e1001230.

Biography

Birth place: Shanghai, China

Education:

- Department of Pathology, Duke University Medical Center

  PhD Candidate (2012-present)

- Shanghai Medical College, Fudan University

  Master of Clinical Medicine (Surgery/Neurosurgery)

  Bachelor of Medicine

Selective publications:

Bao, X., V. Chandramohan, R.P. Reynolds, J.N. Norton, W.C. Wetsel, R.M. Rodriguiz, D.K. Aryal, R.E. McLendon, E.D. Levin, N.A. Petry, M.R. Zalutsky, B.K. Burnett, C.T. Kuan, I.H. Pastan, and D.D. Bigner, *Preclinical toxicity evaluation of a novel immunotoxin, D2C7-(scdsFv)-PE38KDEL, administered via intracerebral convection-enhanced delivery in rats.* Invest New Drugs, 2016. **34**(2): p. 149-58.

Piao, H., C.T. Kuan, V. Chandramohan, S.T. Keir, C.N. Pegram, **X. Bao**, J.E. Mansson, I.H. Pastan, and D.D. Bigner, *Affinity-matured recombinant immunotoxin targeting gangliosides 3'-isoLM1 and 3',6'-isoLD1 on malignant gliomas.* MAbs, 2013. **5**(5): p. 748-62.

Chandramohan, V., **X. Bao**, S.T. Keir, C.N. Pegram, S.E. Szafranski, H. Piao, C.J. Wikstrand, R.E. McLendon, C.T. Kuan, I.H. Pastan, and D.D. Bigner, *Construction of an immunotoxin, D2C7-(scdsFv)-PE38KDEL, targeting EGFRwt and EGFRvIII for brain tumor therapy.* Clin Cancer Res, 2013. **19**(17): p. 4717-27.

Chandramohan, V., **X. Bao**, M. Kato Kaneko, Y. Kato, S.T. Keir, S.E. Szafranski, C.T. Kuan, I.H. Pastan, and D.D. Bigner, *Recombinant anti-podoplanin (NZ-1) immunotoxin for the treatment of malignant brain tumors.* Int J Cancer, 2013. **132**(10): p. 2339-48.

Selective poster presentations:

Preclinical toxicity evaluation of a novel immunotoxin, D2C7-(scdsFv)-PE38KDEL, administered via intracerebral convection-enhanced delivery in rats
The 2015 SNO-SCIDOT Joint Conference on Therapeutic Delivery to the CNS
San Antonia, TX, USA

Immunotoxin and Immune Checkpoint Blockade Combination Immunotherapy for Malignant Gliomas
Basic Science Day 2015, School of Medicine, Duke University
Durham, NC, USA

Immunotoxin and Immune Checkpoint Blockade Combination Immunotherapy for Malignant Gliomas
The 3rd Annual Duke Cancer Institute Scientific Retreat
Durham, NC, USA

Anti-tumor efficacy of D2C7-(scdsFv)-PE38KDEL, a novel immunotoxin targeting EGFRwt and EGFRvIII, by convection-enhanced delivery in orthotopic brain tumor mouse models
The 28th Annual Scientific Meeting of the Society for Immunotherapy of Cancer
National Harbor, MD, USA